University of Strathclyde
Department of Mechanical Engineering

Pattern Formation in Swarming Systems using Bifurcating Potential Fields

by

Derek James Bennet

A thesis presented in fulfilment of the requirements
for the degree of Doctor of Philosophy

2010

Declaration of author's rights

Acknowledgements

I would like to thank my supervisor, Professor Colin McInnes for his support and advice throughout my PhD. He was always there when I needed any help and has been a source of inspiration in completing this thesis.

During the latter stages of my PhD I was lucky enough to spend some time carrying out part of my research at Nihon University, Tokyo, Japan. I would like to thank Professor Kenji Uchiyama for looking after me so well whilst I was there, as well as all of the students at Nihon University. A big thank you also goes to all my friends and staff at the University of Strathclyde.

I would like to dedicate this thesis to my family. In particular, my Mum and Dad, who have always supported and encouraged me throughout my life. I know that without them I would never have been able to complete this thesis.

Abstract

Many future engineering systems may consist of swarms of multiple, mobile autonomous *agents*, operating together to solve engineering problems in new and efficient ways. To enable such systems, this thesis investigates the development of new methodologies for verifiable swarming systems, investigating two areas of generic swarming systems; pattern formation and reconfigurability.

Based on dynamical systems theory and through the new approach of bifurcating artificial potential fields, it is shown that a verifiable swarming system can be constructed, capable of creating reconfigurable, autonomous patterns. Using scale separation of the potential fields and Lyapunov stability methods, swarm verification can be achieved, providing a step towards replacing traditional heuristic methods with a more rigorous analytical approach.

The new methodologies are demonstrated in two safety or mission critical engineering systems; spacecraft formation flying and swarms of unmanned aerial vehicles. For spacecraft formation flying, it is shown that a formation can operate in low-Earth-orbit and deep-space using a second order force model with bounded actuator effort. For swarms of unmanned aerial vehicles, a guidance and control algorithm is developed through a first order velocity field model. In both models, it is shown that the swarm can safely form different patterns and autonomously reconfigure between them.

Contents

List of Figures

List of Tables

Chapter 1

Introduction

1.1 Background

In the near future many engineering systems may consist of multiple, mobile autonomous *agents* that must operate together in a coordinated and safe manner. Recently, various branches of science and technology, in particular biology and robotics, have been investigating the global emergent behaviour that often occurs when swarms of *agents* interact locally [1]. These systems are often termed complex systems as their global behaviour cannot be fully explained by considering the dynamics of each individual *agent* [2]. Biologists are motivated by the development of mathematical models to describe the complex patterns that occur in nature [3], whereas engineers are driven by the need to solve engineering problems in new, efficient and robust ways. Examples of potential swarm engineering applications include; inspection of complicated engineering structures such as turbines with small miniature robots [4], scientific data gathering in formations of unmanned aerial vehicles [5–9] and for interferometric/sparse aperture telescopes in spacecraft formation flying [10, 11]. Figures 1.1 (i) and (ii) show an example of a swarm system in nature and also in an engineering context.

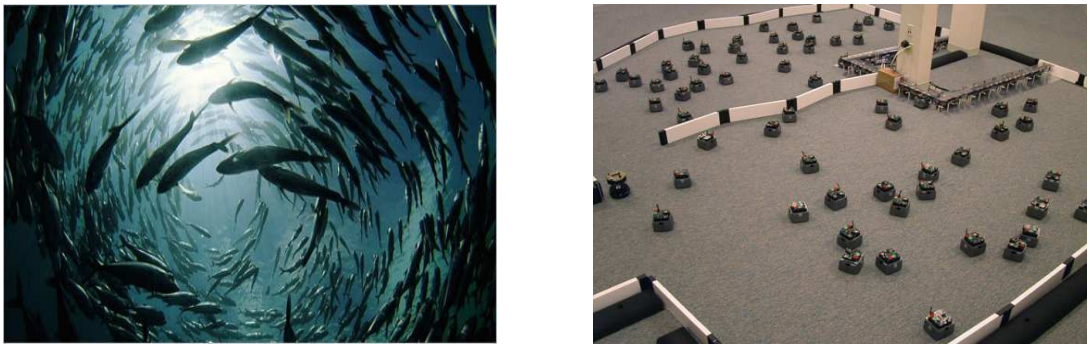

(i) (ii)

Figure 1.1: Examples of swarms (i) school of fish (Getty Images) (ii) robot swarm (MIT)

In nature the term *agent* applies to swarms of social entities, such as insects, that self-organise through local communications and interaction with the environment. This phenomena is apparent on every length scale from formations of bacteria to flocks of birds or schools of fish [12], where one of the key characteristics is that the members in the group maintain a constant separation distance [13]. Instead of a centralised leader architecture, the *agents* in the swarm act in a distributed way, having no *a priori* knowledge of the pattern that they will eventually relax into. The term *emergent behaviour* therefore describes the process in which through local microscopic interactions, macroscopic behaviours occur.

Although biology provides us with a prime example of a complex system there are many examples of others such as; the dynamics of global weather patterns, the economic dynamics of world markets and neuron activity in the brain [14]. In the past decade the study of these types of system has been termed *complex systems theory* and has been suggested as the science of the 21st century. In general they are typically composed of a series of non-linear components, interacting and producing self-organised behaviour [14].

In the engineering context, Parunak defines a swarming system as the "*the useful self-organisation of multiple entities through local interactions*"[15]. The term '*useful*' implies that the swarming system will be effective in an engineering application, having advantages over conventional single entity systems and considering real dynamic complexities such as non-holonomic effects. A swarming system is particularly appealing to an engineer as it can have desirable properties such as

scalability, robustness and flexibility.

To make use of these advantages swarm robotics has developed into a major research area with large international projects currently underway addressing ways in which they can be designed and developed. Originally robot systems were developed based on the artificial intelligence (AI) approach with the desire to model intelligence on an individual basis, aiming at reproducing human cognition [16]. Although partially successful, it soon became apparent that even modeling the simplest of behaviours would be a difficult task. During the mid-1980s Brooks introduced the idea of a behaviour based system to the AI community and has since produced a paradigm shift in the way that robotic systems are designed [17]. His idea was based on a layered subsumption architecture, neglecting any internal model of the environment and creating a completely reactive system, where *agent* behaviours are driven by sensing and communication. This ad-hoc type approach has been investigated by many authors and produced interesting qualitative behaviours such as dispersion, collision avoidance and flocking [18–20].

Another related approach to the control of a swarm robotic system is the work carried out by Beni [21]. His work was based on a cellular automata approach, originally developed by von Neumann [22], and can be considered one of the simplest models of a complex system. In [23] he introduced the term *swarm intelligence* to describe a system that lacks any form of hierarchical control structure, where the *agents* in the system interact locally with each other and also the environment.

Winfield has also introduced the term *swarm engineering* to highlight the key issues that are involved in real, safety-critical applications as opposed to simulation [24]. One of the difficult aspects of swarming technology is how to create verifiable systems, ensuring no undesirable behaviours occur. Therefore, although there have been numerous theoretical approaches developed for swarm robot systems, the implementation of these in real applications will require the development of verifiable swarms.

In order to address these issues this thesis investigates the development of generic swarming systems, considering ways in which verifiable, reliable and realistic

swarm engineered systems can be achieved. Through the use of dynamical systems theory two areas of swarm systems are investigated; **pattern formation** and **reconfigurability**. The new control algorithms developed based on **bifurcating artificial potential fields** are mathematically elegant, computationally efficient and can analytically prove the stability of the system replacing traditional algorithm validation. The algorithms are implemented in engineering applications of particular interest to the author; **spacecraft formation flying** and **unmanned aerial vehicles (UAVs)**.

The following sections of this chapter review the central concepts discussed in the background that are important in swarm engineered systems and provides a review of current modelling techniques used. There is then a discussion on related approaches to pattern formation and reconfigurability in swarming systems, followed by the layout and objectives of this thesis.

1.2 What is Swarm Intelligence?

The term *swarm intelligence* first appeared in the literature as a means to describe a special type of robotic system that would be decentralised and made up of simple and (quasi) identical *agents* [23]. This was particularly appealing for a robot system as a decentralised control scheme lends to simpler robots with the potential for mass production and high redundancy.

In 1999, Bonabeau et al. extended the definition of *swarm intelligence* to include "*any attempt to design algorithms or distributed problem-solving devices inspired by the collective behaviour of social insect colonies and other animal societies*" [25]. They were particularly interested in the way in which social insects such as ants and wasps form colonies. They realised that the ideas that Beni had raised were relevant and true of the characteristics that they found in the swarming behaviour of social insects and suggested that the behaviour was a product of two characteristics; *self-organisation* and *stigmergy*.

1.2.1 Self-organisation

Self-organisation describes the behaviour that a physical system goes through with the emergence of macroscopic patterns from microscopic interactions [26].

An example is crystal growth in snow flakes. Snowflakes form by water vapour in clouds creating ice on dust particles. Depending upon temperature and the spin of the flakes as they fall a variety of different flake patterns emerge through the process of local interactions [27]. An example of a self-organised snow flake is given in Fig. 1.2 (i). Another example of *self-organisation* is the process of magnetisation [28]. A magnetic material consists of an array of small magnets know as *spins*. At high temperatures the *spins* have a random distribution. However, if the temperature of the magnet is reduced the *spins* self-organise into the same direction, as shown in Fig. 1.2 (ii).

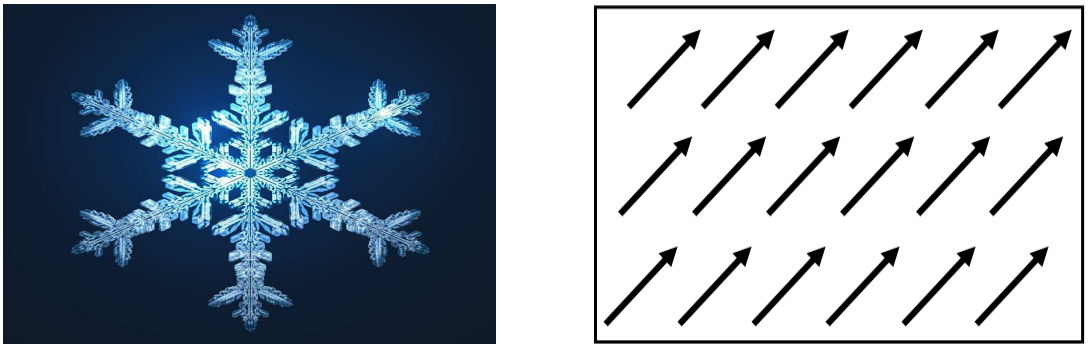

(i) (ii)

Figure 1.2: Examples of self-organisation (i) snowflake formation (Gravner-Griffeath) (ii) spin alignment for magnetisation

1.2.2 Stigmergy

In swarms of social insects *self-organisation* is driven by either direct or in-direct communication. With direct communication, social insects may communicate through some form of sensing such as physical contact. Indirect communication, on the other hand, is when an insect alters the environment resulting in a change in behaviour of other insects. The process of indirect communication is termed *stigmergy* and is important in the collective behaviour that occurs through *swarm intelligence*. One of the best examples of this process is to consider the foraging behaviour of ants. Beckers et al. have been able to show that ants find the shortest path between their nest and a food source by depositing chemical pheromones when they find food [29]. Other ants in the colony are then attracted to this substance and as a result the foraging ants can optimise their search for food.

This idea has proved successful in several applications such as a method of re-routing network traffic in telecommunication systems [30].

1.2.3 Approaches to Modelling Swarm Intelligence

The modelling of *swarm intelligence* has been researched extensively since it was first introduced in the the late 1980s. For this reason there exists numerous methods such as the design of optimisation tools based on the behaviour of social insects to developing simple rules that mimic the flocking behaviour that is found in birds. This section gives a review of some of the most popular approaches to modelling swarm intelligence.

Cellular Automata

Cellular automata are a class of discrete mathematical systems that can be viewed as a simple method of modelling *swarm intelligence*. It was first introduced by von Neumann as a method to achieve self-reproduction and consists of lattice cells that can exist in a number of finite states [22]. The dynamics of such systems are solved discretely with the future state of each cell dependent upon the interaction locally with its neighbouring cells.

One of the most popular examples of cellular automata is Conway's *Game of Life* [31]. It consists of a lattice of cells that can either be dead or alive and the dynamics of the system are solved based on a set of local rules depending upon the condition of the surrounding cells in the simulation. The results showed that through simple local interactions, dynamic behaviours can occur such as the gliding of a pattern across the lattice.

Cellular automata has been applied to various topics such the modeling of fluid behaviour [32], earthquakes [33] and chemical reactions [34].

Reynolds Flocking Boids model

One of the key early papers to demonstrate swarming behaviour in animals was Reynolds boids simulation of flocking birds in 1987 [35]. This heuristic ruled based approach defined the movement of each boid on three simple steering behaviours; separation, alignment and cohesion and produced interesting qualitative

behaviours. The method was also investigated by Heppner and Grenander [36].

Recently the idea has been applied to flocking of autonomous unmanned air vehicles by Crowther [37, 38]. Although producing successful behaviours, demonstrating that swarming behaviour can be replicated through a set of simple rules, the systems lacks any formal validation for the behaviours and therefore limits its ability to be applied to a safety or mission critical system.

Ant Colony Optimisation

Dorigo proposed the idea of using the behaviour of ants that forage for food as an algorithm that would find an optimal path in a graph [39]. This probabilistic method has been shown to have near optimal solutions to the traveling salesman problem where the aim is to find the shortest route to connect a series of cities [40].

Recently the method has been extended and applied successfully to solve problems such as transportation, distribution and logistics in vehicle routing [41], routing and congestion problems in computer networks [42] and the prediction of 3D protein shapes through protein folding in biology [43].

Particle Swarm Optimisation

Particle swarm optimisation (PSO) was introduced by Kennedy and Eberhart and was inspired from the social behaviour of flocking birds or schools of fish [44]. In the algorithm the particles search a multi-dimensional solution space, changing their velocity depending upon a fitness function which is weighted against its position in the solution space and also the influence of its neighbours. The result is that the swarm will flock together, globally optimising the problem at hand.

Although originally conceived of as an optimisation tool [45], PSO has become very popular of late in other applications due to its simplicity and efficiency. It has been applied to various problems such as the selection of the process parameters for pulsed laser micro-machining [46].

1.3 Swarm Robotics

Over the past 20 years swarm robotics has developed into a major research field driven by the need to solve engineering problems in new and efficient ways. A robot is defined by Arkin as "*a machine that is able to extract information from its environment and use knowledge from its world to move safely and in a meaningful and purposeful manner*"[47]. The key issues to be addressed in the area of swarm robotics are;

- How do we control a swarm of robots overcoming real practical and technological constraints such as communication limitations, non-holonomic effects and actuator saturation?
- What technical and societal problems can be addressed and solved using this technology?

To answer the first question researchers have based the development of control systems on the *swarm intelligence* paradigm, with the ultimate aim of developing fully autonomous, distributed systems. These systems are particularly appealing to an engineer as they can have the key advantages of being robust to individual failures, scalable and flexible. They also allow the engineer the opportunity to solve problems that may not have been achievable through the use of a single robot. As a result, swarm robotics has been applied to a range of engineering applications such as swarms of unmanned aerial vehicles and spacecraft formation flying.

At present there are large international projects underway that are addressing the design and development of swarm robot systems. For example, in Europe a number of research institutes are developing swarms of small mobile robots. The European Commission have funded several activities such as the *Swarm-bots* project (2001-2005) and its extension, the *Swarmanoid* project (2006-2010). *Swarm-bots* studied new approaches to the design of self-organising and self-assembling artifacts [48, 49], with *Swarmanoid* extending the research by considering systems of distributed heterogeneous robots [50, 51].

In addition the European Commission has also funded two research projects, *Symbrion* and *Replicator*, between 2008 and 2013. *Symbrion* aims to develop novel

principles of behaviour, adaptation and learning for swarms of robots based on artificial evolution and evolutionary computational approaches [52], with *Replicator* focusing on the development of a swarm of small autonomous mobile micro-robots that are capable of self-assembling into large artificial organisms [53]. Figures 1.3 (i) and (ii) show an example of a *Swarm-bot* and *Symbrion* robots respectively.

(i) (ii)

Figure 1.3: Examples of swarm robots (i) Swarm-bot (Universite Libre de Bruxelles) (ii) Symbrion (University of Stuttgart)

In addition to academic research, a large number of military researchers are investigating ways in which swarming technology can be used. The idea of swarming units of attack, as opposed to single units, has been used throughout military history; such as swarms of U-boats adopting the '*wolf-pack*' strategy during the second world war [54]. Recently, military researchers have been developing ways in which they can take advantage of the benefits of using swarms of robots [14]. For example, in 2008 the US army invested $10 million into a collaborative research project with the aim of developing swarms of unmanned air vehicles[1]. The potential applications of this technology include surveillance of the battlefield or convoy protection. The Office of Naval Research in the US have also sponsored a research collaboration into the development of heterogeneous unmanned network teams between 2008-2011, in particular swarms of unmanned underwater vehicles (UUV). This technology could then be used to identify potential threats and track them, reducing the risk to personnel and improving stealth capabilities. An example of a UAV swarm and UUV is given in Fig. 1.4 (i) and (ii) respectively.

Multiple spacecraft flying in formation is another research application of swarm robot technology. Multiple spacecraft operating together enables a variety of mis-

[1] www.microsystems.umd.edu/index.php, accessed 22/06/09

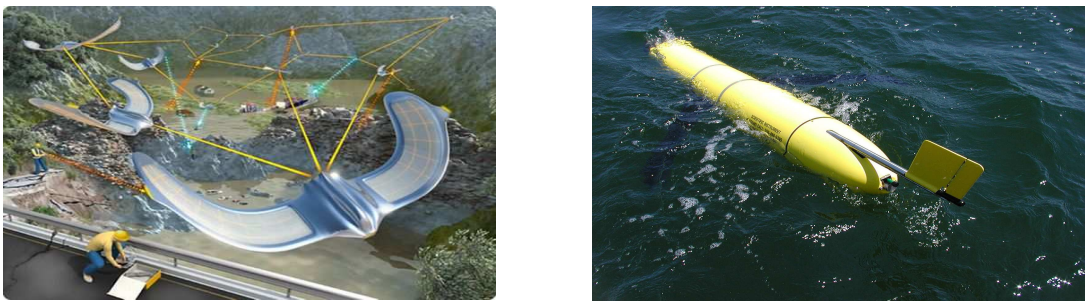

(i) (ii)

Figure 1.4: (i) UAV (US army) (ii) Slocum Glider UUV (Webb Research)

sions that can improve significantly the functionality of the system in comparison with a large single spacecraft [55]. For example, LISA, the Laser Interferometer Space Antenna, is a joint ESA-NASA mission to observe astrophysical and cosmological sources of gravitational waves. It will consist of three spacecraft separated by 5 million kilometers achieving a mission goal that could never be realised with the use of only one spacecraft [56]. ESA are also investigating DARWIN, a mission that will consist of 4 spacecraft equipped with optical telescopes in formation at the Sun-Earth L_2 point searching for earth like planets [11]. Figure 1.5 (i) and (ii) show visualisations of both LISA and DARWIN missions respectively.

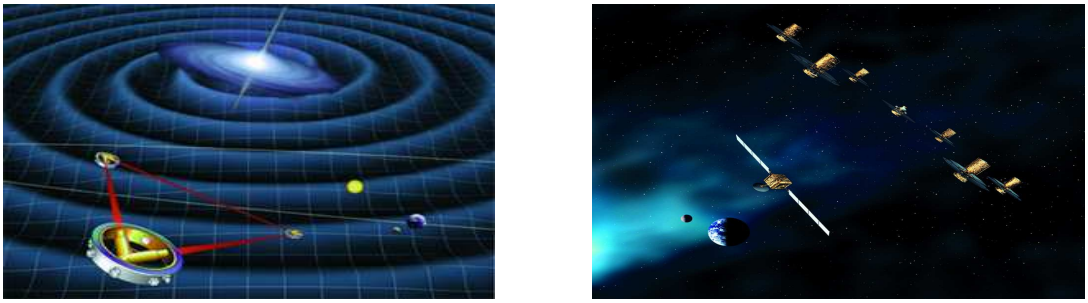

(i) (ii)

Figure 1.5: Examples of spacecraft formation flying (i) LISA (NASA) (ii) DARWIN (ESA)

1.3.1 Swarm Robotics Control Architectures

The control of multiple robots can be split broadly into either centralised or distributed control. Centralised control architectures have proved successful for the control of a small number of robots, with the advantage of achieving a very high level of positional accuracy. The leader-follower architecture is an example of a centralised control law that has proved successful for the control of multiple UAVs. Koo et al. proposed a leader UAV that would determine the trajectories of two follower UAVs, with numerical results showing that the control law can achieve the desired flight formation [57]. The disadvantage of this system is that as the number of UAVs increase, controlling them in a centralised way becomes extremely demanding on the controller, which in turn limits the scalability and robustness of the system.

As opposed to this centralised approach, this thesis is concerned with the development of a distributed control architecture, allowing the development of a robust and flexible system. The behaviour-based approach, introduced by Brooks, is generally regarded as the method of choice for the development of swarm robotic systems of this type. As opposed to the classical AI approach, behavioural robotics is based on a collection of behaviours, which act either dependently or independently to produce a particular behaviour in the robot. Instead of requiring an internal model of the environment, behavioural intelligence is related to the interaction of the robot with its environment and also other robots. It is therefore clear to see the similarities that exist between this description and that of *swarm intelligence*.

Pirjanian states that the success of behavior-based control architectures is dependent upon the *Action Selection Problem*, which is concerned with how the controlled robots decide which of the basic behaviours they will use [58]. There have been several reviews published on behavioural based control architecture for swarm robotics, notably Arkin 1998 [47], Pirjanian 1999 [58] and more recently Bayindir in 2007 [2]. This section gives a discussion of the key approaches to behaviour based control.

Subsumption Architecture

This bottom up approach is based on an arbitration mechanism that consists of a set of layered independent behaviours with a simple inhibition or suppression

mechanism acting between them. Figure 1.6 shows a typical priority-based subsumption architecture, consisting of three basic behaviours, where higher level behaviours subsume the lower behaviours, therefore taking priority in the command of the system.

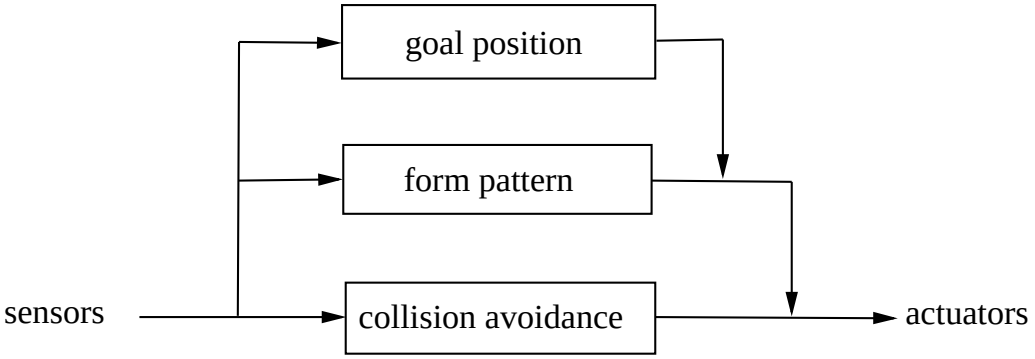

Figure 1.6: Subsumption architecture

Brooks implemented his architecture on single robot platforms such as *Allen* [17] and was able to demonstrate that the subsumption architecture could successfully achieve simple behaviours such as obstacle avoidance. Mataric developed a robot capable of path planning and navigation producing control laws in real time by integrating a map representation into a reactive, subsumption-based mobile robot [59]. She noted that the main advantage of this architecture was that it could operate in an unpredictable, dynamic world.

Parker used the subsumption architecture to simulate the formation of a line pattern of robots that could navigate past an obstacle to reach a goal position [60]. Balch and Arkin extended Parker's work adding other formation patterns such as a column or wedge formation and applied it successfully to the control of two mobile robots [61].

One of the disadvantages of this method is that as more complex layers are added to the system, the complexity in designing the system increases [62]. Also, although this approach has been shown to produce interesting emergent swarm behaviours, the system lacks formality and is therefore difficult to validate which is essential for safety or mission critical applications.

Probabilistic Finite State Automata

The probabilistic finite state automata approach is a method in which robots are modelled as finite state machines, with the use of stochastic Markov processes to describe the behaviour of the swarm [63, 64]. In this mathematical approach the system transitions between different states dependent upon certain probabilities, providing a way to model and analyse the long term behaviour of a swarm robotic system [65].

Lui et al. presented a probabilistic finite state machine model to deal with a swarm foraging task [64]. The approach uses several difference equations to describe a probabilistic finite state machine for the task and they implement the mathematical model in a sensor-based simulation to act as validation. Using eight simulated robots with collision avoidance sensors, three light sensors and a camera to search for food, their results showed excellent agreement with the mathematical model.

Soysal et al. also introduced a model to approach the aggregation problem in swarm robotics [66]. Using a three-state finite state machine based on approach, repel and wait behaviours they showed in simulation that an aggregation task can be achieved.

A disadvantage to this approach is that given a particular global task to solve there is no formal method to design individual behaviours. Also, although this mathematical approach provides an insight to emergent swarm behaviours based on a large number of robots, this approach is difficult to validate without resorting to lengthy algorithm validation techniques.

Distributed Artificial Potential Fields

The artificial potential field (APF) approach is a fusion behaviour based architecture that combines several behaviours of a robot, superimposing them through the use of the APF [16]. It often results in a non-linear dynamic system, that can either be continuous or discrete, with the evolution of the system thus expressed mathematically. This thesis is concerned with the development of swarming systems based on this method and so the results are amenable to formal proof.

The method was first introduced by Khatib to enable obstacle avoidance for manipulators and mobile robots [67]. During the early years of robotics, computational resources were limited and the APF provided a simple and easy computational method for single robot motion planning [68]. It has thus been studied extensively in the area of autonomous path planning for mobile robots [68–73] and more recently has been applied to autonomous swarming systems [74–79]. The basic idea behind this method is to create a global potential field that consists of attractive and repulsive potentials acting on each robot. Depending upon the robot's position in its workspace the negative gradient of the attractive/repuslive scalar potential field can either describe a required velocity or acceleration that will attract the robot to a desired goal position while avoiding obstacles, as shown in the example given in Fig. 1.7.

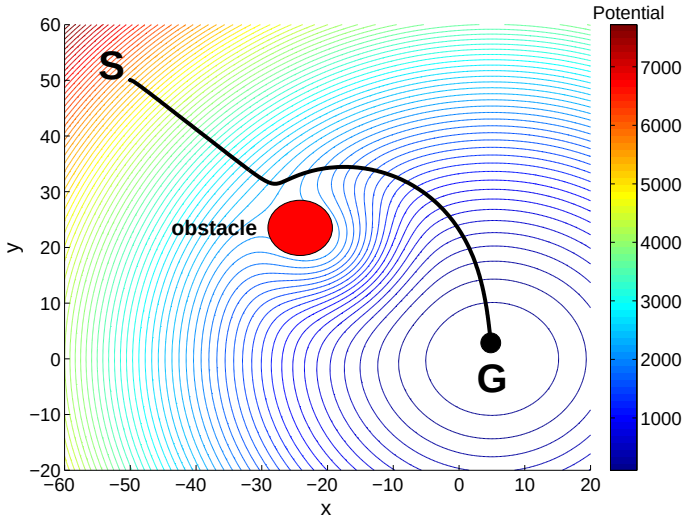

Figure 1.7: Artificial potential field contour plot with start, **S** and goal, **G**

Ideally, the global minimum of the potential field should correspond to the desired equilibrium state of the system. However, one of the limitations of the APF method is that the robot may become trapped in undesired local minima due to the superposition of the repulsive and attractive potential fields. This problem has been investigated extensively with several methods developed to overcome the problem for single and swarm robot platforms [70, 80–83].

A basic approach is to consider the case when a single robot is required to avoid an obstacle and reach a goal position. If the goal position is described by a sym-

metric attractive potential and the obstacle by a circular gaussian function, then no local minima will form [84]. This is limited by the fact that the robot may encounter obstacles that are not circular and thus this method cannot be relied upon for applications where the robot may be required to operate in unknown dynamic environments. A more rigorous method to overcome the local minima problem for a single robot is Borenstein et al. proposed wall-following method [70]. In this approach if a robot encounters an obstacle it will follow the obstacle contour until it escapes the obstacle and can then continue towards the goal position. Another method is to form the APF, U, as a solution to the Laplace equation ($\nabla^2 U = 0$) [5, 85, 86]. By doing so the APF is ensured to have a single global minimum and therefore overcome the local minimum problem.

For swarm robot problems Marcoloni et al. consider the creation of 2D patterns operating in an environment containing unknown obstacles [83]. To overcome local minima they manipulate the swarm so that some robots become *rescuers* that are able to help other robots escape the obstacle. Their results, presented in both simulation and experiment, suggested that this method can successfully lead to escape from local minima although no formal analytical method was provided to prove that it always occurs.

A related approach to Borenstein's wall following method is Mabrouk and McInnes' rolling vortex method [82]. In this approach the robots which are closest to wall have a lower speed compared with those further away and as a result a rolling vortex motion is induced and the swarm formation escapes the local minima reaching the goal position.

In addition, another disadvantage of the APF method is that it normally requires global knowledge of all other *agents* in the swarm [87], as well as *a priori* information of the obstacles in the environment [88]. In real engineered systems this is challenging and limits the scalability of the control algorithm. Furthermore, care has to be taken to ensure that the resulting commanded velocity or force respects non-holonomic constraints for the design of a real robot system. Kyriakopoulos et al. consider this for path planning of a single wheeled vehicle, decomposing the problem by using the potential field method to generate a collision free path and then approximating this path considering non-holonomic constraints [89]. More

recently, Gazi et al. have considered the aggregation, foraging and formation control of a swarm of non-holonomic *agents* [90]. In this approach they combine the APF method with a sliding mode controller that has the advantages of being robust to uncertainties and disturbances in the system dynamics. They successfully show that their unicycle robots can achieve swarming through the interaction of a pairwise repulsive and attractive potential and that the simulated results can respect the non-holonomic constraints.

The application of the APF method to the control of swarms of robots has been studied extensively over the past decade. One of the first approaches was the *social potential field* approach proposed by Reif and Wang [74]. In this distributed-control framework they consider a global controller that defines pair-wise potential functions acting on each robot. Under the assumption that the robot can sense and communicate with all other robots in the swarm a resulting force will act on each robot generating an emergent global behaviour. They based the potential fields on inverse power laws similar to those that are found in molecular dynamics. Their numerical results showed that using point mass robots they are able to form evenly distributed cluster patterns.

A related approach is Spears et al. *artificial physics* method that suggests using laws specifically inspired from natural physics to design distributed robot systems [91]. They note that as the sensors and actuators associated with real small robots are usually simple it is essential that the controls laws are also simple and should therefore be based on local communication. Their results are inspired from the physics-like behaviour that occurs in solids, liquids and gas and show that they can achieve hexagonal and square patterns, obstacle avoidance and coverage tasks.

One of the advantages of the APF approach is that the stability of the system can be investigated mathematically, therefore providing a means to prove the existence or not of certain behaviours. As the APF aims for the system to converge to a minimum energy state, one approach is to use Lyapunov stability methods. Leonard and Fiorelli use this approach to prove the closed loop stability of their swarm based on the system kinetic and artificial potential energy [92]. Their model consists of an attractive force and a local repulsive force that ensures col-

lision avoidance. Lyapunov theory is then used to show that the inclusion of a dissipative velocity term will ensure that the system will relax asymptotically into the equilibrium state. D'Orsogna consider a statistical mechanics approach with the use of *H-stability* of their pairwise potential swarm to indicate whether the swarm will be in a stable or catastrophic state. They also extend their discrete model to the continuum limit, allowing for the study of systems consisting of a very large number of vehicles [93].

The advantages associated with APF have resulted in them being applied to several engineering applications. For example, in the control of multiple spacecraft the APF has been proposed as a control strategy [16]. Future space missions may consist of the assembly of large structures [94], the use of swarms of satellites to explore the magnetosphere [95] or asteroid-belt [96] and for the development of very large virtual telescopes [11]. The ability of autonomous self-assembly is particularly desirable as these missions are often designed for cases when human presence is not available, or when operated at large distances from the Earth and is thus impractical due to communication delays. Izzo has implemented the APF method for a swarm of homogeneous spacecraft in his *equilibrium shaping approach* [16]. His results showed that coherent spatial patterns can be formed and that the method scales well due to the lack of explicit global coordination, resulting in a small amount of data exchange between the spacecraft. Related to this is McQuade's work into the autonomous configuration of satellite functions using generic potential fields [97] and Badawy's use of superquadric artificial potential functions for autonomous on-orbit assembly of a large space structure [98].

In recent years swarms of UAVs have been applied to distributed sensing operations and are particularly suitable for missions that may be repetitive or dangerous [99]. Frew et al. implemented the APF through their Lyapunov based vector field approach [7]. They showed that this approach provides globally stable convergence to a limit cycle behaviour for a single UAV platform and validated the simulation result with the development of a real UAV. In addition, Han et al. implemented the APF and a robust sliding mode controller, showing in simulation that their proposed method can track a desired trajectory [100].

1.3.2 Other approaches

There exists a wide variety of other approaches for the control of more than one robot. The *Symbrion* and *Replicator* projects, discussed previously, aim to produce a robot swarm than can aggregate together to form a multi-robot organism. To achieve this they consider the use of both bio-inspired and evolutionary network approaches, allowing the system the opportunity to combine the advantages of both methods so that it can learn and adapt to a dynamic environment [53].

Related to this is the field of distributed artificial intelligence (DAI) which is concerned with the development of systems that have some form of cognitive ability [16]. As opposed to purely reactive behaviour based approaches, DAI combines reactive and deliberative *agents* into a hybrid controller, where a deliberative *agent* possesses an internal view of the environment and has the ability to adapt and learn. The disadvantages of these approaches are that they are more computationally expensive in comparison with simpler architectures, such as APF.

In spacecraft formation flying, Scharf et al. [101] and Lawton [102] discuss several formation control architectures. The multiple-input-multiple-output (MIMO) methodology considers the relative states of the formations as a single plant [103]. The advantage of this approach is that optimality can be guaranteed, however, the controller can become unstable with the failure of one spacecraft. The virtual structure architecture is a centralised control method where all spacecraft in the formation are part of a virtual rigid structure where changes in the position of each spacecraft are communicated with a formation controller and the appropriate alterations are made to the structure [104]. The approach has the advantage of maintaining a formation well during manoeuvres [105]. However, it does not perform well if the formation shape is time-varying and is also susceptible to failure as it is centralised control [106].

Another approach is to use the centralised leader-follower (L/F) architecture, as discussed earlier, where one spacecraft obtains information on a desired trajectory and follower spacecraft tracks the leader [107, 108]. The Landsat-7 and Earth Observing-1 (EO-1) satellites are examples of a real hierarchical L/F mission and is generally considered the first mission to demonstrate formation flying [55]. The two satellites in this formation do not communicate with each other directly.

Instead a central controller determines Landsat-7's position and sends this information to EO-1 determining the future orbits of both spacecraft [109]. Again the limitation of this system is that it is also dependent upon the central controller and is therefore susceptible to failure. In addition, as the number of spacecraft increase, the workload required to maintain a formation discretely will increase significantly. Cyclic controller architectures are similar to the L/F, however each spacecraft is connected in a non-hierarchical way [110].

For swarms of UAVs control architectures include Reynolds flocking model [35] as discussed earlier. Another approach is to use graph theory to represent the local interactions and spatial distribution of a swarm of UAVs in either an undirected or directed graph [111, 112]. The graph consists of vertices or *agents* that are connected together by edges. In the undirected case pairs of *agents* communicate with each other to maintain separation distance whereas in the directed case only one of the pair tries to maintain their position relative to each other.

1.3.3 Problem Areas

This section discusses related approaches to the two swarming problem themes that are investigated in this thesis: pattern formation and reconfigurability.

Pattern formation

Pattern formation is an important area of swarming systems as real engineered systems are often required to form particular patterns that can be used in a practical way [113]. Reviews of pattern formation in swarm robotics can be found by Bahceci et al. [114] and Bayindir et al. [2].

Through the use of a pairwise attractive and repulsive potential field, D'Orsogna proposed a self-propelling swarming system that is capable of forming different patterns, such as a rotating ring or cluster [78]. In the model it is assumed that all *agents* have information on the position of all other *agents* in the swarm. However, this becomes unrealistic as the number of *agents* increase. Leonard et al. overcomes this issue by considering the use of a pairwise interaction potential field that acts in a small region surrounding the robots so that if two robots are far enough apart they do not affect each other. Their simulated results showed

the successful generation of patterns such as an equilateral triangle and hexagonal lattice [92].

A practical implementation of this is the *Swarm-bots* project where the mobile robots can connect and disconnect from each other, as discussed in **Section 1.3** [48]. This approach consists of homogeneous small robots governed by local attraction and repulsion. Using local sensing the robots are attracted towards other robots with a red light and will avoid robots with blue lights. The results consist of 16 robots that successfully self-assemble, forming patterns.

Reconfigurability

In swarming systems the ability to autonomously change pattern is advantageous as it allows increased flexibility. In nature, recent work has suggested that swarms of animals can switch patterns in a very simple way with a limited amount of information exchange. Nabet et al. have demonstrated this in their coupled dynamic animal swarm model, that consists of two groups of informed and uninformed individuals, with the results showing that the system can bifurcate into two groups in a stable manner [115].

Varghese and McKee have noted that much of the work carried out to date in swarm robotics has not been concerned with the transformation of swarm patterns [116]. They highlight the need for a mathematical tool to describe the transition between different patterns and to achieve this in a particle based simulation. Although their results showed a reconfiguration of a circle pattern to a line, avoiding an obstacle, it has the disadvantage of requiring path planning for each individual robot and so is not an autonomous formation.

1.4 Thesis Objectives

The objectives of the work presented are to:

- Develop new methodologies for verifiable swarming systems, replacing traditional heuristic methods with a more rigorous analytical approach.
- Investigate two areas of generic swarming systems; pattern formation and reconfigurability.
- Demonstrate the implementation of these methodologies in engineering systems.

To achieve these objectives this thesis considers the development of new methodologies for swarming systems based on bifurcating APFs. The difficulties encountered in the development of real autonomous swarm robot systems result in the view that control laws should be designed based on a simple, verifiable methodology. The APF method is therefore ideally suited to this requirement. In addition, there are an array of tools that exist in dynamical systems theory which can be utilised to develop new ways in which to approach swarming problems.

To demonstrate the proposed method two engineering applications are investigated; spacecraft formation flying and swarms of unmanned aerial vehicles. Using these applications it is shown that the proposed new algorithms can be used successfully in both first order velocity field and second order force controllers.

The key contribution to knowledge that this thesis presents is that;

> *Through the new approach of bifurcating APFs, a verifiable swarming system will self-organise, capable of creating reconfigurable, autonomous patterns.*

Specifically, it is shown that self-organised swarm behaviour can be manipulated through a simple parameter change to the system such that the swarm can transition between static and dynamic patterns. In addition, Lyapunov stability methods are used to provide a means of analytically proving that desired behaviours will occur.

1.5 Thesis Layout

An introduction to swarming systems was discussed in **Chapter 1** indicating the need for new methodologies for the development of verifiable swarming systems. By meeting this requirement, many new and exciting engineering systems can be realised in safety or mission critical applications, such as spacecraft formation flying and swarms of unmanned aerial vehicles. The concept of *swarm intelligence* was identified as a method that can be used to develop such systems. Although there are numerous approaches to the control of multiple robots, the artificial potential field method was identified as the control architecture of choice for this thesis.

In **Chapter 2** a review of dynamical systems theory is provided explaining the methods used throughout this thesis. Particular attention is paid to classical bifurcation theory which provides the key contribution in this thesis. In addition, stability techniques are discussed allowing for analytical proof for swarm pattern formation.

The key contributions of this thesis are explained in **Chapters 3** and **4**. Firstly, **Chapter 3** discusses the control model developed based on the new approach of bifurcating artificial potential fields. The model consists of a steering and repulsive potential field, with both velocity and force controllers considered. The steering potential is used to command the formation to a desired equilibrium position, with the repulsive potential field ensuring collision avoidance and an equally spaced final formation. The stability of the system is also discussed, showing that the swarm model can be verifiable. **Chapter 4** shows the results of pattern formation and reconfigurability in the swarm model developed.

In **Chapter 5** the model is extended to consider real world effects that are essential for implementation in a real system, such as actuator saturation and communication limitations. The advantages of the model are also demonstrated, highlighting the fact that the system is scalable, robust and flexible.

Chapters 6 and **7** apply the new control methodologies to the two engineered systems considered in this thesis. **Chapter 6** considers SFF applications, implemented through a second order force swarm controller. Firstly, the model is

applied to the two-body problem utilising Hill's equations of motion to create a formation of spacecraft that can orbit the Earth and form various patterns. Secondly, the model is applied to the three-body problem, placing the formation at the Sun-Earth Lagrange L_2 position.

In **Chapter 7** swarms of unmanned aerial vehicles are considered through the use of a first order velocity field control system. The desired velocity field acting on each UAV can be transformed into a set of commands that control the aerodynamic surfaces of each UAV. A 6 degree of freedom (DOF) linearised guidance model is developed to verify that the proposed algorithm can successfully control a formation of UAVs. A review and discussion of future work presented in this thesis is given in **Chapter 8**.

1.6 Simulation Methodology

In all the simulated results shown in this thesis, the dynamics of each *agent* are expressed as either a first order velocity field or second order force controller and transformed into a set of coupled first order ordinary differential equations (ODEs). The solution to the set of ODEs is obtained using Matlab's (version 7.5) standard ODE solver, **ode45**, that employs a variable step size Runge-Kutta integration method[2]. In addition, each *agent* is given random initial positions and velocities using Matlab's **randn** function, unless stated otherwise.

[2]www.mathworks.com, accessed 7/05/2010

1.7 Papers Authored

1. Bennet D.J. and McInnes C.R. *Pattern Transition in Spacecraft Formation Flying via the Artificial Potential Field Method and Bifurcation theory.* In 3rd International Symposium on Formation Flying, Missions and Technologies, Noordwijk, The Netherlands, April 23-25, 2008.

2. Bennet D.J. and McInnes C.R. *Distributed control of Multi-robot Systems using Bifurcating Potential Fields.* In Towards Autonomous Robotic Systems, TAROS 08, Edinburgh, UK, 1st-3rd Sept 2008.

3. Bennet D.J. and McInnes C.R. *Spacecraft Formation Flying using Bifurcating Potential Fields.* In 59th International Astronautical Congress, IAC-08-C1.6.4, Glasgow, UK, 29th Sept - 3rd Oct. 2008.

4. Suzuki, M., Uchiyama, K., Bennet, D.J. and McInnes, C.R. *Three Dimensional Formation Flying using Bifurcating Potential Fields*, AIAA-2009-5884, AIAA Guidance, Navigation and Control Conference, Chicago, August 9-13th, 2009.

5. Bennet D.J and McInnes C.R. *Verifiable Control of a Swarm of Unmanned Aerial Vehicles*, Proceedings of the Institution of Mechanical Engineers, Part G, Journal of Aerospace, 223 (7): 939-953, 2009.

6. Bennet D.J and McInnes C.R. *Distributed Control in Multi-Robot Systems using Bifurcating Potential Fields*, Journal of Robotics and Autonomous Systems, 58 (3): 256-264, 2010.

Chapter 2

Dynamical Systems Theory

The purpose of this chapter is to review the concepts from dynamical systems theory that are used throughout this thesis. In **Section 2.2**, both first order velocity field and second order force controllers, expressed as continuous ordinary differential equations (ODEs), are introduced with **Section 2.3** considering APFs with respect to Lyapunov stability theory. The concept of bifurcation theory is then discussed in **Section 2.4** that provides a mathematical tool allowing reconfigurability in the swarm model considered in this thesis.

2.1 Introduction

Dynamical systems theory provides a means of mathematically describing the long term behaviour of a system and can be expressed as either a discrete or continuous time system. In a dissipative dynamical system the phase space contracts to a subset of that space known as an attractor. By expressing the APF as a set of continuous ordinary differential equations a swarm system can be attracted to a particular subset, allowing for the emergence of different swarm patterns.

Dynamical systems can be either linear or non-linear. A linear dynamical system is limited to fixed point attractors where all phase space trajectories converge to a single point. In the real world, as very few systems can be modelled by linear differential equations, non-linear equations are often used. Complexity theory has shown that although a dynamical system is normally deterministic, the use of non-linear equations gives rise to a wide array of new behaviours that linearity cannot. For example, non-linear dynamical systems can lead to periodic

behaviours such as limits cycles.

As very few ODEs have an exact solution, numerical methods must be used to solve the system of equations. Although the system has to be solved in this way there exists several qualitative methods to study differential equations that can be used to determine certain characteristics of the system. For example, using the phase plane approach, properties such as equilibrium, stability and periodicity can be investigated. These methods will be demonstrated in the following sections.

2.2 Ordinary Differential Equations

As stated both force and velocity controllers for a swarm of *agents* are considered. To solve a system of ordinary differential equations it is useful to write them as a set of first order ODEs. A first order system of autonomous ordinary differential equations has the form;

$$\frac{dx_1}{dt} = F_1(x_1, \ldots, x_n) \qquad \ldots \qquad \frac{dx_n}{dt} = F_n(x_1, \ldots, x_n) \tag{2.1}$$

where, x_i $(i = 1 - n)$ are the state variables of the system.

Given a set of initial conditions, within the time span $a < t < b$ (where a and b are real), the system of equations can be solved numerically. Therefore, knowing the initial state of the system, the future state can be determined. It is assumed that the *existence-uniqueness* theorem holds so that there exists one solution to the system of first order differential equations for a set of initial conditions. The phase-paths of the system therefore, do not cross guaranteeing the existence of a unique solution. This is a significant advantage for safety or mission-critical systems compared to non-deterministic stochastic path planners [117].

2.2.1 Second Order Controller

Consider a point mass model in which the motion of an *agent* is governed by Newton's 2^{nd} law, as defined in Eq. 2.2, where the actuator control force is a function of the position coordinate, x, only;

$$\ddot{x} = f(x) \tag{2.2}$$

From the conservation of energy, the potential energy, U, of the system can then be expressed as;

$$U(x) = -\int f(x)dx + C \tag{2.3}$$

for some constant, C.

Equation 2.2 can be reduced to its first order equivalent by replacing $\dot{x}$ with a new variable y;

$$\dot{x} = y \tag{2.4}$$

$$\dot{y} = -\frac{dU}{dx} \tag{2.5}$$

From Eq. 2.5 it can be seen that the negative gradient of the APF represents the control force or acceleration acting on each *agent*. Therefore, by including some form of dissipation in Eq. 2.5, the system can be attracted to the minimum energy state.

2.2.2 First Order Controller

The second approach is to consider that each *agent* will be defined by a velocity field, as described by Eq. 2.6 and 2.7;

$$\dot{x} = X(x, y) \tag{2.6}$$

$$\dot{y} = Y(x, y) \tag{2.7}$$

with *agent* velocity defined by the pair $(\dot{x}, \dot{y})$.

The resulting velocity field can then be used to attract each *agent* to a particular equilibrium condition. In addition, the velocity field can be transformed into a set of commands that can control forward speed, u, and heading angle, ψ, as

shown in Eq. 2.8 and 2.9;

$$u = (\dot{x}^2 + \dot{y}^2)^{0.5} \tag{2.8}$$

$$\psi = tan^{-1}\left(\frac{\dot{y}}{\dot{x}}\right) \tag{2.9}$$

It should be noted that for such a 2D system the *Poincaré-Bendixon* theorem states that the phase paths can either return to an original point, giving a closed path, reach an equilibrium point or approach a limit cycle. For the single *agent* case therefore, phase paths cannot cross and therefore, no chaotic solutions can exist. Again, this is a significant advantage for safety or mission critical systems.

2.3 Artificial Potential Fields

As explained in **Section 1.3.1**, the APF method consists of regions of low and high potential corresponding to goal states and obstacles respectively. For real, safety critical applications the APF should be designed such that the control method can guarantee a smooth convergence to the final equilibrium state. To achieve this Lyapunov's stability theory can be used to ensure that the attractive APF will converge to the desired state. Linearisation techniques are also employed to determine the local stability properties of the system.

2.3.1 Lyapunov Stability

Lyapunov stability theory was developed by Aleksandr M. Lyapunov in his doctoral thesis entitled *The general problem of the stability of motion* at Moscow University in 1892 [118] and is extremely useful in the development of non-linear control systems [119, 120]. Lyapunov suggested the following two methods when considering the stability of a non-linear system;

- **Lyapunov's Second (or Direct) Method** allows the determination of the stability of the system without requiring a solution. As this method has the advantage of not requiring the solution of a non-linear differential equation, it can be used to analytically prove the stability of the system.
- **Lyapunov's Indirect Method** investigates the local stability of the system through the use of linearisation techniques. Assuming a solution to

the system can be found, linearisation can be applied to find the system response if perturbed whilst in its equilibrium position.

Using these two Lyapunov criteria the stability of the dynamical system can be investigated. The system is termed *Lyapunov stable* if all solutions starting near an equilibrium point, x_o, remain there and *Lyapunov asymptotically stable* if all solutions to the system converge to the equilibrium point. A *Lyapunov unstable system* is the opposite to both of these where the solution of the system moves away from the equilibrium point. Figure 2.1 shows these three conditions.

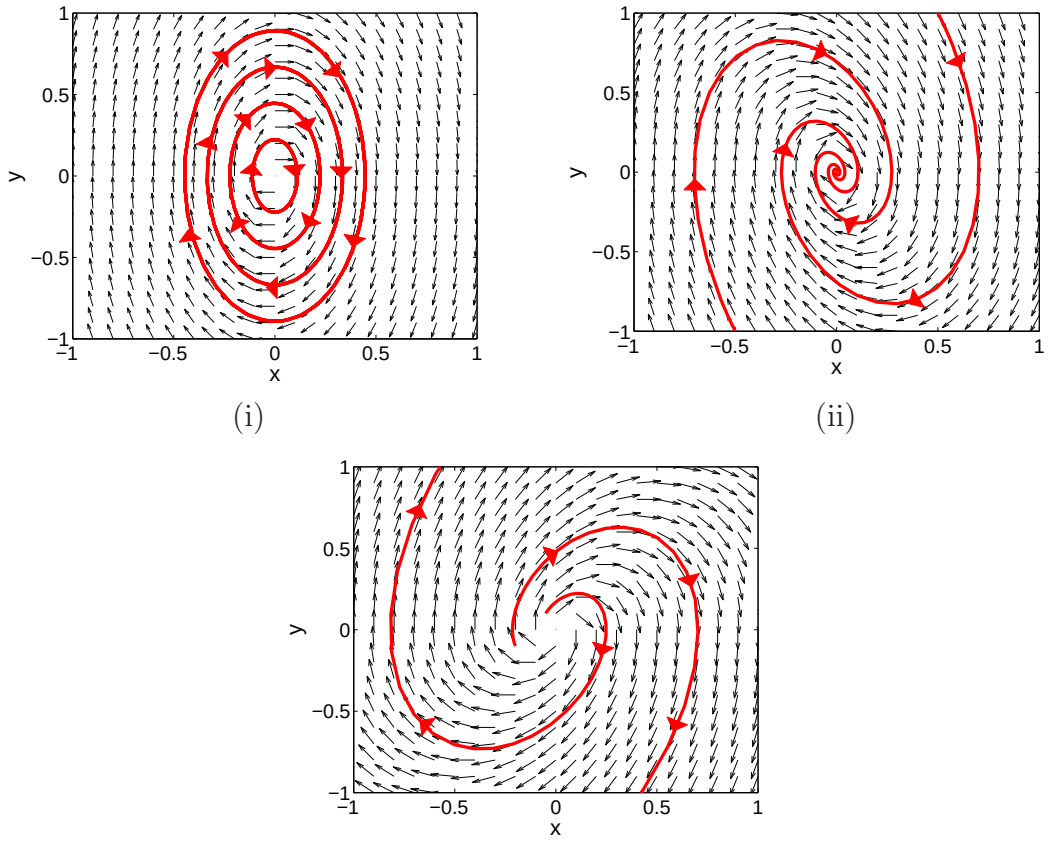

Figure 2.1: Lyapunov stability (i) stable (ii) asymptotically stable (iii) unstable

Lyapunov's Second Method

Lyapunov's Second Method consists of finding a scalar Lyapunov function, L, that can be used to determine the stability of a system without explicitly solving the differential equation. The aim of the APF method is to attract the system to

a desired equilibrium state so that if Lyapunov's Second Method can be satisfied, global convergence of the system to the final state can be guaranteed. To ensure this the system should be defined such that the conditions given in Table 2.1 hold true.

Table 2.1: Lyapunov's Second Theorem stability conditions

$x \neq x_o$	$x = x_o$
$L(x) > 0$	$L(x_o) = 0$
$\dot{L}(x) < 0$	$\dot{L}(x_o) = 0$

where, x_o represents the equilibrium state of the system.

From Table 2.1, if L is defined such that it is a positive definite function and its time derivative, $\dot{L}$, is negative definite then the system is asymptotically Lyapunov stable. Using this theorem it can be shown analytically that swarm patterns will be achieved and is discussed in **Chapter 3**. It should be noted that the existence of local minima can lead to $\dot{L} = 0$ for $x \neq x_o$.

Lyapunov's Indirect Method

Considering the first order equivalent of the dynamical system described by Eq. 2.2 and assuming x_o is an equilibrium point of the system, linearisation techniques can be used to investigate the local stability of the system if perturbed from the equilibrium state. Defining $\delta x = x - x_o$ and Taylor series expanding about fixed point to linear order, the eigenvalues of the system can be found using;

$$\delta \dot{x} = J \delta x \tag{2.10}$$

where the Jacobian matrix, J, evaluated at the fixed point is;

$$J = \left. \frac{\partial f(x)}{\partial x} \right|_{x_o} \tag{2.11}$$

The eigenvalues from Eq. 2.11 therefore describe the linear behaviour of the system with properties summarised in Table 2.2. As can be seen if the eigenvalues of the system are in the open left half of the complex plane then the system can be considered as linearly asymptotically stable.

Table 2.2: Eigenvalue Classification

Type	Eigenvalues	Classification
Real, distinct and opposite signs	+ve and -ve real	Saddle
Real, distinct and same signs	-ve	Stable node
	+ve	Unstable node
Complex conjugates	Complex, -ve real	Stable spiral
	Complex, +ve real	Unstable spiral
	Purely imaginary, no real	Centre

In addition, the *Hartman-Grobman theorem* states that if at least one eigenvalue has a real part then the equilibrium position can be considered as hyperbolic. This allows for a qualitative idea of the behaviour of the non-linear system in the neighbourhood of the equilibrium. If at least one eigenvalue has positive real part this implies non-linear instability. However, if all eigenvalues have negative real part this implies non-linear stability.

2.3.2 Attractive Potential Field

Before considering the swarm model that is discussed in **Chapter 3**, it is useful to illustrate, with a simple point mass *agent*, how the APF method can be used in a verifiable way to attract it to a goal position. Firstly, consider a simple 2D attractive parabolic potential, $U_{att,p}$ with position, $\mathbf{x}$, and goal position, $\mathbf{x}_g$;

$$U_{att,p} = \frac{\alpha_p}{2}|\mathbf{x} - \mathbf{x}_g|^2 \tag{2.12}$$

where α_p controls the amplitude of the parabolic potential.

Expressing this potential in a two-dimensional second order force model results in;

$$\dot{\mathbf{x}} = \mathbf{v} \tag{2.13}$$

$$\dot{\mathbf{v}} = -\nabla U_{att,p} - \sigma\mathbf{v} \tag{2.14}$$

where,

$$\nabla = [\partial/\partial x \;\; \partial/\partial y]^T \tag{2.15}$$

and σ controls the amplitude of the velocity dissipation.

The Lyapunov function, L, is choosen as the total energy of the system so that for a unit mass system;

$$L = \frac{1}{2}\mathbf{v}^2 + U_{att,p} \tag{2.16}$$

The rate of change of the Lyapunov function can be expressed as;

$$\frac{dL}{dt} = \left(\frac{\partial L}{\partial \mathbf{x}}\right)\dot{\mathbf{x}} + \left(\frac{\partial L}{\partial \mathbf{v}}\right)\dot{\mathbf{v}} \tag{2.17}$$

Then, substituting Eq. 2.13 and 2.14 into Eq. 2.17, it can be seen that for $\sigma > 0$;

$$\frac{dL}{dt} = -\sigma\mathbf{v}^2 < 0 \tag{2.18}$$

As L is positive definite and $\dot{L}$ is negative definite then the system is asymptotically Lyapunov stable, with the goal an attractor since, $\dot{L} = 0$ only at $\mathbf{x} = \mathbf{x}_g$.

To investigate the local stability Lyapunov's Indirect method is used. Assuming that the equilibrium states are $\mathbf{x}_0$ and $\mathbf{v}_0$ the Jacobian matrix for the system is;

$$J = \left.\begin{pmatrix} \partial\dot{\mathbf{x}}/\partial\mathbf{x} & \partial\dot{\mathbf{x}}/\partial\mathbf{v} \\ \partial\dot{\mathbf{v}}/\partial\mathbf{x} & \partial\dot{\mathbf{v}}/\partial\mathbf{v} \end{pmatrix}\right|_{\mathbf{x}_o,\mathbf{v}_o} \tag{2.19}$$

The Jacobian, J, is then a 2×2 matrix given by;

$$J = \begin{pmatrix} 0 & 1 \\ -\alpha_p & -\sigma \end{pmatrix} \tag{2.20}$$

The eigenvalues, λ, for the system are found from $det(J - \lambda\mathbf{I}) = 0$ giving $\lambda = -\frac{1}{2}(\sigma \pm \sqrt{(\sigma^2 - 4\alpha_p)}$. Choosing $\sigma > 0$ and $\alpha_p > 0$, the eigenvalues are always either negative real or complex with negative real part as $-\sigma \pm \sqrt{(\sigma^2 - 4\alpha_p)} \not> 0$. The equilibrium position can therefore be considered as linearly stable, as expected.

Figures 2.2 and 2.3 show the results of a simple point mass *agent* that is desired to reach a goal position at the origin using the parabolic potential.

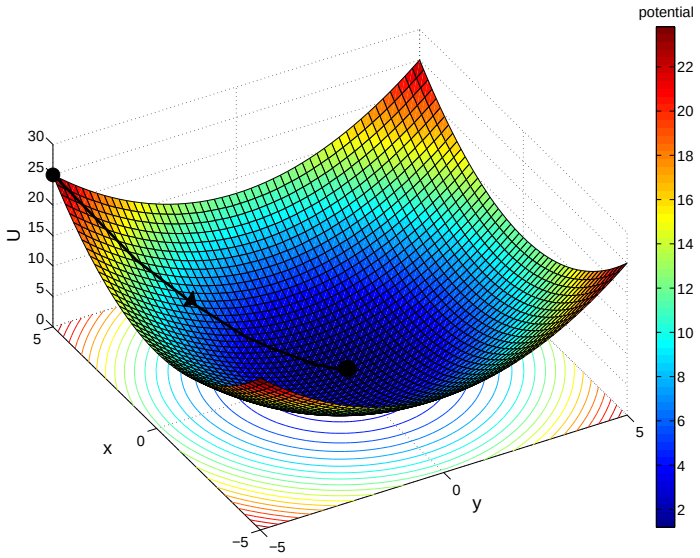

Figure 2.2: Attractive potential function ($\alpha = 1$ and $\sigma = 1$)

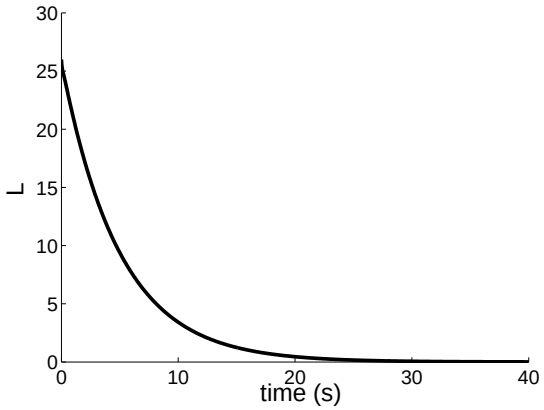

Figure 2.3: Lyapunov function

As can be seen from Fig. 2.2 that the *agent* successfully travels down the gradient of the attractive potential function and reaches the desired equilibrium position, with Fig. 2.3 indicating that the Lyapunov stability criteria has been satisfied.

2.3.3 Repulsive Potential Field

In real applications it is important that obstacle and *agent* collision avoidance is ensured. Referring to Eq. 2.12 a repulsive potential field, U_{rep}, is added, as shown in Eq. 2.21;

$$U_{total} = U_{att} + U_{rep} \tag{2.21}$$

This repulsive potential field can be used for avoidance of both single and multiple obstacles and also for collision avoidance in a swarming system.

Obstacle Collision Avoidance

There are many methods for modeling obstacles such as power-law, superquadric and harmonic functions [84, 121]. As discussed previously in **Section 1.3.1**, a disadvantage of the APF method is that local minima may form with the inclusion of the repulsive potential field. As the objective of this chapter is to demonstrate basic principles, the artificial repulsive potential will be expressed such that the local minima problem will be avoided. Consider a single obstacle represented by a gaussian potential function [121], $U_{rep,ob}$, as shown in Eq. 2.22;

$$U_{rep,ob} = C_{ob} \exp\left\{-\frac{1}{L_{ob}}|\mathbf{x} - \mathbf{x}_{obs}|^2\right\} \tag{2.22}$$

where, C_{ob} is a scaling parameter, L_{ob} is the width of the gaussian function and $\mathbf{x}_{obs}$ is the position of the obstacle.

Therefore, considering the simple 2D case of attracting an *agent* to a goal position whilst avoiding an obstacle, Eq. 2.13 and 2.14 are altered to the form shown in Eq. 2.23 and 2.24. As stated in **Section 1.3.1**, the spherical symmetry of the attractive and repulsive potential field results in no local minima forming (only an unstable saddle).

$$\dot{\mathbf{x}} = \mathbf{v} \tag{2.23}$$

$$\dot{\mathbf{v}} = -\nabla U_{att,p} - \nabla U_{rep,ob} - \sigma\mathbf{v} \tag{2.24}$$

It can be shown that for an obstacle with effective dimension, D_e, the scaling parameter, C_{ob}, to ensure collision avoidance should be chosen such that [121];

$$C_{ob} = \frac{\alpha_p(D_e + |\mathbf{x}_{obs}| - |\mathbf{x}_g|)}{6\exp^{-3D_e}} \tag{2.25}$$

Figures 2.4 and 2.5 show the case for an effective dimension, $D_e = 0.5$, $\alpha_p = 1$, $C_{ob} = 4.6$ and $L_{ob} = 0.17$. From Fig. 2.4 it can be seen that the *agent* successfully avoids the obstacle and reaches the desired goal position at the origin, with Fig. 2.5 indicating that Lyapunov's stability criteria has been satisfied.

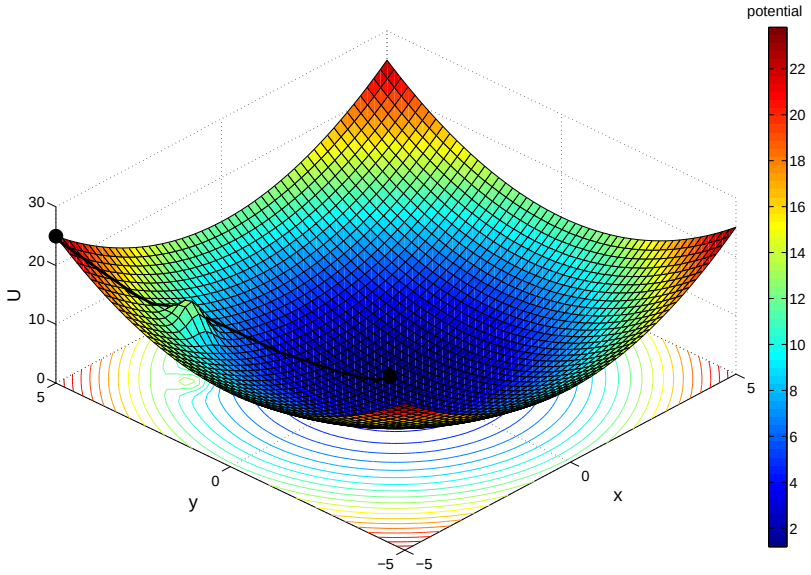

Figure 2.4: Obstacle collision avoidance

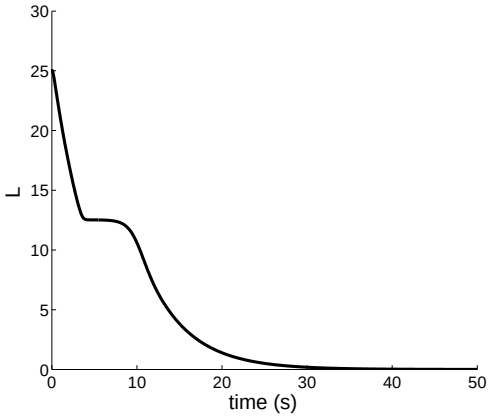

Figure 2.5: Lyapunov function for obstacle collision avoidance

Agent Collision Avoidance

In the multi-*agent* case it is important that collision avoidance between the *agents* is assured. To achieve this consider a repulsive potential field that is a simple pairwise exponential function, based on a generalised Morse potential [87], as shown in Eq. 2.26;

$$U_{ij}^{R} = \sum_{j,j\neq i} C_r \exp^{-\frac{|\mathbf{x}_{ij}|}{L_r}} \tag{2.26}$$

where C_r and L_r represent the amplitude and length-scale of repulsive potential respectively and $|\mathbf{x}_{ij}| = |\mathbf{x}_i - \mathbf{x}_j|$.

The total repulsive force on the i^{th} *agent* is dependent upon the position of all the other $(N-1)$ *agents* in the formation. The repulsive potential is therefore used to ensure collision avoidance as the *agents* are steered towards the goal state.

To illustrate this consider the case where there are two *agents* that must avoid each other to reach their respective goal positions, as shown in Fig. 2.6.

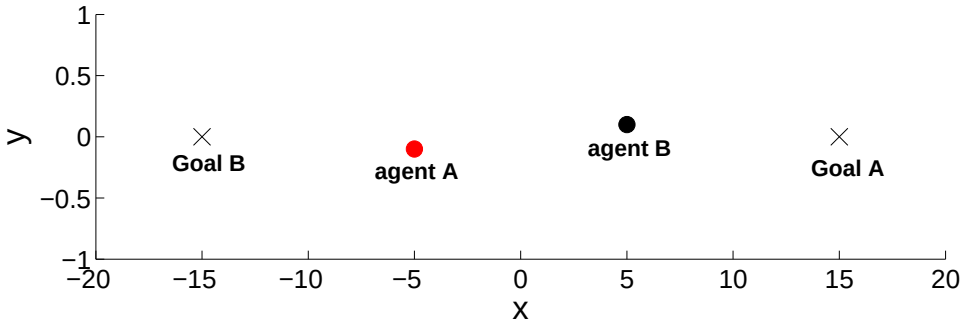

Figure 2.6: *Agent* collision avoidance initial conditions

From Fig. 2.7 it can be seen that the two *agents* successfully reach their desired goal position, avoiding any collisions.

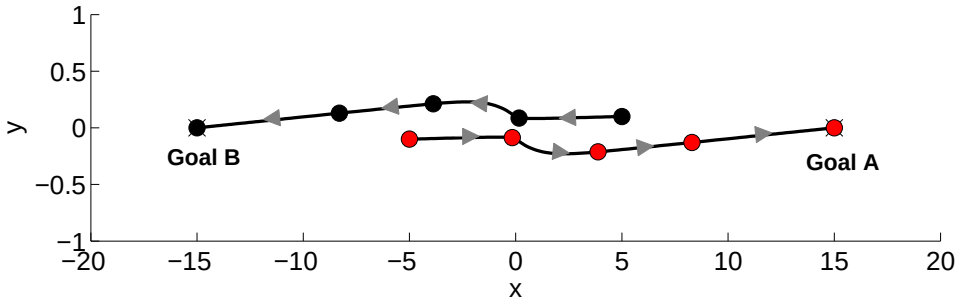

Figure 2.7: Collision avoidance simulation ($C_r = 10$, $L_r = 2$, $\sigma = 5$ and $\alpha_p = 1$)

2.4 Bifurcation Theory

Bifurcation theory studies the qualitative change in behaviour of a system due to a smooth system parameter change. In this section various bifurcations are discussed that lead to a simple and verifiable new approach for reconfigurability in swarming systems. Both static and dynamic bifurcations are considered allowing for transitions between fixed point and periodic attractors.

2.4.1 Pitchfork Bifurcation

Consider the two-dimensional system described by Eq. 2.27 and 2.28;

$$\dot{x} = y \tag{2.27}$$

$$\dot{y} = x(\mu - x^2) - y \tag{2.28}$$

where μ is the bifurcation parameter.

From the discussion given in **Section 2.2.1**, the pitchfork bifurcation APF can be defined as;

$$U_{pitchfork} = \frac{x^4}{4} - \frac{\mu x^2}{2} \tag{2.29}$$

Figure 2.8 shows the potential for $\mu = -10$ and $\mu = 5$. For $\mu = -10$ there is one stable equilibrium point at $x_o = 0$, as indicated by Fig. 2.8. For $\mu = 5$ the system bifurcates into 3 equilibrium points, with the original equilibrium becoming unstable at $x_o = 0$ and two new symmetrically stable equilibrium points emerging at $x_o = \pm\sqrt{\mu}$.

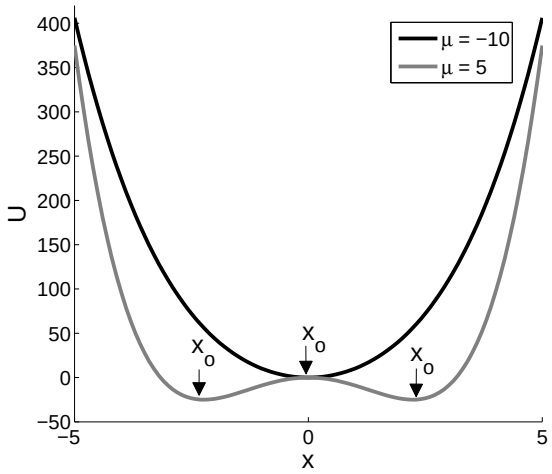

Figure 2.8: Pitchfork potential

Figures 2.9 and 2.10 show the pitchfork phase-space portrait and bifurcation diagram for the pitchfork bifurcation. As expected for $\mu < 0$ there is one stable spiral to the equilibrium position and for $\mu > 0$ there are two stable spirals to the two stable equilibrium positions.

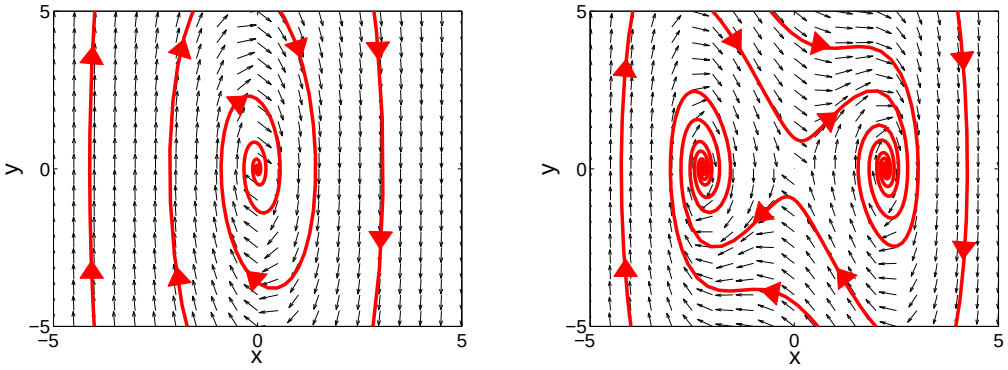

(i) (ii)

Figure 2.9: Phase-space portrait for pitchfork potential (i) $\mu = -10$ (ii) $\mu = 5$

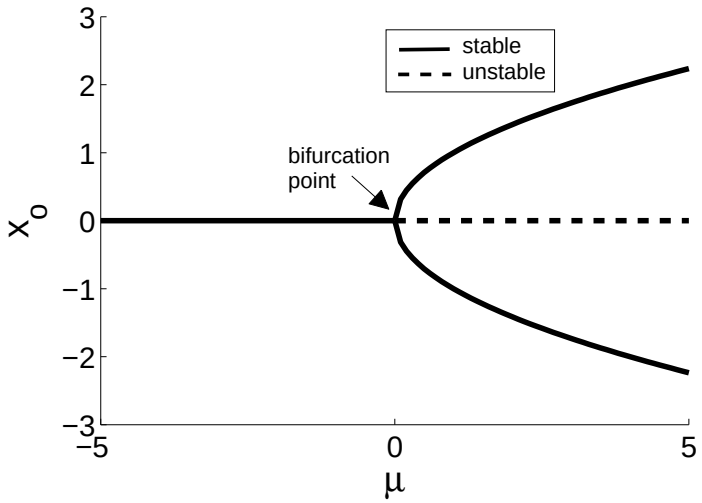

Figure 2.10: Bifurcation diagram for pitchfork potential

2.4.2 Transcritical Bifurcation

The transcritical artificial potential function is given by Eq. 2.30;

$$U_{transritcal} = \frac{x^3}{3} - \frac{\mu x^2}{2} \tag{2.30}$$

Depending upon the choice of the bifurcation parameter, μ, the potential field can have several different forms as shown in Fig. 2.11.

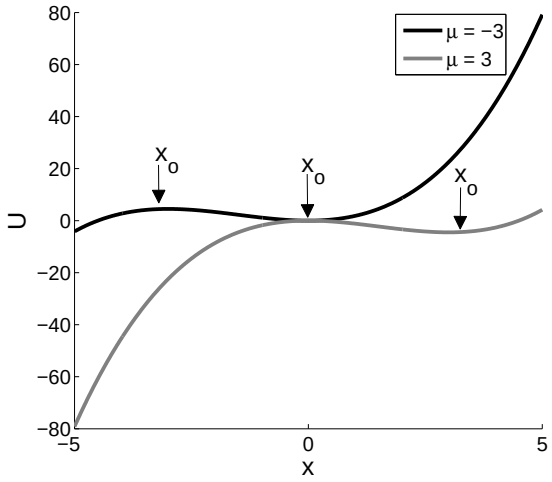

Figure 2.11: Transcritical potential

Expressing the potential field in the form of Eq. 2.27 and 2.28, Fig. 2.12 shows phase-space portrait for μ negative and positive.

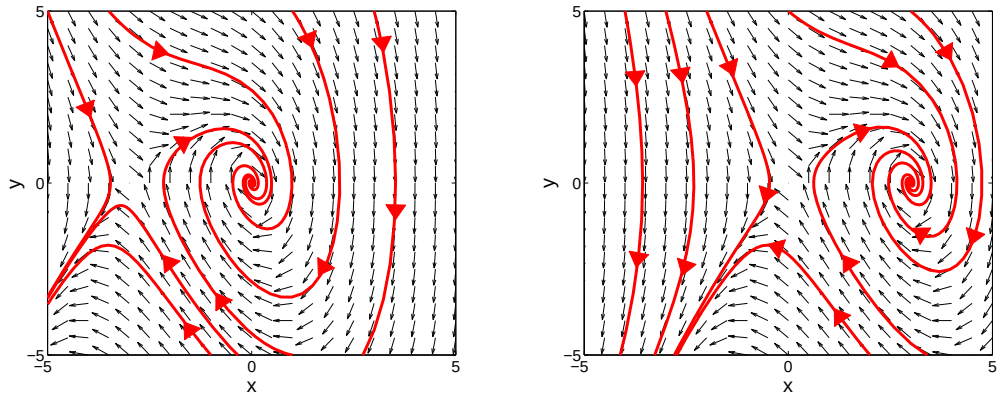

(i) (ii)

Figure 2.12: Phase-space portrait for transcritical potential (i) $\mu = -3$ (ii) $\mu = 3$

The transcritical bifurcation diagram is shown in Fig. 2.13 indicating that a bifurcation occurs in the system at $\mu = 0$. For $\mu < 0$ there are two equilibrium points with a stable node at the origin and an unstable node located at $x_o = \mu$. For $\mu > 0$, the equilibrium positions switch in behaviour so that the stable node at the origin becomes unstable and $x_o = \mu$ becomes stable.

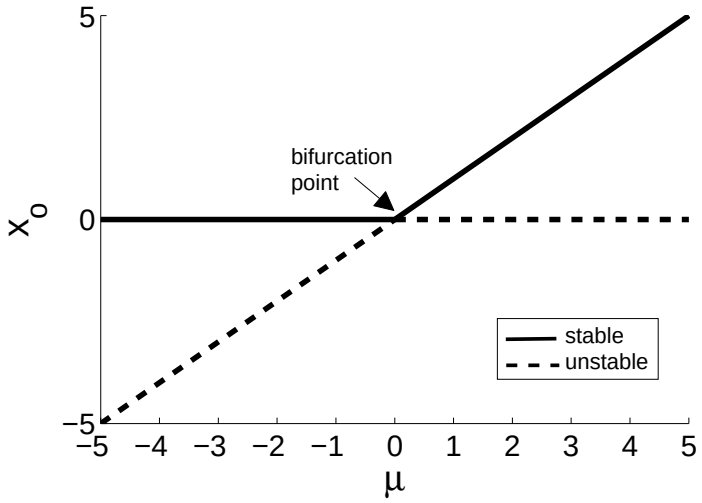

Figure 2.13: Bifurcation diagram for transcritical potential

2.4.3 Cusp Catastrophe

An extension to the 1-parameter bifurcation equations is to consider 2-parameter bifurcations such as the Cusp catastrophe, developed by Thom [122]. Equation

2.31 shows the 1D cusp catastrophe potential energy equation that is dependent upon two bifurcation parameters, μ_1 and μ_2;

$$U_{cusp} = \frac{\mu_1}{2}x^2 + \mu_2 x + \frac{1}{4}x^4 \tag{2.31}$$

Figure 2.14 shows the variation of equilibrium position with bifurcation parameter and the mapping of this potential function onto the $\mu_1 - \mu_2$ plane. It can be seen that the system behaviour changes as μ_1 and μ_2 are altered. The results are very similar to a phase diagram from thermodynamics [123]. As pressure and temperature are varied different phases can be achieved which is analogous to the different patterns which can be achieved as the bifurcation parameters are altered, as will be demonstrated later in **Chapter 4**.

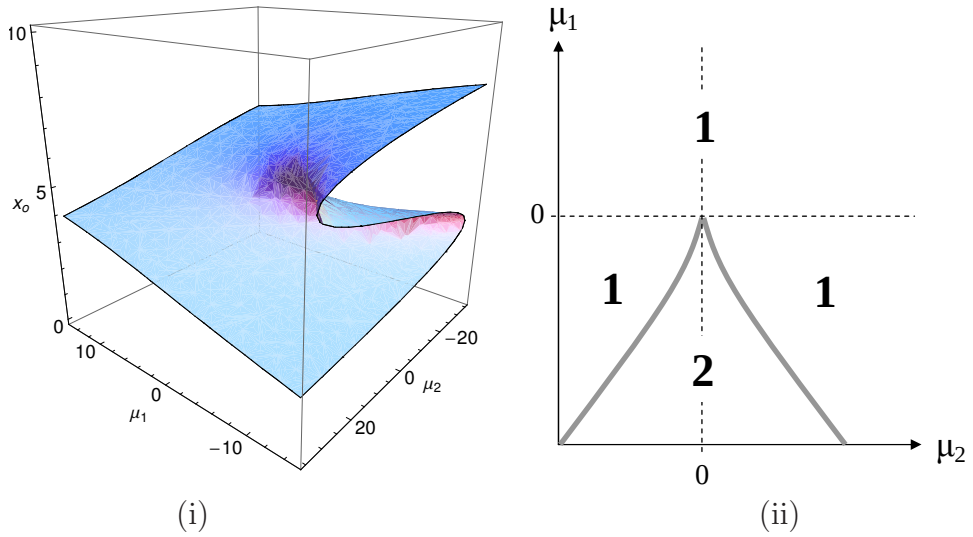

Figure 2.14: Cusp catastrophe (i) surface (ii) mapping on μ_1-μ_2 plane, indicating number of stable equilibrium positions

Setting $\mu_2 = 0$ results in the pitchfork bifurcation equation. However, for $\mu_1 > 0$ and all μ_2 there is only one equilibrium state. For $\mu_1 < 0$ and for all μ_2 there are either 1 or 2 equilibrium states as shown. Maintaining μ_1 at a constant negative value and alternating μ_2 from negative to positive, a loop is obtained switching between one and two equilibrium positions. The system can therefore be tipped into the upper or lower branches of the pitchfork equation as shown in Fig. 2.15. Thus, if the system is in the bi-stable state, control over the position of a single equilibrium state can be achieved through the variation of the parameters in the bifurcation equation.

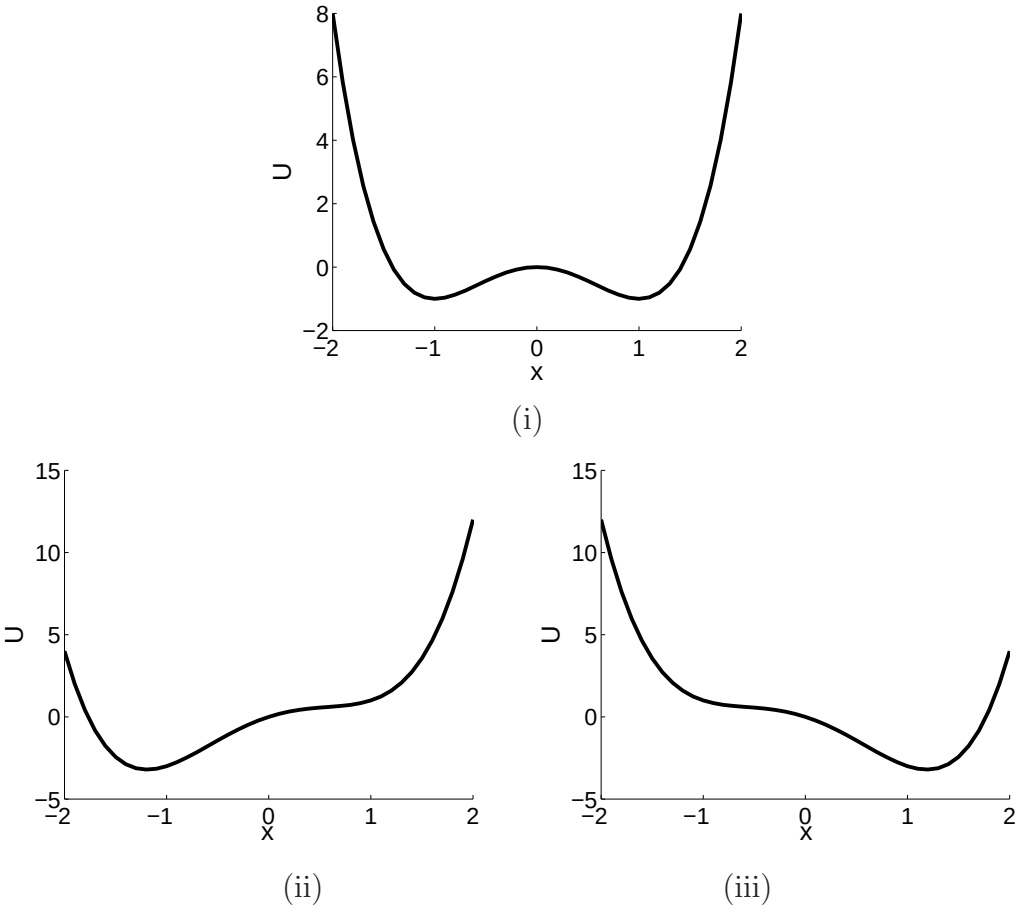

Figure 2.15: Cusp catastrophe: (i) $\mu_1 < 0$, $\mu_2 = 0$ (ii) $\mu_1 < 0$, $\mu_2 > 0$ (iii) $\mu_1 < 0$, $\mu_2 < 0$

2.4.4 Hopf Bifurcation

In bifurcation theory the Hopf bifurcation is a dynamic bifurcation about a fixed point of a dynamical system that generates a limit cycle as the bifurcation parameter μ changes. An example of a Hopf bifurcation is given in Eq. 2.32 and 2.33;

$$\dot{x}_i = \mu x_i + y_i - x_i(x_i^2 + y_i^2) \tag{2.32}$$

$$\dot{y}_i = -x_i + \mu y_i - y_i(x_i^2 + y_i^2) \tag{2.33}$$

Figures 2.16 (i) and (ii) show the phase-plane created when $\mu < 0$ and $\mu > 0$. As the bifurcation parameter becomes positive, a pair of complex eigenvalues cross the imaginary axis and the limit cycle behaviour is induced.

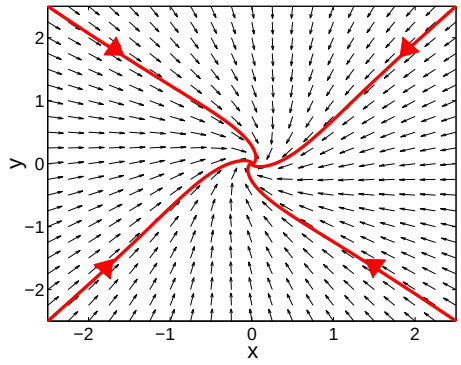

(i)

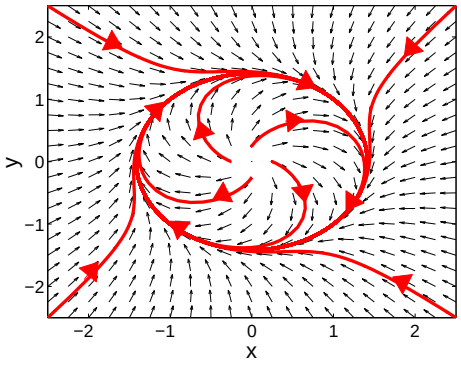

(ii)

Figure 2.16: Phase-space portrait for Hopf bifurcation (i) $\mu = -2$ (ii) $\mu = 2$

As μ increases the size of limit cycle also increases allowing for a varying size of limit cycle, as shown in Fig. 2.17.

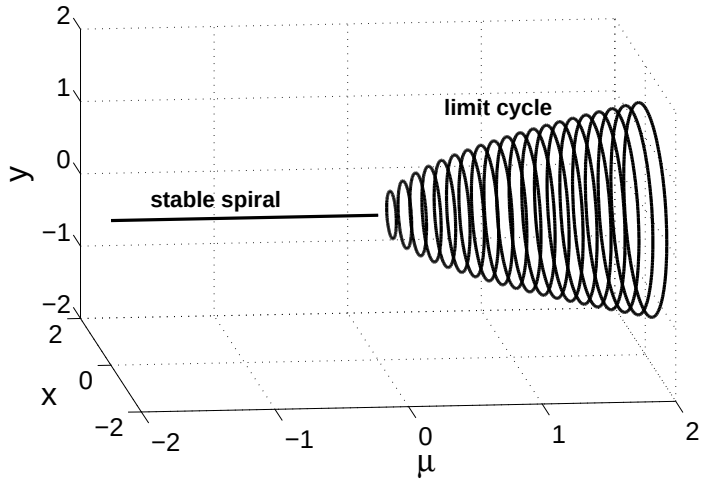

Figure 2.17: Hopf bifurcation diagram

2.5 Summary

This chapter has considered basic concepts and tools from dynamical systems theory that are used in this thesis. Two control approaches based on ordinary differential equations were introduced that will be used to control the swarm formation. These are the second order force controller, based on Newton's 2^{nd} law, and a first order velocity field controller.

The concept of APFs was introduced considering both attractive and repulsive potentials. Using Lyapunov stability criteria, the attractive APF can be designed such that global convergence to the goal state can be guaranteed. Using Lyapunov's Second method this can be shown analytically without requiring a solution to the system and is considered one of the advantages of the swarm model developed in this thesis. If a solution to the system can be obtained another useful approach when considering the stability of the system is to use linearisation methods. Using this approach once the *agent* in the system has reached a goal state, linearisation can be used to determine the local stability properties of the system.

In real applications it is important that collision avoidance is ensured. Using the APF method it was shown that the inclusion of a repulsive potential field can allow for both obstacle and *agent* collision avoidance.

Chapter 3

Swarm System Model

This chapter considers the swarming model proposed in this thesis based on the methods discussed in **Chapter 2**. Firstly, the basic swarm model is introduced with respect to both second order force and first order velocity field controllers. Before considering this model further, **Section 3.1.1** considers basic swarm properties of a system based on a pairwise potential function. In **Section 3.2** the stability of the proposed swarming model is investigated with respect to both force and velocity field examples. The pitchfork bifurcation potential is used to demonstrate the stability of a 2D static formation, whereas the Hopf bifurcation is used as an example when considering the stability of a 2D dynamic formation.

3.1 Swarm Model

Consider a swarm of homogeneous autonomous *agents* ($1 \leq i \leq N$) that are interacting through an artificial potential field. It will be initially assumed that all *agents* can communicate with each other and are fully actuated. Equations 3.1 and 3.2 show the second order equations of motion with mass, m, position, $\mathbf{x}_i$ and velocity, $\mathbf{v}_i$;

$$\frac{d\mathbf{x}_i}{dt} = \mathbf{v}_i \tag{3.1}$$

$$m\frac{d\mathbf{v}_i}{dt} = -\nabla_i U^S(\mathbf{x}_i) - \nabla_i U^R(\mathbf{x}_{ij}) - \sigma\mathbf{v}_i \tag{3.2}$$

From Eq. 3.2 it can be seen that the virtual force experienced by each *agent* is dependent upon the gradient of two different artificial potential functions and a dissipative term. The first term in Eq. 3.2 is defined as the steering potential,

U^S, which will control the formation, whereas the second term in Eq. 3.2 is the pairwise collision avoidance repulsive potential, U^R, as defined in Eq. 2.26. Equation 3.3 shows the first order velocity field equivalent to the second order force equations.

$$\frac{d\mathbf{x}_i}{dt} = -\nabla_i U^S(\mathbf{x}_i) - \nabla_i U^R(\mathbf{x}_{ij}) \tag{3.3}$$

3.1.1 Pair-wise Potential Field

Before considering this model further, it is useful to establish some basic properties of a system of *agents* interacting through an internal pair-wise potential function and a dissipative term, as shown in Eq. 3.4;

$$m\dot{\mathbf{v}}_i = -\nabla_i U(\mathbf{x}_{ij}) - \sigma \mathbf{v}_i \tag{3.4}$$

In molecular dynamics, molecules are often represented as particles that interact through pair-wise potential functions. An example of such a potential is the Morse pair-wise potential function that has been considered by D'Orsogna as a method for controlling a swarm of *agents* [87]. The Morse potential has the form shown in Eq. 3.5 and Fig. 3.1;

$$U(\mathbf{x}_{ij}) = \sum_{j,j\neq i} \left[C_r \exp^{-\frac{|\mathbf{x}_{ij}|}{L_r}} - C_a \exp^{-\frac{|\mathbf{x}_{ij}|}{L_a}} \right] \tag{3.5}$$

where, C_a,C_r and L_a,L_r represent the amplitude and range of the attractive and repulsive potential respectively, chosen to provide weak long-range attraction and strong short-range repulsion.

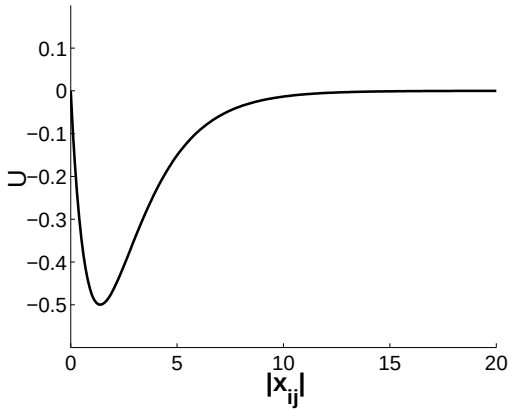

Figure 3.1: Morse pair-wise potential function ($C_a = 2, L_a = 2, C_r = 2, L_r = 1$)

Using this potential function it can be seen that the force experienced by each *agent* in the swarm is dependent upon the position of all other *agents*, as shown in the example given in Fig. 3.2.

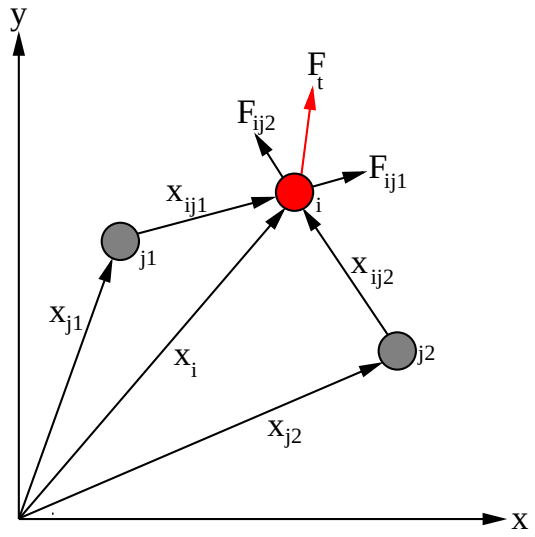

Figure 3.2: Pair-wise interaction forces ($\mathbf{F}_t = \mathbf{F}_{ij1} + \mathbf{F}_{ij2}$)

Taking the dot product of the velocity vector with Eq. 3.4 and summing over all the *agents* results in;

$$\sum_i m\mathbf{v}_i \cdot \dot{\mathbf{v}}_i = -\sum_i \sigma \mathbf{v}_i^2 - \sum_i \nabla_i U(\mathbf{x}_{ij}) \cdot \mathbf{v}_i \tag{3.6}$$

Thus, the rate of change of total effective energy, E, of the system is continually decreasing, as shown in Eq. 3.7, until the system reaches an equilibrium state,

which can be considered analogous with *Lyapunov's second theorem*;

$$\frac{dE}{dt} = -\sigma \sum_i \mathbf{v}_i^2 \leq 0 \tag{3.7}$$

where, $E = \frac{1}{2}\sum_i m\mathbf{v}_i^2 + \frac{1}{2}\sum_i U(\mathbf{x}_{ij})$.

Also, taking the cross product of the position vector with Eq. 3.4 and summing over all the *agents* results in;

$$\sum_i m\mathbf{x}_i \times \dot{\mathbf{v}}_i = -\sum_i \sigma \mathbf{x}_i \times \mathbf{v}_i - \sum_i \mathbf{x}_i \times \nabla_i U(\mathbf{x}_{ij}) \tag{3.8}$$

Defining the angular momentum, $\mathbf{H} = \sum_i \mathbf{x}_i \times \mathbf{v}_i$, it can be shown that angular momentum will be continually decreasing until the system reaches an equilibrium state, as shown in Eq. 3.9;

$$\frac{d\mathbf{H}}{dt} = -\left(\frac{\sigma}{m}\right)\mathbf{H} \tag{3.9}$$

since, $\sum_i \mathbf{x}_i \times \nabla_i U(\mathbf{x}_{ij}) = 0$ due to internal symmetry in the swarm ($\mathbf{x}_i \times \mathbf{x}_j = -\mathbf{x}_j \times \mathbf{x}_i$).

Finally, consider the velocity and acceleration vector of the center-of-mass, shown in Eq. 3.10 and 3.11;

$$\dot{\mathbf{R}}_c = \frac{\sum_i m\mathbf{v}_i}{\sum_i m} \tag{3.10}$$

$$\ddot{\mathbf{R}}_c = \frac{\sum_i m\dot{\mathbf{v}}_i}{\sum_i m} \tag{3.11}$$

By summing over all the *agents* in Eq. 3.4, it can be shown that the swarm can be controlled through its center-of-mass, as shown in Eq. 3.12;

$$m\ddot{\mathbf{R}}_c = -\sigma\dot{\mathbf{R}}_c \tag{3.12}$$

where, $\sum_i \nabla_i U(\mathbf{x}_{ij}) = 0$ due to internal symmetry in the swarm.

To illustrate this consider the case of a swarm of 50 *agents* interacting together through the Morse potential field. By altering Eq. 3.4 to form shown in Eq. 3.13 the centre-of-mass of the swarm can be attracted to the origin.

$$m\dot{\mathbf{v}}_i = -\nabla_i U(\mathbf{x}_{ij}) - \alpha \mathbf{x}_i - \sigma \mathbf{v}_i \tag{3.13}$$

where, α controls the amplitude of this new term.

Again, summing over all the *agents* in the system, Eq. 3.13 reduces to;

$$m\ddot{\mathbf{R}}_c + \sigma\dot{\mathbf{R}}_c + \alpha\mathbf{R}_c = 0 \tag{3.14}$$

Therefore, the eigenvalues for Eq. 3.14 are $\lambda_{1,2} = \frac{1}{2m}\left[-\sigma \pm \sqrt{(\sigma^2 - 4\alpha m)}\right]$. For $\sigma > 0$ and $\alpha > 0$ the eigenvalues are always either negative real or complex with negative real part so that the centre-of-mass of the swarm can be considered stable. Figure 3.3 demonstrates this with the formation relaxing into an equally spaced static cluster pattern.

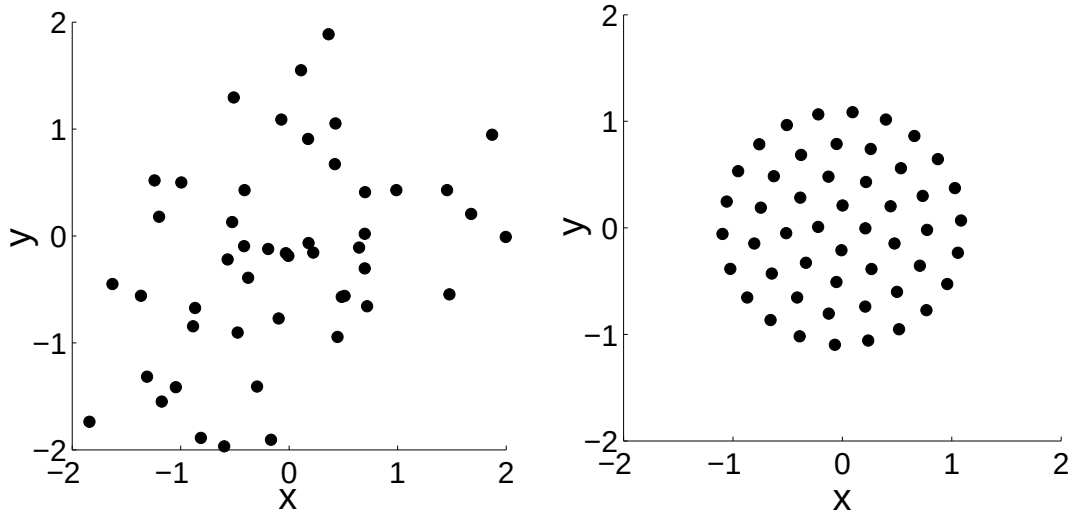

(i) (ii)

Figure 3.3: Pair-wise pattern formation (i) random initial conditions (ii) equally spaced cluster ($C_a = 2, L_a = 2, C_r = 2, L_r = 1, m = 1, \sigma = 1, \alpha = 2$)

Figures 3.4 and 3.5 show the motion of the centre-of-mass and total angular momentum respectively. The eigenvalues of the system are $\lambda_{1,2} = -0.5 \pm 1.32\text{i}$ so that the centre-of-mass follows a stable spiral to the origin, as confirmed in Fig. 3.4. It can also be seen in Fig. 3.5 that the rate of change of angular momentum is continually decreasing until equilibrium is reached, as stated in Eq. 3.9.

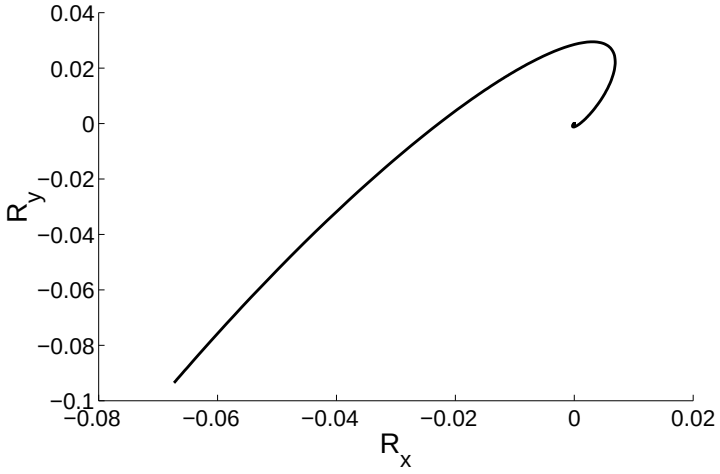

Figure 3.4: Motion of centre-of-mass to origin ($\mathbf{R}_c = \mathrm{R}_x\mathbf{i} + \mathrm{R}_y\mathbf{j}$)

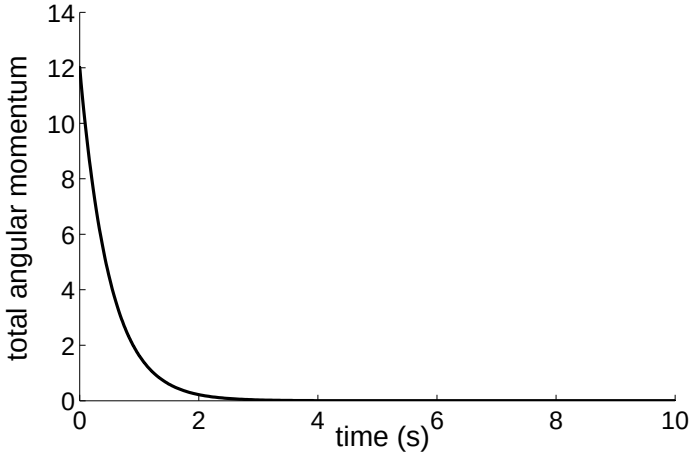

Figure 3.5: Total angular momentum

In addition to driving the swarm centre-of-mass to a desired static position, the swarm centre-of-mass can track a desired trajectory. For example, for the swarm centre-of-mass to follow a circular or elliptical path, Eq. 3.15 can be used;

$$m \begin{bmatrix} \dot{v}_x \\ \dot{v}_y \end{bmatrix} = \begin{bmatrix} -\sigma v_x - \nabla_i U(x_{ij}) - \alpha(x_i - \xi \sin(t)) \\ -\sigma v_y - \nabla_i U(y_{ij}) - \alpha(y_i - \zeta \cos(t)) \end{bmatrix} \tag{3.15}$$

where, t is time and ξ,ζ control the amplitude of the desired trajectory.

Two cases are considered for varying values of ξ and ζ, as summarised in Table 3.1. The results are shown in Fig. 3.6 and 3.7 for the formation at different times with random initial conditions. From these results it can be seen that the swarm center-of-mass can track the path defined by the parameters ξ and ζ whilst maintaining a swarm cluster formation. If ξ and ζ are equal a circular path will be obtained for the formation, as shown in Fig. 3.6. However, if ξ, ζ are different an elliptical path can be generated, as shown in Fig. 3.7.

Table 3.1: Swarm centre-of-mass parameters

path	C_a	L_a	C_r	L_r	m	σ	α	ξ	ζ
circular	2	2	2	1	1	2	10	2	2
ellipse	2	2	2	1	1	2	10	4	2

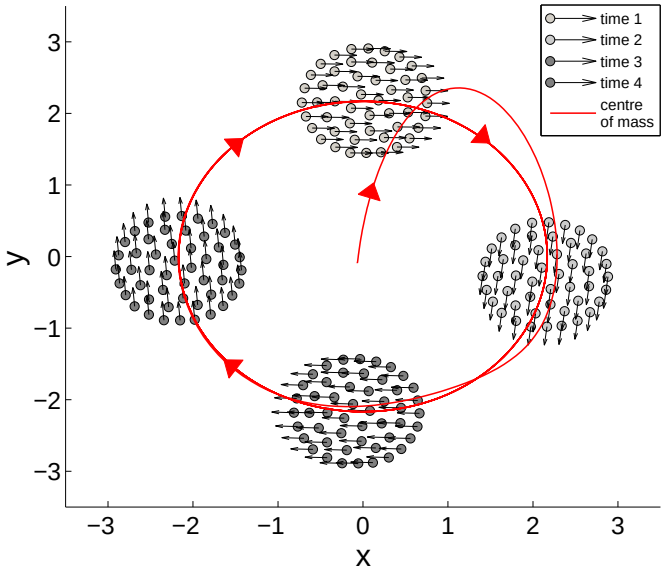

Figure 3.6: Swarm centre-of-mass circular path

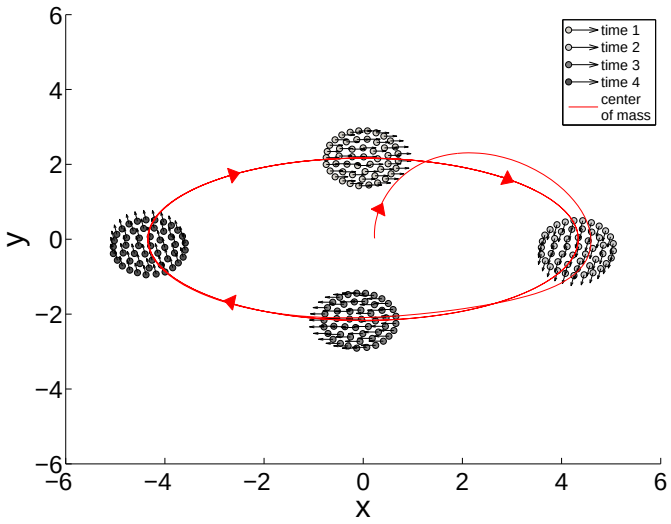

Figure 3.7: Swarm centre-of-mass elliptical path

Therefore, some useful properties of a swarm system based on a pair-wise potential field have been discussed that will become useful in the following sections.

3.2 Stability

The stability of the swarm model introduced in **Section 3.1** is discussed in the following sections. It will be shown that there exists a scale separation between the steering and repulsive terms such that each *agent* in the swarm moves under the influence of a long-range steering potential, but with short range collision avoidance. This assumption allows collisions to be treated separately in the stability analysis. For the second order force system the pitchfork bifurcation is used as an example when considering the stability of a system that is desired to create 2D static patterns. For the first order velocity field case the Hopf bifurcation is used as an example when considering the stability of a 2D dynamic pattern formation.

3.2.1 Artificial Potential Function Scale Separation

From the swarm model discussed in **Section 3.1**, it is known that the dynamics of each *agent* is dependent upon the gradient of two different artificial potential functions. The steering and repulsive potential are a function of position only with length scale R and L_r respectively, as shown in Eq. 3.16 and 3.17;

$$U^S = f(X, R) \tag{3.16}$$

$$U^R = C_r \exp^{-X/L_r} \tag{3.17}$$

where for illustration a simple one-dimensional (1D) system with position coordinate X is considered.

Defining an outer region dependent upon the steering potential only and an inner region dependent upon the repulsive potential only it can be shown that these two regions are separated so that each *agent* moves under the influence of the long-range steering potential but with short range collision avoidance (for $L_r/R << 1$). This effectively creates a boundary layer between them, as illustrated in Fig. 3.8, where the position of the boundary layer is dependent upon the parameters chosen in the steering and repulsive potentials. This can then be used to determine the non-linear stability properties of the system considering the steering potential only.

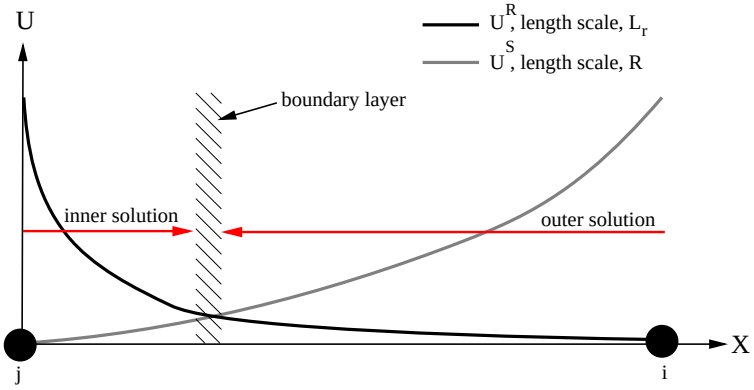

Figure 3.8: Artificial potential function scale separation

For 1D motion of an *agent* of mass m and damping constant σ;

$$m\frac{dV}{dt} = -\frac{dU^R}{dX} - \frac{dU^S}{dX} - \sigma V \tag{3.18}$$

so that,

$$mV\frac{dV}{dX} = \frac{C_r}{L_r}\exp^{-X/L_r} - \frac{dU^S}{dX} - \sigma V \tag{3.19}$$

Scaling X such that $S = X/R$, then;

$$\frac{1}{R}mV\frac{dV}{dS} = \frac{C_r}{L_r}\exp^{-\frac{R}{L_r}S} - \frac{1}{R}\frac{dU^S}{dS} - \sigma V \tag{3.20}$$

Now define $\varepsilon = \dfrac{L_r}{R} << 1$ so that;

$$mV\frac{dV}{dS} = \frac{C_r}{\varepsilon}\exp^{-\frac{S}{\varepsilon}} - \frac{dU^S}{dS} - \sigma RV \tag{3.21}$$

Let $\varepsilon \to 0$ in order to consider 'far-field' dynamics which form a singularly perturbed system [124];

$$\lim_{\varepsilon\to 0}\frac{1}{\varepsilon}\exp^{(-S/\varepsilon)} = 0 \tag{3.22}$$

Therefore, at large separation distances the repulsive potential vanishes allowing the consideration of the steering potential only when investigating the stability of the system, under the assumption that $\epsilon << 1$.

Conversely defining a stretched variable $\overline{S} = \dfrac{S}{\varepsilon}$ it is found that the 'near-field' dynamics are defined by;

$$mV\frac{dV}{d\overline{S}} = C_r\exp^{-\overline{S}} - \varepsilon R\left(\frac{1}{L_r}\frac{dU^S}{d\overline{S}} + \sigma V\right) \tag{3.23}$$

and letting $\varepsilon \to 0$;

$$mV\frac{dV}{d\overline{S}} = C_r\exp^{-\overline{S}} \tag{3.24}$$

Thus, at small separations the steering potential vanishes. Therefore, it has be shown that a scale separation exists in the model between the repulsive and steering terms allowing for the treatment of collisions as separate in the subsequent stability analysis.

3.2.2 Relationship Between Second and First Order Systems

Considering the second order system as defined in Eq. 3.18, the velocity field can be defined as follows;

$$\frac{m}{\sigma}\frac{dV}{dt} = -\frac{1}{\sigma}\frac{dU^S}{dX} - \frac{1}{\sigma}\frac{dU^R}{dX} - V \tag{3.25}$$

Assuming that $m/\sigma << 1$ so that the system is overdamped,

$$-\frac{1}{\sigma}\frac{dU^S}{dX} - \frac{1}{\sigma}\frac{dU^R}{dX} - V = 0 \tag{3.26}$$

thus,

$$\frac{dX}{dt} = -\frac{1}{\sigma}\frac{dU^S}{dX} - \frac{1}{\sigma}\frac{dU^R}{dX} \tag{3.27}$$

Assuming that the second-order system is over-damped, the dynamics of the swarm of *agents* can be reduced to the form shown in Eq. 3.28.

$$\frac{d\mathbf{x}_i}{dt} = -\nabla_i U^S(\mathbf{x}_i) - \nabla_i U^R(\mathbf{x}_{ij}) \tag{3.28}$$

The first order system is therefore also said to move under the influence of a long-range steering potential but with short-range collision avoidance.

3.2.3 Second Order Force Swarm System

Consider a steering potential based on the pitchfork bifurcation as shown in the first two terms of Eq. 3.29. The aim of this potential is to drive each *agent* to a goal distance, r, from the origin in the $x-y$ plane thus forming a symmetric ring. The last term in Eq. 3.29 is to ensure that the formation is created in the $x-y$ plane, where α controls the amplitude of this quadratic potential. Using this as an example potential field the stability of the second order system can be investigated.

$$U^S(\mathbf{x}_i;\mu,\alpha) \;=\; -\frac{1}{2}\mu\left(\rho_i - r\right)^2 + \frac{1}{4}\left(\rho_i - r\right)^4 + \frac{1}{2}\alpha z_i^2 \tag{3.29}$$

where cylindrical polar coordinates (ρ_i, z_i) are used, neglecting the θ term as the potential field is rotationally symmetric.

As discussed in **Section 2.4.1**, depending on the sign of μ, the steering potential can have two distinct forms as the bifurcation parameter, μ, is altered from negative to positive. The equilibrium states of the potential occur whenever

$\partial U/\partial \rho_i = 0$ and $\partial U/\partial z_i = 0$. Therefore;

$$\frac{\partial U}{\partial \rho_i} = -\mu(\rho_i - r) + (\rho_i - r)^3 \tag{3.30}$$

$$\frac{\partial U}{\partial z_i} = \alpha z_i \tag{3.31}$$

If $\mu \leq 0$, equilibrium occurs when $\rho_i = r$. If $\mu > 0$ equilibrium occurs when $\rho_i = r$, $r \pm \sqrt{\mu}$. Therefore, a single ring will bifurcate to a double ring using μ as a control parameter.

For a function consisting of two variables the stability of the system is determined from the sign of the determinant of the Hessian matrix [125], D, given in Eq. 3.32;

$$D = \frac{\partial^2 U}{\partial \rho_i^2}\frac{\partial^2 U}{\partial z_i^2} - \left[\frac{\partial^2 U}{\partial \rho_i \partial z_i}\right]^2 \tag{3.32}$$

The conditions for stability are as follows;
(i) $D > 0$, $\partial^2 U/\partial \rho_i^2 > 0 \Longrightarrow$ equilibrium point is a stable minimum.
(ii) $D > 0$, $\partial^2 U/\partial \rho_i^2 < 0 \Longrightarrow$ equilibrium point is a unstable maximum.
(iii) $D < 0 \Longrightarrow$ equilibrium point is a saddle.

The second derivatives of the potential are shown in Eq. 3.33, 3.34 and 3.35;

$$\frac{\partial^2 U}{\partial \rho_i^2} = -\mu + 3(\rho_i - r)^2 \tag{3.33}$$

$$\frac{\partial^2 U}{\partial z_i^2} = \alpha \tag{3.34}$$

$$\frac{\partial^2 U}{\partial \rho_i \partial z_i} = 0 \tag{3.35}$$

From Eq. 3.34, choosing $\alpha > 0$, $\partial^2 U/\partial z_i^2 > 0$. From Eq. 3.33 it can be seen that $\partial^2 U/\partial \rho_i^2 \gtrless 0$ depending on the value of μ. Therefore, the properties of the equilibrium state, ρ_o, are shown in Table 3.2;

Table 3.2: Stability of equilibrium states of artificial potential function

μ	ρ_o	$\partial^2 U/\partial\rho_i^2$	Stability
< 0	r	> 0	stable minimum
> 0	r	< 0	unstable maximum
	$r + \sqrt{\mu}$	> 0	stable minimum
	$r - \sqrt{\mu}$	> 0	stable minimum

Linear stability: 1-parameter static bifurcation

Using Lyapunov's indirect method, as discussed in **Section 2.3.1**, an eigenvalue analysis can be performed on the linearised equations of motion assuming that at large separation distances the repulsive potential can be neglected through scale separation as explained in **Section 3.2.1**. Therefore, the second order equations of motion for the swarm model are re-cast as;

$$\begin{aligned} \begin{pmatrix} \dot{\mathbf{x}}_i \\ \dot{\mathbf{v}}_i \end{pmatrix} &= \begin{pmatrix} \mathbf{v}_i \\ -\sigma\mathbf{v}_i - \nabla_i U^S(\mathbf{x}_i) \end{pmatrix} \\ &= \begin{pmatrix} f(\mathbf{x}_i, \mathbf{v}_i) \\ g(\mathbf{x}_i, \mathbf{v}_i) \end{pmatrix} \end{aligned} \tag{3.36}$$

Let $\mathbf{x}_o$ and $\mathbf{v}_o$ denote fixed points with $\dot{\mathbf{x}}_i = \dot{\mathbf{v}}_i = 0$ so that;

$$f(\mathbf{x}_o, \mathbf{v}_o) = 0 \tag{3.37}$$

$$g(\mathbf{x}_o, \mathbf{v}_o) = 0 \tag{3.38}$$

Thus, $\mathbf{v}_o = 0$ and $\nabla U^S = 0$ at equilibrium. This occurs when $\rho_o = r$ if $\mu < 0$ and $\rho_o = r, r \pm \sqrt{\mu}$ if $\mu > 0$, with $z_o = 0$. Defining $\delta\mathbf{x}_i = \mathbf{x}_i - \mathbf{x}_o$ and $\delta\mathbf{v}_i = \mathbf{v}_i - \mathbf{v}_o$ and Taylor Series expanding about the fixed points to linear order, the eigenvalues of system can be found. The Jacobian, $\mathbf{J}$, is defined as;

$$\mathbf{J} = \left(\begin{array}{cc} \frac{\partial}{\partial \mathbf{x}_i}(f(\mathbf{x}_i, \mathbf{v}_i)) & \frac{\partial}{\partial \mathbf{v}_i}(f(\mathbf{x}_i, \mathbf{v}_i)) \\ \frac{\partial}{\partial \mathbf{x}_i}(g(\mathbf{x}_i, \mathbf{v}_i)) & \frac{\partial}{\partial \mathbf{v}_i}(g(\mathbf{x}_i, \mathbf{v}_i)) \end{array} \right) \Bigg|_{\mathbf{x}_o, \mathbf{v}_o} \tag{3.39}$$

This is then a 4×4 matrix given by;

$$\mathbf{J} = \left(\begin{array}{cccc} 0 & 0 & 1 & 0 \\ 0 & 0 & 0 & 1 \\ -\frac{\partial^2 U}{\partial \rho_i^2} & -\frac{\partial^2 U}{\partial \rho_i \partial z_i} & -\sigma & 0 \\ -\frac{\partial^2 U}{\partial \rho_i \partial z_i} & -\frac{\partial^2 U}{\partial z_i^2} & 0 & -\sigma \end{array} \right) \Bigg|_{\mathbf{x}_o, \mathbf{v}_o} \tag{3.40}$$

As shown previously, if $\mu < 0$ equilibria of the system occur when $\mathbf{x}_o = (r, 0)$ and $\mathbf{v}_o = 0$. Evaluating the Jacobian matrix given in Eq. 3.40 it is found that;

$$\mathbf{J} = \left(\begin{array}{cccc} 0 & 0 & 1 & 0 \\ 0 & 0 & 0 & 1 \\ \mu & 0 & -\sigma & 0 \\ 0 & -\alpha & 0 & -\sigma \end{array} \right) \tag{3.41}$$

The corresponding eigenvalue spectrum is therefore;

$$\lambda = \left\{ \begin{array}{l} 1/2(-\sigma \pm \sqrt{(\sigma^2 - 4\alpha)}) \\ 1/2(-\sigma \pm \sqrt{(\sigma^2 + 4\mu)}) \end{array} \right. \tag{3.42}$$

As $\alpha > 0$, $\sigma > 0$ and $\mu < 0$ the eigenvalues are always either negative real or complex with negative real part as $-\sigma \pm \sqrt{(\sigma^2 - 4\alpha)} \not> 0$ and $-\sigma \pm \sqrt{(\sigma^2 + 4\mu)} \not> 0$. The equilibrium position can therefore be considered as linearly stable.

If $\mu > 0$ equilibrium of the system occurs when $\mathbf{x}_{o1} = (r, 0)$, $\mathbf{x}_{o2} = (r + \sqrt{\mu}, 0)$ and $\mathbf{x}_{o3} = (r - \sqrt{\mu}, 0)$ with $\mathbf{v}_i = 0$. The Jacobian matrix evaluated at the three different equilibrium positions is given by Eq. 3.43, 3.44 and 3.45 respectively as;

$$\mathbf{J}_1 = \left(\begin{array}{cccc} 0 & 0 & 1 & 0 \\ 0 & 0 & 0 & 1 \\ \mu & 0 & -\sigma & 0 \\ 0 & -\alpha & 0 & -\sigma \end{array} \right) \tag{3.43}$$

$$\mathbf{J}_2 = \left(\begin{array}{cccc} 0 & 0 & 1 & 0 \\ 0 & 0 & 0 & 1 \\ -2\mu & 0 & -\sigma & 0 \\ 0 & -\alpha & 0 & -\sigma \end{array} \right) \tag{3.44}$$

$$\mathbf{J}_3 = \begin{pmatrix} 0 & 0 & 1 & 0 \\ 0 & 0 & 0 & 1 \\ -2\mu & 0 & -\sigma & 0 \\ 0 & -\alpha & 0 & -\sigma \end{pmatrix} \tag{3.45}$$

The eigenvalues for $\mathbf{J}_1$ are;

$$\lambda = \begin{cases} 1/2\left(-\sigma \pm \sqrt{(\sigma^2 - 4\alpha)}\right) \\ 1/2\left(-\sigma \pm \sqrt{(\sigma^2 + 4\mu)}\right) \end{cases} \tag{3.46}$$

Considering the second pair of eigenvalues in Eq. 3.46 it can be show that $-\sigma \pm \sqrt{(\sigma^2 + 4\mu)} > 0$, since $\sigma^2 + 4\mu > \sigma^2$ and therefore there is always at least one positive real eigenvalue. This equilibrium position is therefore always linearly unstable.

The eigenvalues for $\mathbf{J}_2$ and $\mathbf{J}_3$ are;

$$\lambda = \begin{cases} 1/2\left(-\sigma \pm \sqrt{(\sigma^2 - 4\alpha)}\right) \\ 1/2\left(-\sigma \pm \sqrt{(\sigma^2 - 8\mu)}\right) \end{cases} \tag{3.47}$$

Again as $\alpha > 0$, $\sigma > 0$ and $\mu > 0$, the eigenvalues are always either negative real or complex with negative real part as $-\sigma \pm \sqrt{(\sigma^2 - 4\alpha)} \not> 0$ and $-\sigma \pm \sqrt{(\sigma^2 - 8\mu)} \not> 0$. The equilibrium positions can therefore be considered as linearly stable.

Non-linear stability: 1-parameter static bifurcation

Using Lyapunov's second method the non-linear stability of the system can be investigated allowing an analytical proof that the swarm will relax into the minimum energy configuration. Again using the assumption of scale separation, the Lyapunov function, L, is defined as the total energy of the system, where $U^S(\mathbf{x}_i)$ is given in Eq. 3.29, so that, for unit mass;

$$L = \sum_i \left(\frac{1}{2}\mathbf{v}_i^2 + U^S(\mathbf{x}_i)\right) \tag{3.48}$$

where, $L > 0$ other than at the goal state when $L = 0$.

The rate of change of the Lyapunov function can be expressed as;

$$\frac{dL}{dt} = \left(\frac{\partial L}{\partial \mathbf{x}_i}\right)\dot{\mathbf{x}}_i + \left(\frac{\partial L}{\partial \mathbf{v}_i}\right)\dot{\mathbf{v}}_i \tag{3.49}$$

Then, substituting Eq. 3.36 into Eq. 3.49 it can be seen that;

$$\frac{dL}{dt} = -\sigma \sum_i \mathbf{v}_i^2 \leq 0 \tag{3.50}$$

As stated previously in **Section 2.3.1**, a problem arises in the use of superimposed artificial potential functions as $\dot{L} \leq 0$. This implies that $\dot{L}$ could equal zero in a position other than the goal minimum suggesting that the system may become trapped in a local minimum. However, under the assumption of the scale separation, as there is a smooth, well defined symmetric potential field and equilibrium only occurs at the goal states, the local minima problem can be avoided and the system will relax into the desired goal position.

For the more general case when scale separation cannot be assumed, a similar analysis to that shown in **Section 3.1.1** can be used. Therefore, taking the dot product of the velocity vector with Eq. 3.2 and summing over all *agent* states results in;

$$\sum_i m\mathbf{v}_i \cdot \dot{\mathbf{v}}_i = -\sum_i \sigma \mathbf{v}_i^2 - \sum_i \nabla_i U^S(\mathbf{x}_i) \cdot \mathbf{v}_i - \sum_i \nabla_i U^R(\mathbf{x}_{ij}) \cdot \mathbf{v}_i \tag{3.51}$$

Thus, the rate of change of the total effective energy is then;

$$\frac{dE}{dt} = -\sigma \sum_i \mathbf{v}_i^2 \leq 0 \tag{3.52}$$

where, $E = \frac{1}{2}\sum_i m\mathbf{v}_i^2 + \sum_i U^S(\mathbf{x}_i) + \frac{1}{2}\sum_i U^R(\mathbf{x}_{ij})$.

This is a similar result to that obtained above, however, it now takes into consideration the repulsive potential field. Again, the total effective energy of the system is continually decreasing. However, the system may relax into a minimum energy configuration other than that given by the minimum of the desired steering potential. For example, considering the case when $r = 0$, each *agent* in the swarm will be driven to the origin of the system. However, due to the interaction with the repulsive potential, the *agents* will be forced apart with the steering and repulsive potential balancing such that the system will relax into a locally

minimum energy cluster configuration. In this situation the scale separation argument does not hold true, however, it does provide a tool to enable analytical investigation of the stability of the problem.

3.2.4 First Order Velocity Field Swarm System

In this example consider the case of a first order velocity field that is based on the Hopf bifurcation, as discussed in **Section 2.4.4** and shown in Eq. 3.53;

$$\begin{pmatrix} \dot{x}_i \\ \dot{y}_i \\ \dot{z}_i \end{pmatrix} = \begin{pmatrix} \mu x_i + y_i - x_i(x_i^2 + y_i^2) - \dfrac{\partial U^R}{\partial x_i} \\ -x_i + \mu y_i - y_i(x_i^2 + y_i^2) - \dfrac{\partial U^R}{\partial y_i} \\ -\alpha z_i - \dfrac{\partial U^R}{\partial z_i} \end{pmatrix} \tag{3.53}$$

For $\mu > 0$ each *agent* in the swarm will be attracted to a limit cycle with radius, $r = \sqrt{\mu}$, with the addition of the repulsive potential field creating an equally spaced ring formation in the $x - y$ plane.

Linear stability: 1-parameter dynamic bifurcation

Similar to the analysis performed in **Section 3.2.3**, the velocity field described by Eq. 3.53 is recast to determine the linear stability of the system;

$$\begin{aligned} \begin{pmatrix} \dot{x}_i \\ \dot{y}_i \\ \dot{z}_i \end{pmatrix} &= \begin{pmatrix} \mu x_i + y_i - x_i(x_i^2 + y_i^2) \\ -x_i + \mu y_i - y_i(x_i^2 + y_i^2) \\ -\alpha z_i \end{pmatrix} \\ &= \begin{pmatrix} m(\mathbf{x}_i) \\ n(\mathbf{x}_i) \\ p(\mathbf{x}_i) \end{pmatrix} \end{aligned} \tag{3.54}$$

Similarly, letting $\mathbf{x}_o$ denote fixed points with $\dot{x}_i = \dot{y}_i = \dot{z}_i = 0$ then;

$$m(x_o, y_o, z_o) = 0 \tag{3.55}$$

$$n(x_o, y_o, z_o) = 0 \tag{3.56}$$

$$p(x_o, y_o, z_o) = 0 \tag{3.57}$$

The Jacobian, $\mathbf{J}$, is then a 3×3 matrix given by;

$$\mathbf{J} = \left(\begin{array}{ccc} \frac{\partial}{\partial x_i}(m(\mathbf{x}_i)) & \frac{\partial}{\partial y_i}(m(\mathbf{x}_i)) & \frac{\partial}{\partial z_i}(m(\mathbf{x}_i)) \\ \frac{\partial}{\partial x_i}(n(\mathbf{x}_i)) & \frac{\partial}{\partial y_i}(n(\mathbf{x}_i)) & \frac{\partial}{\partial z_i}(n(\mathbf{x}_i)) \\ \frac{\partial}{\partial x_i}(p(\mathbf{x}_i)) & \frac{\partial}{\partial y_i}(p(\mathbf{x}_i)) & \frac{\partial}{\partial z_i}(p(\mathbf{x}_i)) \end{array} \right) \Bigg|_{x_o, y_o, z_o} \tag{3.58}$$

Thus, it can be shown that;

$$\mathbf{J} = \left(\begin{array}{ccc} \mu & 1 & 0 \\ -1 & \mu & 0 \\ 0 & 0 & -\alpha \end{array} \right) \tag{3.59}$$

The corresponding eigenvalue spectrum is therefore;

$$\lambda_{1,2,3} = \ -\alpha, \mu \pm i \tag{3.60}$$

From the eigenvalue spectrum given in Eq. 3.60 it can be seen that for $\mu < 0$ and $\alpha > 0$ the equilibrium position is linearly stable, indicating a stable spiral to that position. Alternatively, if $\mu > 0$, the eigenvalues will now be either positive real or positive real with complex conjugate. Therefore, as the complex eigenvalues cross the imaginary axis at $\mu = 0$, the system is said to have bifurcated from a stable spiral into the oscillatory limit cycle motion.

Non-linear stability: 1-parameter dynamic bifurcation

Again Lyapunov's second theorem is used to determine the non-linear stability of the system. As the z-direction motion is decoupled from the x and y motion, as shown in Eq. 3.54, consider a Lyapunov function, L, defined as;

$$L = \frac{1}{2} \sum_i \left[x_i^2 + y_i^2 \right] \tag{3.61}$$

Therefore,

$$\frac{dL}{dt} = \sum_i \left[\frac{\partial L}{\partial x_i} \dot{x}_i + \frac{\partial L}{\partial y_i} \dot{y}_i \right] \tag{3.62}$$

$$\frac{dL}{dt} = \sum_i \left[\rho_i^2 (\mu - \rho_i^2) \right] \tag{3.63}$$

For $\mu < 0$ and $\alpha > 0$, $\dot{L} \leq 0$ so that ρ_i is always decreasing until $L = 0$ so each *agent* would be attracted to the equilibrium position located at the origin. Alternatively, if $\mu > 0$ and $\alpha > 0$, $\dot{L} > 0$ if $\rho_i^2 < \mu$ and $\dot{L} < 0$ if $\rho_i^2 > \mu$ so the system is attracted to a limit cycle of radius, $\rho_i = \sqrt{\mu}$, in the $x - y$ plane, with $z_i = 0$.

3.3 Summary

This chapter introduced the swarm model considered in this thesis showing that it consists of steering and repulsive potential that are used to command each *agent* and prevent collisions respectively. To demonstrate some useful swarming principles a swarm model based on a pair-wise potential was introduced in **Section 3.1**, showing how basic patterns can be formed and also how the centre-of-mass of the swarm can be controlled. **Section 3.2** considered the stability of the proposed swarming model. Firstly, it was shown that there exists a scale separation between the steering and repulsive potentials so that each *agent* moves under the influence of a long-range steering potential but with short range collision avoidance. The stability of both the second and first order models was investigated. As an example, the pitchfork bifurcation equation was used to demonstrate the linear and non-linear stability of the second order swarm model so that static 2D patterns will form under the assumption of scale separation. An energy analysis was also performed for the more general case when this assumption cannot be made, showing that the swarm system will relax into a locally minimum energy configuration. The linear and non-linear stability analysis was also repeated for a first order system with consideration to dynamic pattern formation through the Hopf bifurcation.

Chapter 4

Pattern Formation and Reconfigurability

This chapter considers the swarm model discussed in **Chapter 3**, demonstrating both swarm pattern formation and reconfigurability. Firstly, in **Section 4.1.1**, it is shown that a swarm of *agents* can be attracted to different states. In **Section 4.1.2** pattern formation using bifurcation theory is demonstrated, with **Section 4.1.3** showing examples of other potentials that can lead to different swarm patterns. Finally, **Section 4.2** considers reconfigurability in a swarm using the new approach of bifurcating potential fields. In all the examples given in this chapter, the point-mass swarm of *agents* are given random initial conditions with following constant parameters; $C_r = 1$, $L_r = 0.5$ and $\sigma = 2$, unless stated otherwise.

4.1 Pattern Formation

4.1.1 Swarm Attractors

Depending on the form of the steering potential, the swarm model can be attracted to different states. A simple quadratic potential is used in the following examples, based on a dissipative second order dynamical system.

$0D$ Attractor

Consider a steering potential defined as;

$$U^S = \frac{\alpha}{2}|\mathbf{x}_i|^2 \tag{4.1}$$

where, $\mathbf{x}_i = (x_i, y_i, z_i)^T$.

Using this steering potential each *agent* in the swarm will be attracted to the origin with the repulsive potential causing a cluster pattern to emerge, as shown in Fig. 4.1.

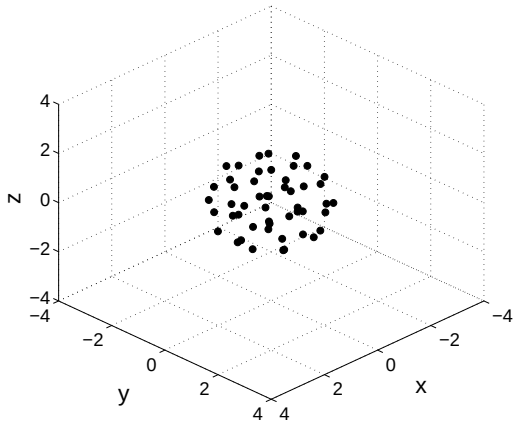

Figure 4.1: 0D Attractor - ball cluster ($n = 50, \alpha = 1$)

Therefore, although each *agent* in the swarm is attracted to a $0D$ point, a $3D$ ball pattern will emerge as the swarm interacts through the repulsive potential.

$1D$ Attractor

In order to attract the swarm to a 1D line pattern in the x-direction, the steering potential energy can be defined as;

$$U^S = \frac{\alpha}{2}(y_i^2 + z_i^2) \tag{4.2}$$

From the results shown in Fig. 4.2 it can be seen that a line pattern can be achieved in the x-direction with the repulsive potential causing the separation distance between the *agents* to increase in the x-direction.

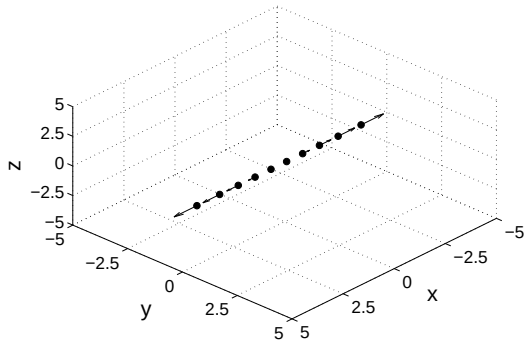

Figure 4.2: 1D Attractor - line ($n = 10, \alpha = 1$)

$2D$ Attractor

By forming a potential gradient in only one direction, the swarm can be attracted to a $2D$ plane using the following steering potential;

$$U^S = \frac{\alpha}{2} z_i^2 \tag{4.3}$$

From the results shown in Fig. 4.3 it can be seen that the swarm is attracted to the $x - y$ plane with the repulsive potential causing the swarm of *agents* to disperse, with the velocity of the swarm approaching zero as the repulsive term approaches zero.

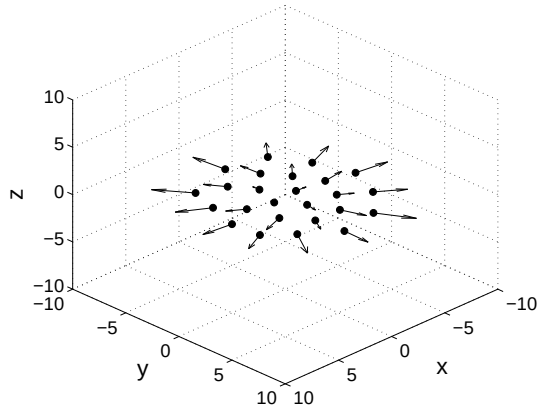

Figure 4.3: 2D Attractor - dispersion of swarm ($n = 25, \alpha = 1$)

No Attractor

In this case the swarm is not attracted to any state, allowing the swarm to interact through the repulsive potential field only, using the second order system shown in Eq. 4.4;

$$m\frac{d\mathbf{v}_i}{dt} = -\nabla_i U^R(\mathbf{x}_{ij}) - \sigma\mathbf{v}_i \tag{4.4}$$

From the results shown in Fig. 4.4 it can be seen that the swarm of *agents* interact together with the repulsive potential again forcing the *agents* to disperse, with the velocity of the swarm approaching zero as the repulsive potential approaches zero.

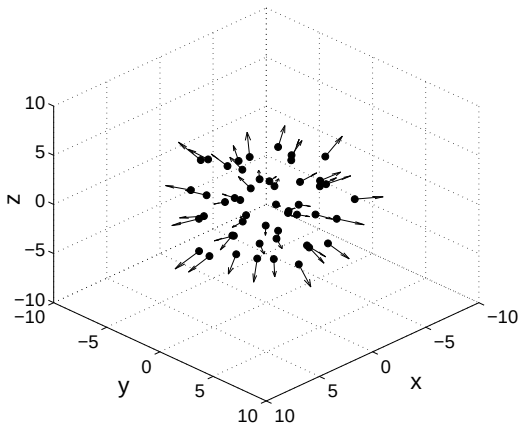

Figure 4.4: 3D dispersion of swarm ($n = 50$)

This section has demonstrated the way in which the steering potential can be used to attract the swarm to a particular state. It will now be shown how different swarm patterns can be achieved using bifurcation of the steering potential.

4.1.2 Bifurcation Patterns

Using the bifurcation equations discussed in **Section 2.4**, several different patterns can be formed. This section introduces these patterns, with **Section 4.2** demonstrating how bifurcation theory can be used to transition between these patterns through a simple parameter change.

Pitchfork Bifurcation

Using the pitchfork bifurcation potential various swarm patterns can be achieved depending upon the type of attractor used. Firstly, consider a $0D$ attractor based on the pitchfork steering potential, as shown in Eq. 4.5;

$$U^S = \frac{1}{4}(x_i^4 + y_i^4 + z_i^4) + \frac{1}{2}(\mu_x x_i^2 + \mu_y y_i^2 + \mu_z z_i^2) \tag{4.5}$$

Therefore, depending upon the sign of the bifurcation parameters, μ_x, μ_y and μ_z, the number of attractors will change, as summarised in Table 4.1.

Table 4.1: Pitchfork bifurcation parameters - $0D$ attractor

μ_x	< 0	> 0	< 0	< 0	< 0	> 0	> 0	> 0
μ_y	< 0	< 0	> 0	< 0	> 0	> 0	< 0	> 0
μ_z	< 0	< 0	< 0	> 0	> 0	< 0	> 0	> 0
attractors	1	2	2	2	4	4	4	8

For $\mu_x, \mu_y, \mu_z < 0$ there is only one equilibrium position so the swarm is attracted to a point at the origin, as discussed in **Section 4.1.1**. Figure 4.5 confirms this for a swarm of 50 *agents*, with a $3D$ cluster formation forming as expected.

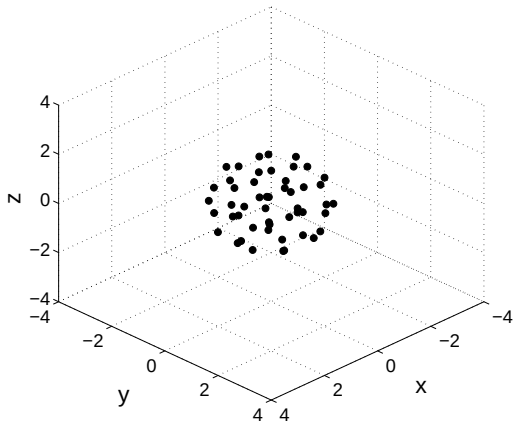

Figure 4.5: $3D$ cluster formation ($n = 50, \mu_x = -5, \mu_y = -5, \mu_z = -5$)

Figures 4.6, 4.7 and 4.8 show the results for the case when the bifurcation parameters are chosen such that there at 2, 4 and 8 attractor positions respectively. Depending upon each *agent* initial conditions, they are driven towards one of the attracting positions, resulting in the cluster formations shown. It should be noted that the split of *agents* is largely uncontrolled, however, future work will investigate the probability of an even split and its sensitivity to initial conditions.

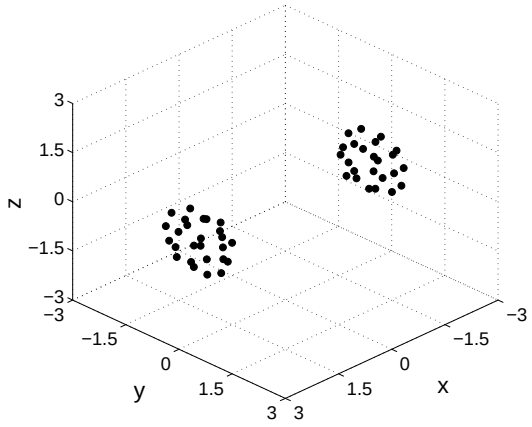

Figure 4.6: Two cluster formations ($n = 50, \mu_x = 5, \mu_y = -5, \mu_z = -5$)

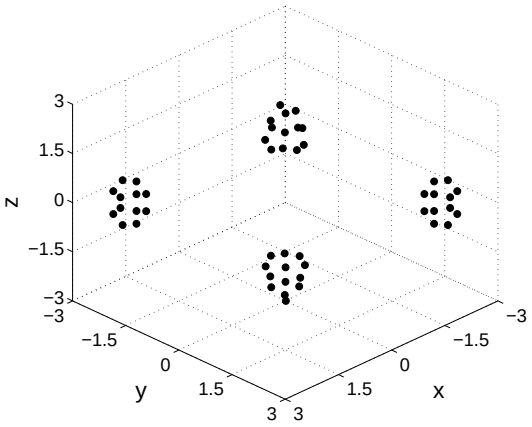

Figure 4.7: Four cluster formations ($n = 50, \mu_x = 5, \mu_y = 5, \mu_z = -5$)

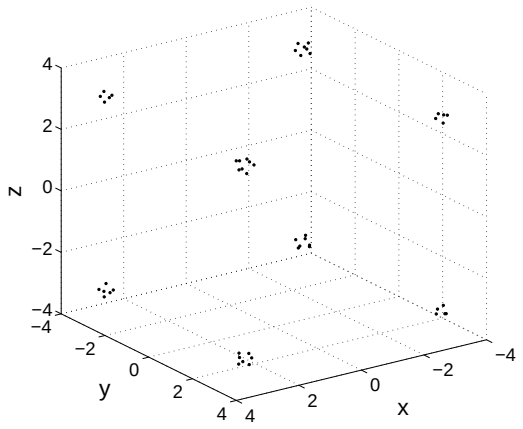

Figure 4.8: Eight cluster formations ($n = 50, \mu_x = 5, \mu_y = 5, \mu_z = 5$)

Next, consider the pattern formation based on a $1D$ pitchfork bifurcation attractor, as shown in Eq. 4.6;

$$U^S = -\frac{1}{2}(\mu_y y_i^2 + \mu_z z_i^2) + \frac{1}{4}(y_i^4 + z_i^4) \tag{4.6}$$

Again, depending on the sign of the bifurcation parameters, μ_y and μ_z, the number of fixed point attractors can be altered, as summarised in Table 4.2.

Table 4.2: Pitchfork bifurcation parameters - $1D$ attractor

μ_y	< 0	> 0	< 0	> 0
μ_z	< 0	< 0	> 0	> 0
attractors	1	2	2	4

In **Section 4.1.1** it was shown that line pattern will be forced apart due to the repulsive potential. In order to achieve a fixed line length with equal spacing, Eq. 4.6 can be altered to include constraining potential, U_c, as follows;

$$U^S = -\frac{1}{2}(\mu_y y_i^2 + \mu_z z_i^2) + \frac{1}{4}(y_i^4 + z_i^4) + U_c \tag{4.7}$$

where,

$$U_c = A_c \exp\{-\frac{1}{L_c}(x_i - x_{w1})^2\} + A_c \exp\{-\frac{1}{L_c}(x_i - x_{w2})^2\} \tag{4.8}$$

and A_c and L_c represent the amplitude and length scale of the potential and x_{w1}, x_{w2} represent the bounds of the constraining potential.

As an example, consider the constraining potential defined such that it is desired to form an equally spaced line in the x-direction, with bounds choosen so that $x_{w1,2} = \pm 6$, as shown in Fig. 4.9. To ensure that the *agents* do not escape the constraining potential, $A_c > \frac{1}{2}v_{max}^2$, where v_{max} is the maximum velocity of an *agent*.

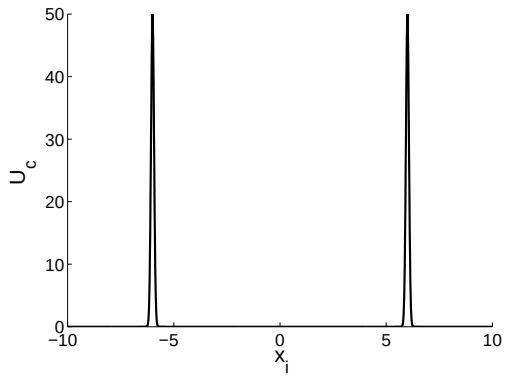

Figure 4.9: Constraining potential ($A_c = 50, L_c = 0.05$)

The results shown in Fig. 4.10, 4.11 and 4.12 consider a constraining potential between $x_{w1,2} = \pm 6$. It can be seen that the swarm can be attracted to the three different formation patterns, assuming random initial condition within the bounds of $x_i = \pm 6$. Firstly, for $\mu_y < 0, \mu_z < 0$ a line pattern is formed as expected. For $\mu_y > 0, \mu_z < 0$ and $\mu_y < 0, \mu_z > 0$ there are now two equilibrium positions with two line patterns forming in either the $x - z$ or $x - y$ plane. If $\mu_y > 0, \mu_z > 0$ there are then four attractors and thus four lines form, as shown in Fig. 4.12.

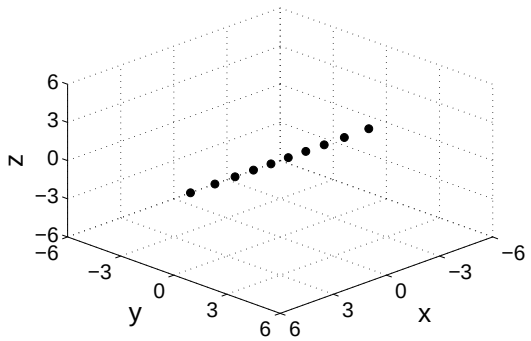

Figure 4.10: Line formation ($n = 10, \mu_y = -5, \mu_z = -5$)

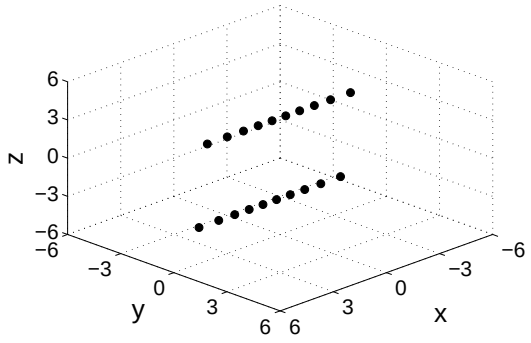

Figure 4.11: Two line formations ($n = 20, \mu_y = 5, \mu_z = -5$)

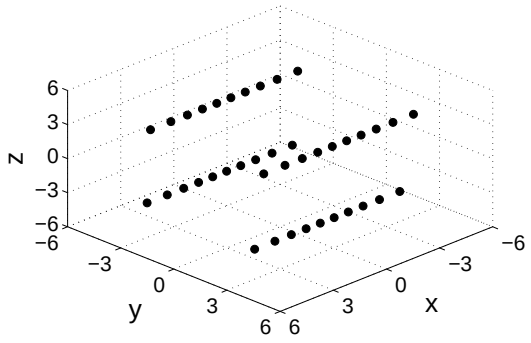

Figure 4.12: Four line formations ($n = 40, \mu_y = 5, \mu_z = 5$)

It was shown in **Section 4.1.1** that to attract the swarm to a particular $2D$ plane, a simple quadratic potential can be used with the results indicating that a swarm, under the influence of a purely repulsive potential field, would disperse in that plane. The pitchfork bifurcation equation, shown previously in Eq. 3.29, will now be used to form patterns in that plane.

$$U^S(\mathbf{x}_i; \mu, \alpha) = -\frac{1}{2}\mu\left(\rho_i - r\right)^2 + \frac{1}{4}\left(\rho_i - r\right)^4 + \frac{1}{2}\alpha z_i^2 \tag{4.9}$$

where, $\rho_i = (x_i^2 + y_i^2)^{0.5}$ and r is scalar.

The results shown in Fig. 4.13-4.16 consider varying values of n, μ and r. For $\mu < 0$ and $r = 3$ an equilateral triangle formation can be achieved, as shown Fig. 4.13. This can be extended to a square formation for $n = 4$ and so on, eventually achieving the ring state, as shown in Fig. 4.14. For $\mu > 0$, Fig. 4.15 shows the double ring formation that can be achieved, with Fig. 4.16 showing the cluster

pattern when $\mu < 0$ and $r = 0$.

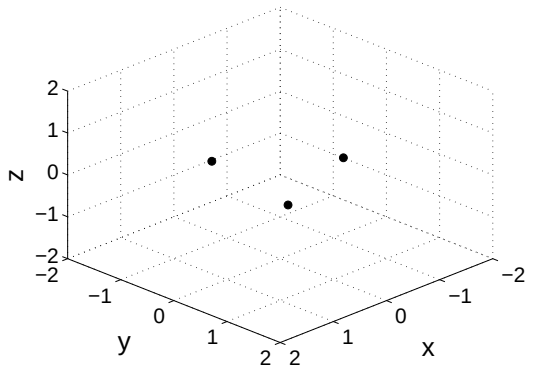

Figure 4.13: Triangle formation ($n = 3, \mu = -5, r = 2$)

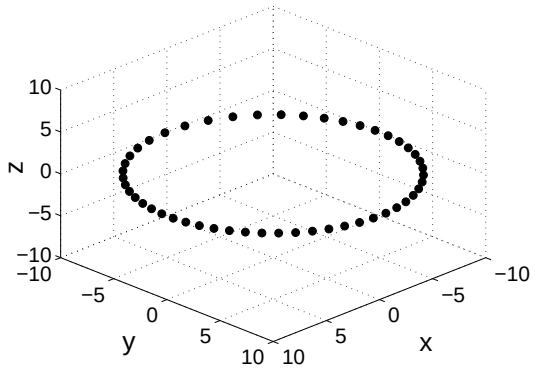

Figure 4.14: Ring formation ($n = 50, \mu = -5, r = 10$)

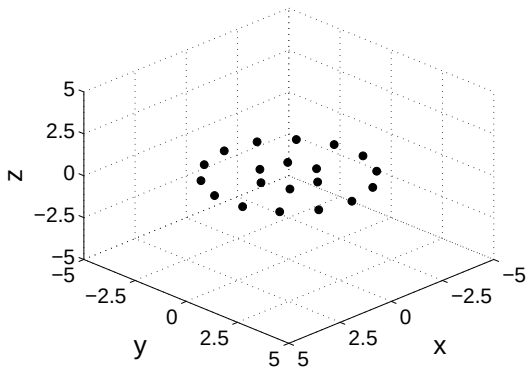

Figure 4.15: Double ring formation ($n = 20, \mu = 5, r = 2$)

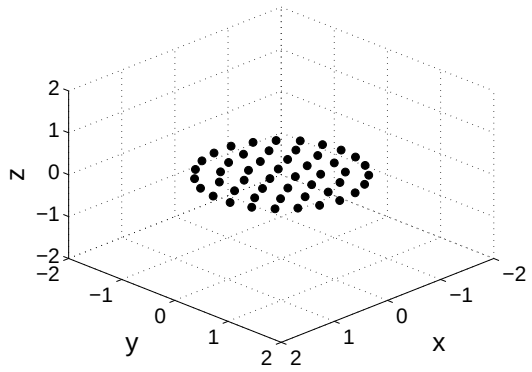

Figure 4.16: Cluster formation ($n = 50, \mu = -5, r = 0$)

Referring back to Eq. 4.4, a pitchfork steering potential can be used to form $3D$ patterns using Eq. 4.10;

$$U^S(\mathbf{x}_i; \mu) = -\frac{1}{2}\mu \left(|\mathbf{x}_i| - r\right)^2 + \frac{1}{4}\left(|\mathbf{x}_i| - r\right)^4 \tag{4.10}$$

From the results shown in Fig. 4.17 and 4.18 it can be seen that for $\mu < 0$ a spherical formation is achieved with radius equal to r. For $\mu > 0$ a double sphere formation can be achieved, with inner and outer sphere radius of $r_i = 3.6$ and $r_o = 6.4$ as expected ($r_{i,o} = r \pm \sqrt{\mu}$), as confirmed in Fig. 4.19 and 4.20

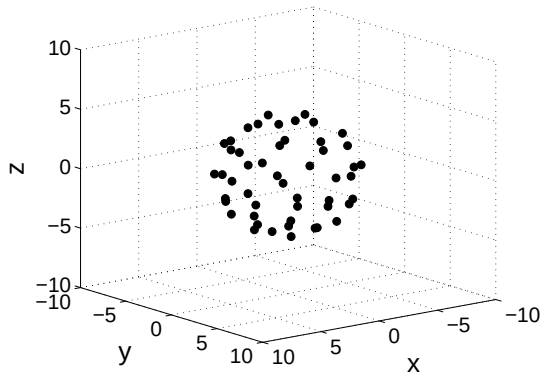

Figure 4.17: Sphere formation ($n = 50, \mu = -5, r = 5$)

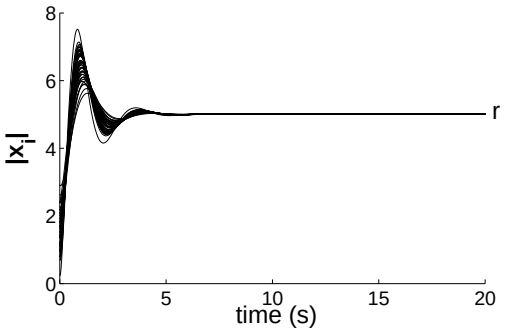

Figure 4.18: Sphere formation radius

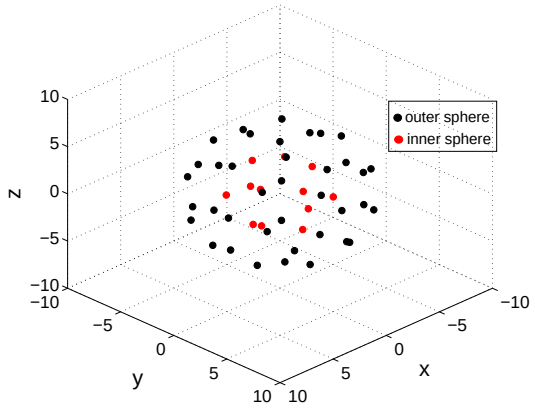

Figure 4.19: Double sphere formation ($n = 50, \mu = 2, r = 5$)

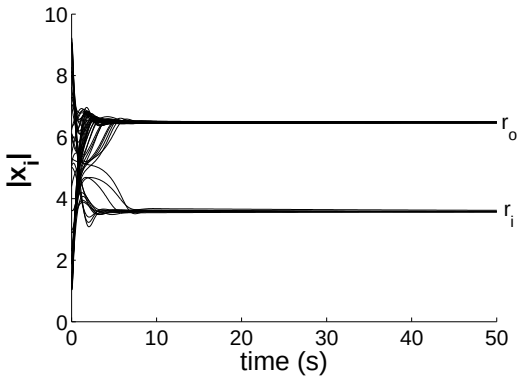

Figure 4.20: Double sphere radius

Therefore, using the pitchfork bifurcation potential a swarm of *agents* can be attracted to different states, forming a variety of different static patterns. Similar static patterns to that shown in this section can be achieved using the transcritical and cusp bifurcation equations.

Hopf Bifurcation

From **Section 2.4.4** it is known that the Hopf bifurcation can lead to either fixed point or periodic limit cycle attractors. Using the swarming model described by Eq. 3.53, Fig. 4.21 and 4.22 show the formation patterns that can achieved for $\mu < 0$ and $\mu > 0$ respectively.

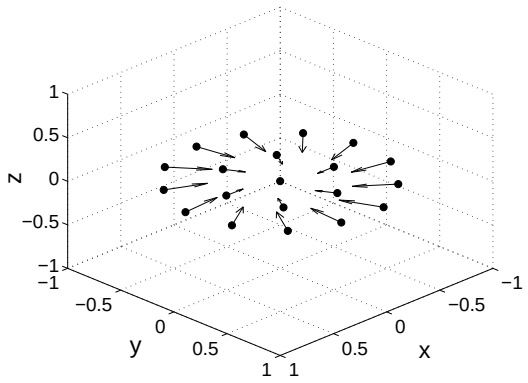

Figure 4.21: Hopf bifurcation cluster pattern ($n = 20, \mu = -5$)

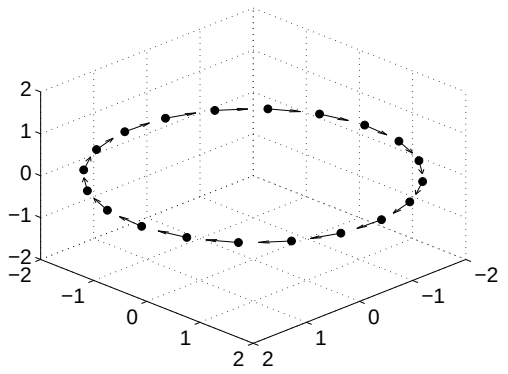

Figure 4.22: Hopf bifurcation rotating ring pattern ($n = 20, \mu = 5$)

From the results it can be seen that the swarm relaxes into a rotating cluster pattern for $\mu < 0$, as shown in Fig. 4.21. In this case the velocity field directs each *agent* to the origin, however, due to the interaction with the repulsive potential, the swarm balances such that a rotating cluster pattern is achieved. Figure 4.22 shows the rotating ring formation for the case when $\mu > 0$ when the system is attracted to a limit cycle.

4.1.3 Other Swarm Patterns

In addition to the bifurcation potential patterns, there are several other potentials that can be used to form patterns as discussed in the following examples.

Grid Formation

In order to generate a grid formation in a plane, the following steering potential can be used;

$$U^S = A_x \cos(M_x x_i) A_y \sin(M_y y_i) + \frac{1}{2} z_i^2 \tag{4.11}$$

where, A_x, A_y and M_x, M_y control the amplitude and spatial frequency of the terms.

An example of the grid potential is shown in Fig. 4.23, that results in the formation of multiple potential wells.

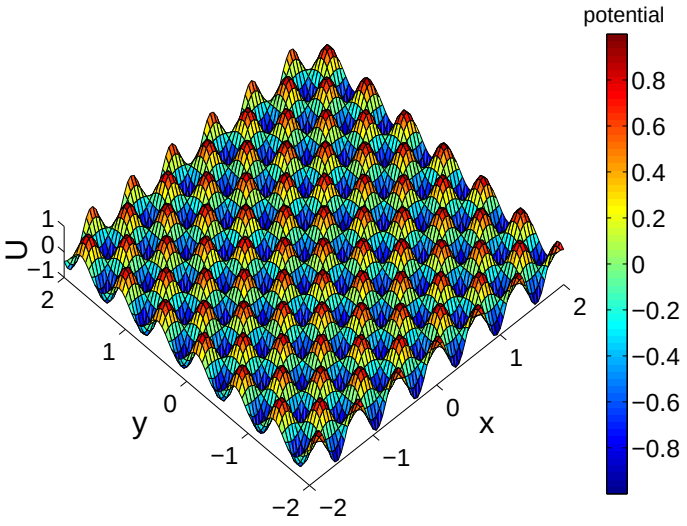

Figure 4.23: Grid potential ($A_x = -1$, $A_y = 1$, $M_x = 10$ and $M_y = 10$)

From the results shown in Fig. 4.24, a swarm grid formation can be achieved. By inclusion of a constraining potential in both the x and y directions ($x_{w1,2} = \pm 1, y_{w1,2} = \pm 1.5$) and giving each *agent* random initial condition within these bounds, each *agent* in the swarm will relax into the minimum of the potential with the repulsive potential ensuring that two *agents* do not remain in the same potential, therefore, creating the grid formation as shown. It should be noted that if the initial conditions were unbound, there is no guarantee that swarm will self-organise into the grid formation shown, with gaps most likely to occur in the final formation.

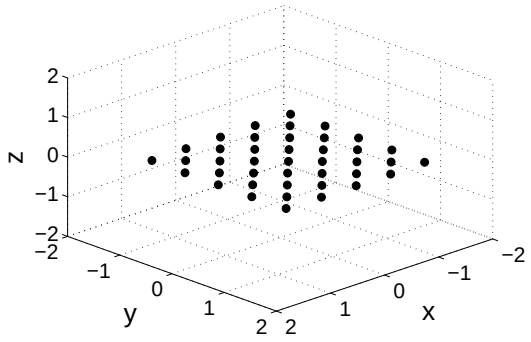

Figure 4.24: Grid formation ($n = 41$, $A_x = -1$, $A_y = 1$, $M_x = 10$ and $M_y = 10$)

Multiple Ring Formation

The pitchfork bifurcation allowed for the formation of either a single or double ring configuration. This can be extended to multiple rings by considering the following steering potential equation;

$$U^S = A_m \cos(\eta \rho_i) + \frac{1}{2} z_i^2 \tag{4.12}$$

where, A_m and η control the amplitude and spatial frequency of the term.

Figure 4.25 shows the potential function consisting of multiple ring minimum energy states. The wavelength of the cosine function is given by $2\pi/\eta$ so that by increasing the value of η results in smaller ring radii.

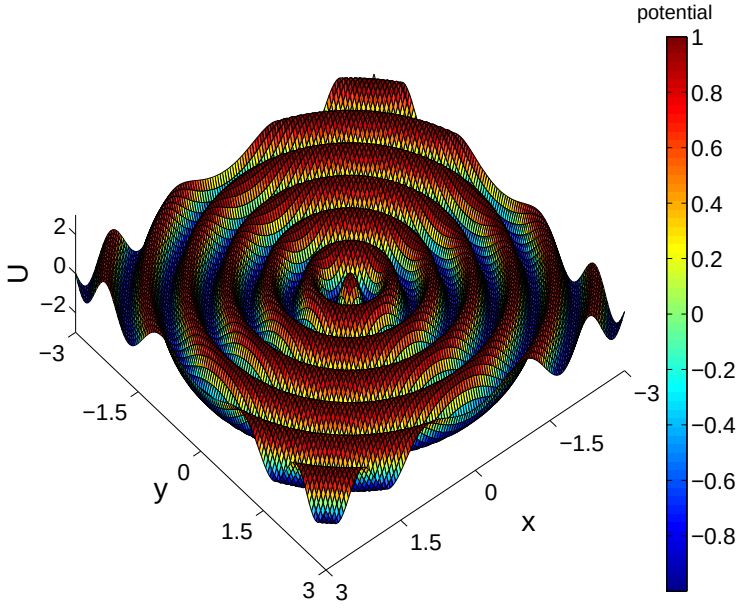

Figure 4.25: Multiple ring potential ($A_m = 1$ and $\eta = 10$)

From the results shown in Fig. 4.26 it can be seen that the swarm formation can relax into a equally spaced multiple ring configuration, assuming random initial conditions within the bounds of a constraining potential in both the x and y directions ($x_{w1,2} = \pm 3, y_{w1,2} = \pm 3$).

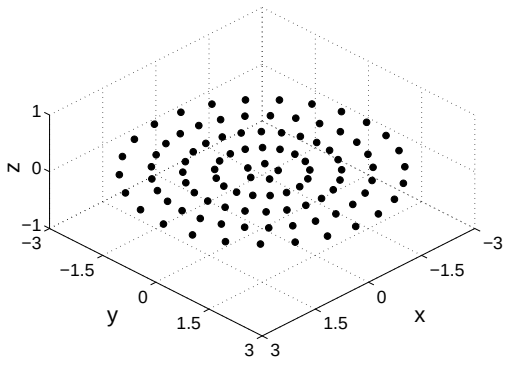

Figure 4.26: Multiple ring formation ($n = 100$, $A_m = 1$ and $\eta = 10$)

Therefore, for illustration both the grid and multiple ring formation were demonstrated with respect to the swarm formations in the $x - y$ plane, although both can be easily extended to the $1D$ and $3D$ formation pattern cases.

Orientation of the Formations

The results thus far have considered formation patterns in a particular plane. In real applications it may be desired for the swarm pattern to form in a different plane. To achieve this the directional cosine matrix (DCM) [126] approach can be used by rotating the x and y axis by an angle ϕ and θ respectively as follows;

$$\mathbf{C}_1(\phi) = \begin{bmatrix} 1 & 0 & 0 \\ 0 & \cos(\phi) & \sin(\phi) \\ 0 & -\sin(\phi) & \cos(\phi) \end{bmatrix} \tag{4.13}$$

$$\mathbf{C}_2(\theta) = \begin{bmatrix} \cos(\theta) & 0 & -\sin(\theta) \\ 0 & 1 & 0 \\ \sin(\theta) & 0 & \cos(\theta) \end{bmatrix} \tag{4.14}$$

The DCM is then defined in Eq. 4.15, with Eq. 4.16 showing the new position vector, $\mathbf{x}'_i$ as a function of the DCM and $\mathbf{x}_i$;

$$DCM = \begin{bmatrix} \cos(\theta) & 0 & -\sin(\theta) \\ \sin(\phi)\sin(\theta) & \cos(\theta) & \sin(\phi)\cos(\theta) \\ \cos(\phi)\sin(\theta) & -\sin(\phi) & \cos(\phi)\cos(\theta) \end{bmatrix} \tag{4.15}$$

$$\begin{bmatrix} x_i' \\ y_i' \\ z_i' \end{bmatrix} = DCM \begin{bmatrix} x_i \\ y_i \\ z_i \end{bmatrix} \tag{4.16}$$

As an example consider the formation of a ring pattern, orientated such that $\phi = 45^o$ and $\theta = 45^o$ using the pitchfork bifurcation shown in Eq. 3.29.

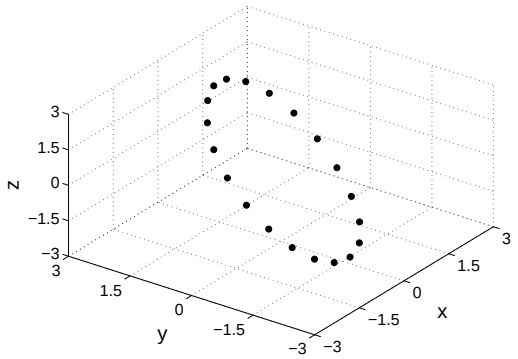

Figure 4.27: Orientation of the pitchfork bifurcation ($n = 20, \mu = -5$, $r = 3$)

Therefore, from the results it can be seen that ring swarm pattern can be orientated by transforming the potential field.

Rotation of the Formation

McInnes has shown how vortex-like swarming can be achieved through artificial potential field methods [127]. Equation 3.1 and 3.2 are altered to include a dissipative orientation term, Λ_i, instead of a velocity dependent term, as shown in Eq. 4.17 and 4.18;

$$\frac{d\mathbf{x}_i}{dt} = \mathbf{v}_i \tag{4.17}$$

$$m\frac{d\mathbf{v}_i}{dt} = -\nabla_i U^S(\mathbf{x}_i) - \nabla_i U^R(\mathbf{x}_{ij}) - \Lambda_i \tag{4.18}$$

where,

$$\Lambda_i = \sum_{j,i\neq j} C_o(\mathbf{v}_{ij}.\hat{\mathbf{x}}_{ij}) \exp^{-|\mathbf{x}_{ij}|/L_o} \hat{\mathbf{x}}_{ij} \tag{4.19}$$

and, $\mathbf{v}_{ij}$ represents the relative velocity vector between *agents*, C_o, L_o represent the strength and range over which the orientation function interacts respectively and $(\hat{.})$ denotes a unit vector.

The purpose of the orientation term is to locally align *agent* velocity vectors, resulting in a vortex rotation. Using a similar procedure to that discussed in **Section 3.1.1**, it can be shown that the swarm system will dissipate energy, while conserving momentum therefore relaxing into rotating formation. Again, considering the use of the pitchfork bifurcation as the basis of the steering potential as described by Eq. 3.29, taking the dot product of the velocity vector with Eq. 4.18 and summing over all *agent* states it can be shown that [128];

$$\frac{dE}{dt} = -\sum_i \mathbf{v}_i \Lambda_i \leq 0 \tag{4.20}$$

Also, taking the cross product of the position vector with Eq. 4.18 and summing over all *agent* states it can be shown that;

$$\frac{d\mathbf{H}}{dt} = 0 \tag{4.21}$$

Figure 4.28 shows the final configuration for a swarm of 20 *agents*. The swarm therefore dissipates energy, relaxing into the equally spaced ring configuration and conserves angular momentum resulting in the rotating ring pattern.

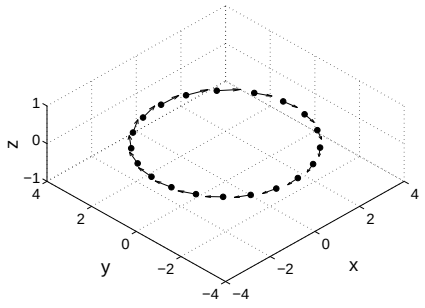

Figure 4.28: Rotation of the ring formation ($n = 20, \mu = -5$, $r = 3$, $C_o = 5$ and $L_o = 1$)

4.2 Reconfigurability

4.2.1 Transcritical Bifurcation

As explained in **Section 2.4.2**, the transcritical bifurcation allows for the switching in position of a single stable equilibrium position dependent upon the sign of the bifurcation parameter, μ. Using this bifurcation potential it can be shown that the position of a single line configuration can be altered by a simple parameter change of μ. Consider a swarm of 10 *agents* that are desired to form a line in the x-direction at three different y-positions, with $z = 0$. To achieve this the transcritical potential, shown in Eq. 4.22 can be used, with $x_{w1,2} = \pm 5$.

$$U^S = \frac{1}{3}y_i^3 - \frac{1}{2}\mu y_i^2 + \frac{1}{2}z_i^2 + U_c \tag{4.22}$$

Figure 4.29 shows the evolution of the y position of the swarm, where it is desired to form a line in the x-direction at $y = 8$, then $y = 4$ and $y = 0$.

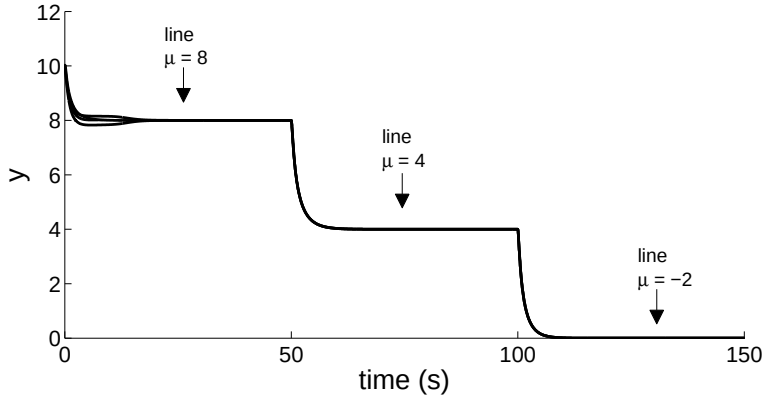

Figure 4.29: Evolution of swarm in the y-direction

Figures 4.30 (i)-(vi) show the results for the system indicating that the system can successfully transition between the desired line positions. Giving the system random initial conditions in the x and z direction, with $y = 10$, the system can be successfully attracted to the first equilibrium position located at $y = \mu = 8$, as shown in Fig. 4.30 (ii). Bifurcating the system such that $\mu = 4$ and $\mu = -2$ the system will then transition autonomously to a new line position located at $y = 4$ and $y = 0$, as confirmed by Fig. 4.30 (iv) and (vi). It should be noted that although the self-organised pattern has been proven analytically —to always occur, the path of each *agent* may be different depending upon initial conditions.

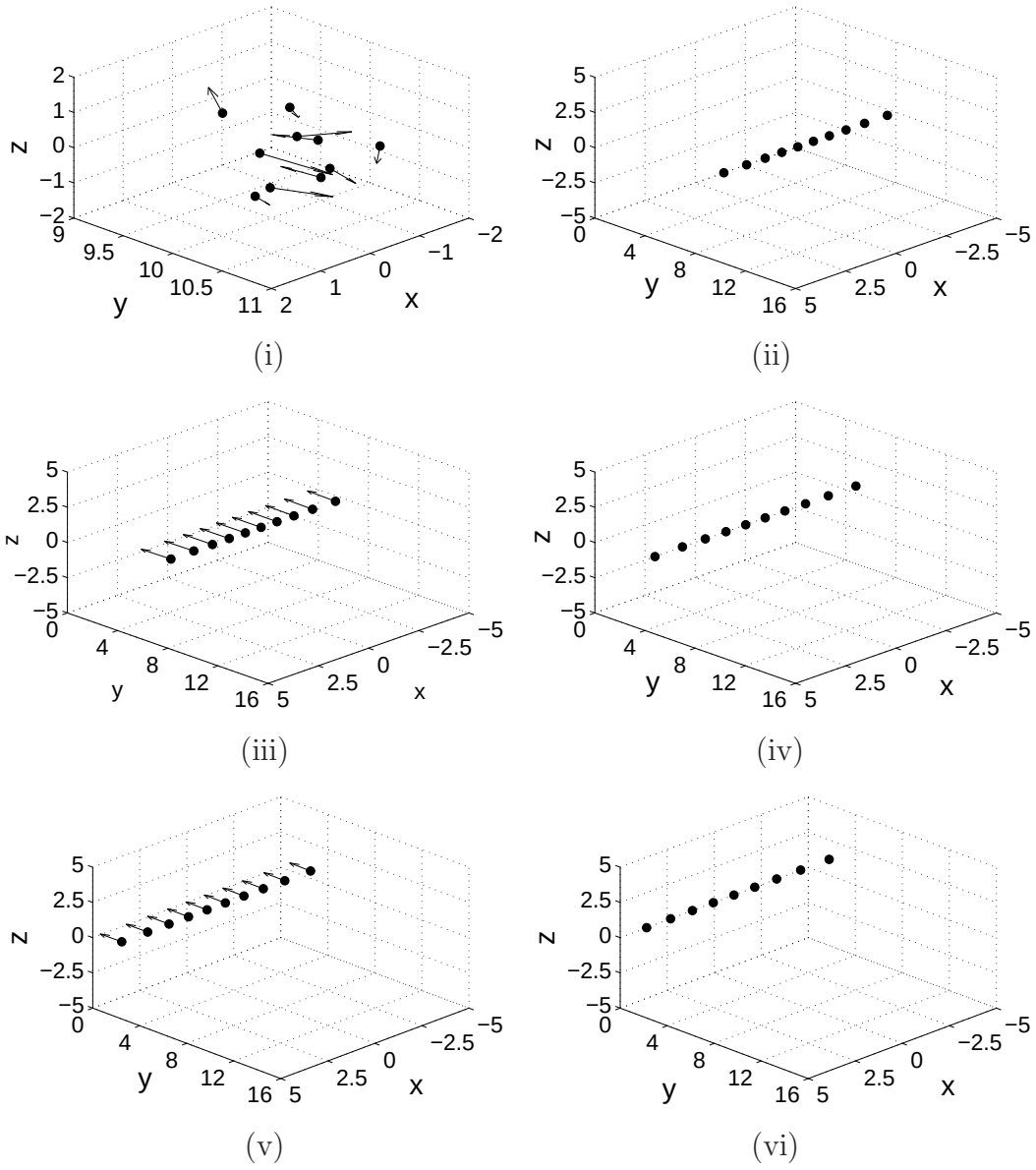

Figure 4.30: Transcritical bifurcation (i) initial conditions (ii) line located at $y = 8$, $(\mu = 8, t = 49s)$ (iii) bifurcation of the system $(\mu = 4, t = 50s)$ (iv) line located at $y = 4$ $(t = 99s)$ (v) bifurcation of the system $(\mu = 0, t = 100s)$ (vi) line located at $y = 0$ $(t = 150s)$

4.2.2 Pitchfork Bifurcation

Using the pitchfork bifurcation a swarm can transition between different $2D$ formation patterns through a simple parameter change. Figure 4.31 shows the evolution of a swarm of 40 *agents* that are desired to form a double ring pattern and then bifurcate into a cluster and then a single ring formation.

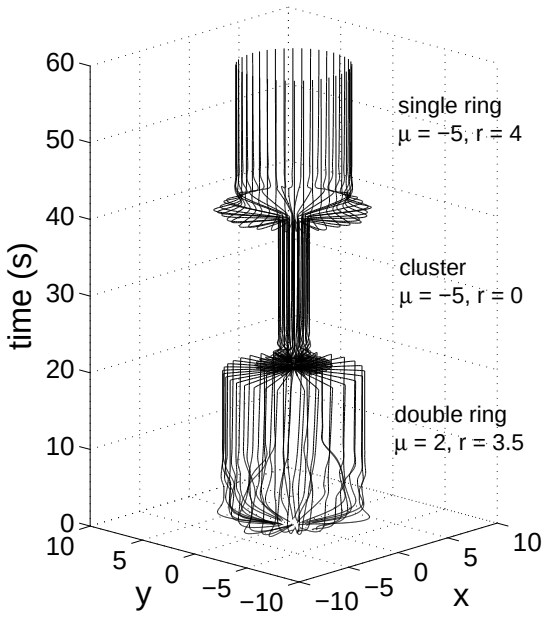

Figure 4.31: Evolution of swarm in the $x - y$ plane

Figures 4.32 (i)-(vi) show the results for the pitchfork bifurcating system indicating that the desired swarm patterns were achieved. The first pattern corresponds to the case when there are two stable equilibrium positions with $\mu > 0$, resulting in the *agents* falling into a double ring pattern, as shown in Fig. 4.32 (ii). The bifurcation parameter is then altered such that $\mu < 0$ and $r = 0$ thus forcing each *agent* to the origin with the repulsive potential causing an equally spaced cluster to form, as shown in Fig. 4.32 (iv). The swarm then bifurcates once more so that $r = 5$ and an equally spaced ring pattern emerges, as shown in Fig. 4.32 (vi).

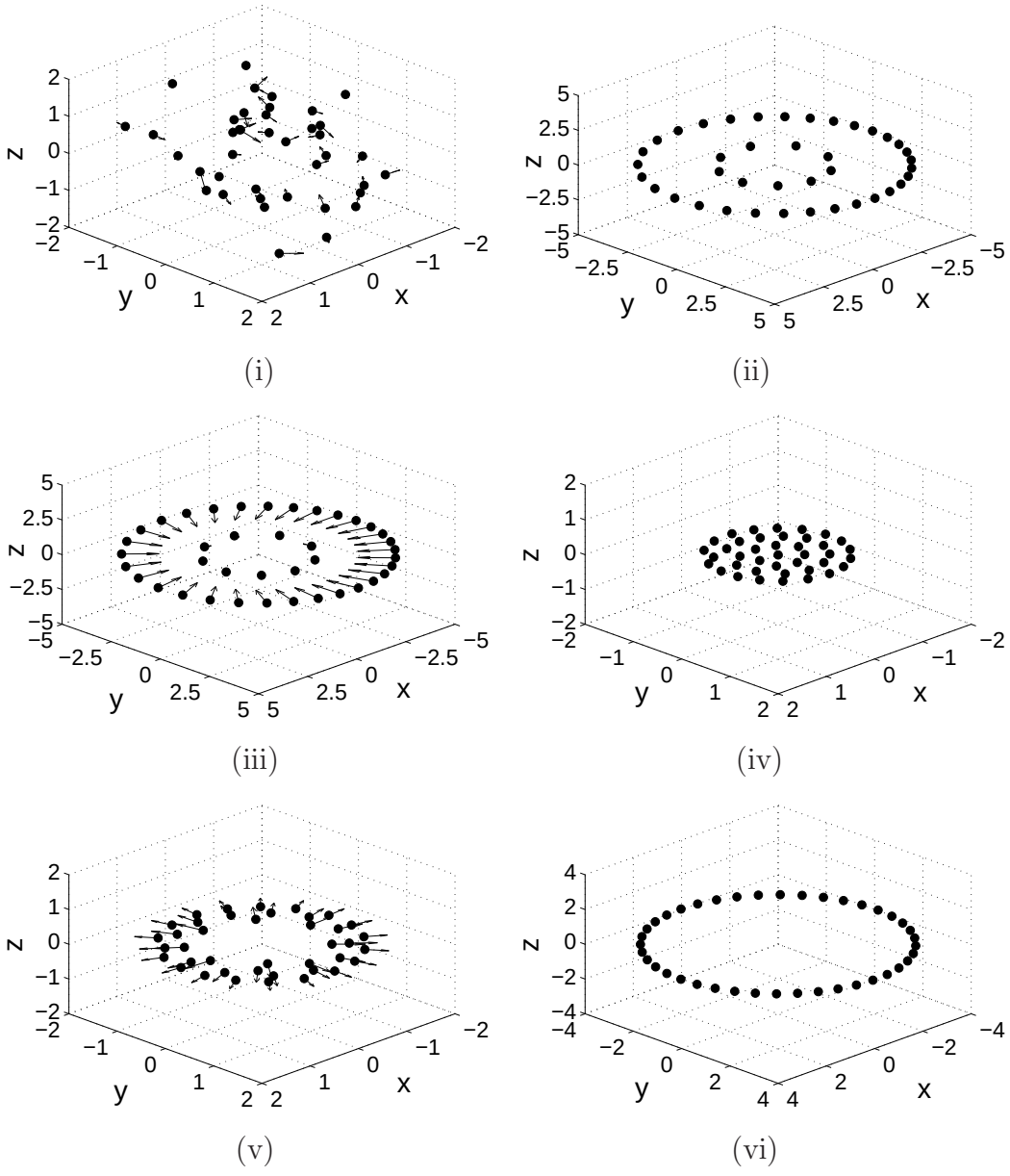

Figure 4.32: Pitchfork bifurcation (i) random initial conditions (ii) double ring ($r_o = 4.9, r_i = 2.1, \mu = 2, r = 3.5, t = 19s$) (iii) bifurcation of the system ($\mu = -5, r = 0, t = 20s$) (iv) cluster ($t = 39s$) (v) bifurcation of the system ($\mu = -5, r = 4, t = 40s$) (vi) ring, radius = 4, ($t = 60s$)

4.2.3 Cusp Catastrophe

As stated in **Section 2.4.3**, the cusp catastrophe is a 2-parameter bifurcation that can be viewed as analogous with a phase diagram in thermodynamics. Referring back to Fig. 2.14 (ii), it can be seen that the number of attractors can be altered as the bifurcation parameters μ_1 and μ_2 change. To demonstrate this consider the formation of a double sphere pattern, that then bifurcates into the upper and lower branches of the potential, forming a large and small sphere. Figure 4.33 shows the evolution of the swarm of *agents* from the origin of the system.

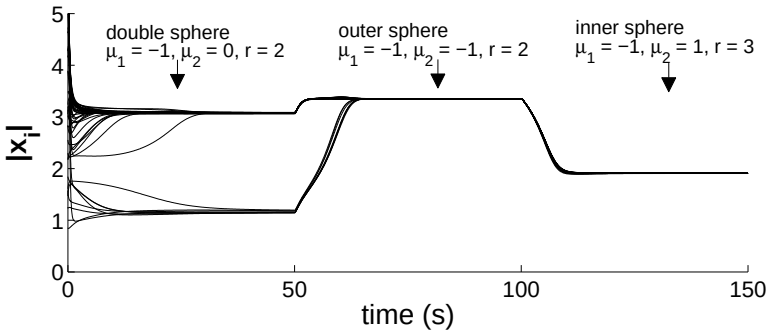

Figure 4.33: Evolution of the cusp catastrophe

Figures 4.34 (i)-(vi) show the results of the simulation indicating that the system successfully transitions between the desired patterns. Depending on the initial conditions, each *agent* will be attracted to one of the double sphere equilibrium states, with the system eventually relaxing into the minimum energy configuration, as shown in Fig. 4.34 (ii). Bifurcating the system so that $\mu_2 = -1$, the system will be attracted into the outer ring state, as shown in Fig. 4.34 (iv). Finally, bifurcating the system again such that $\mu_2 = 1$ and $r = 3$ the system will be attracted to a smaller sphere, as shown in Fig. 4.34 (vi). It should be noted that the formation of both the double ring and double sphere pattern is dependent upon *agent* initial conditions. In both the examples shown in **Section 4.2.2** and **4.2.3** the system was choosen such that the swarm bifurcates from two stable equilibrium positions to one equilibrium position. If the system is desired to go in the other direction from the single to a double equilibrium position, there is no guarantee that the swarm will relax into either the double ring or double sphere pattern. Nevertheless, the results still demonstrate that bifurcation theory can provide a means to transition between different formation patterns.

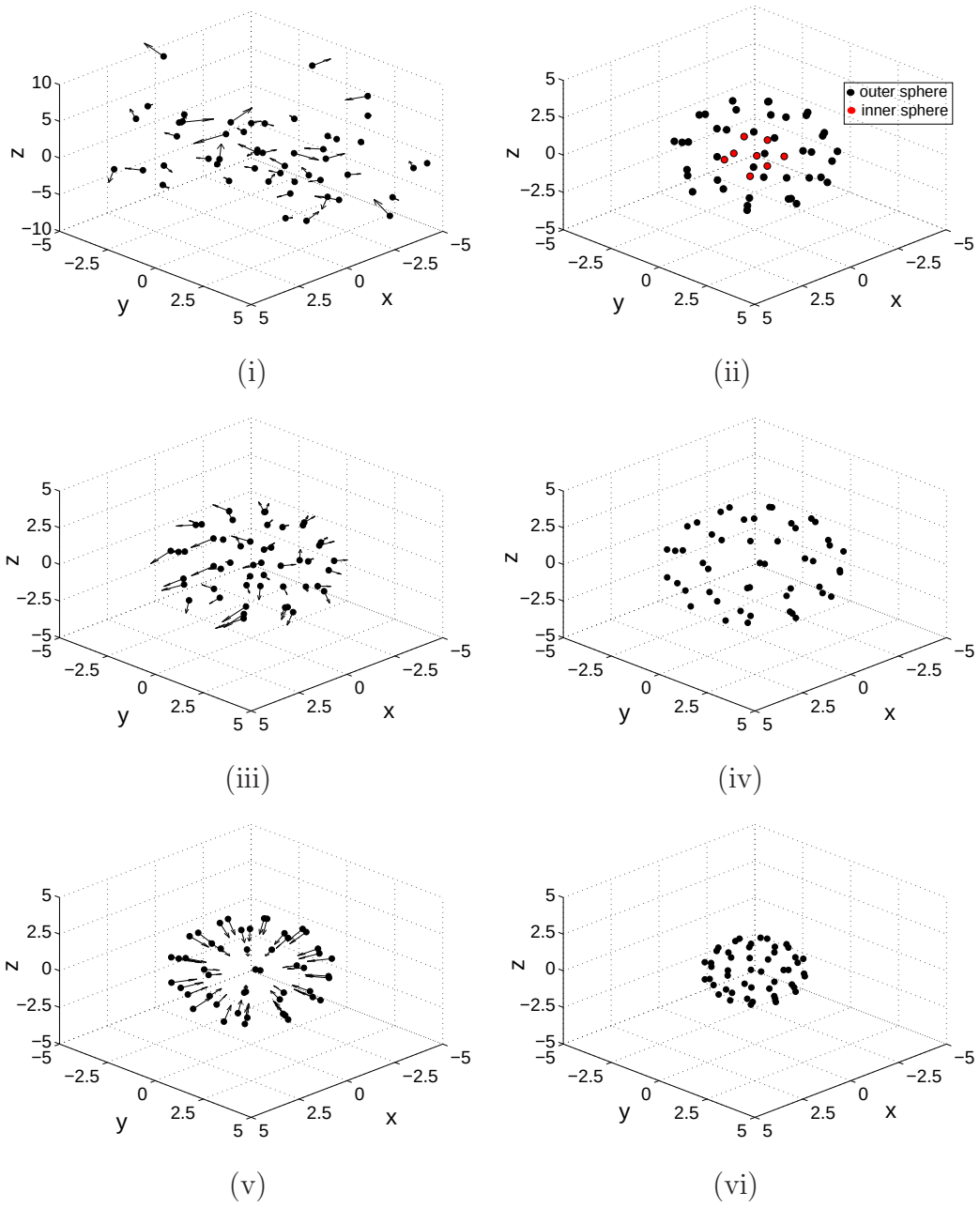

Figure 4.34: Cusp catastrophe (i) random initial conditions (ii) double sphere ($r_o = 3, r_i = 1, \mu_1 = 1, \mu_2 = 0, r = 2, t = 49s$) (iii) bifurcation of the system ($\mu_1 = -1, \mu_2 = -1, r = 2, t = 50s$) (iv) outer single sphere, radius = 3.3 ($t = 99s$) (v) bifurcation of the system ($\mu_1 = -1, \mu_2 = 1, r = 3, t = 100s$) (vi) inner single sphere, radius = 1.7 ($t = 150s$)

4.2.4 Hopf Bifurcation

Consider a swarm of 20 *agents* that are desired to form a rotating cluster pattern, then an equally spaced rotating ring and finally return back to the rotating cluster pattern. To achieve this the Hopf bifurcation can be used to autonomously reconfigure the swarm by altering the bifurcation parameter. Using the first order velocity field as described by Eq. 3.53, Fig. 4.35 shows the time evolution for the swarm system.

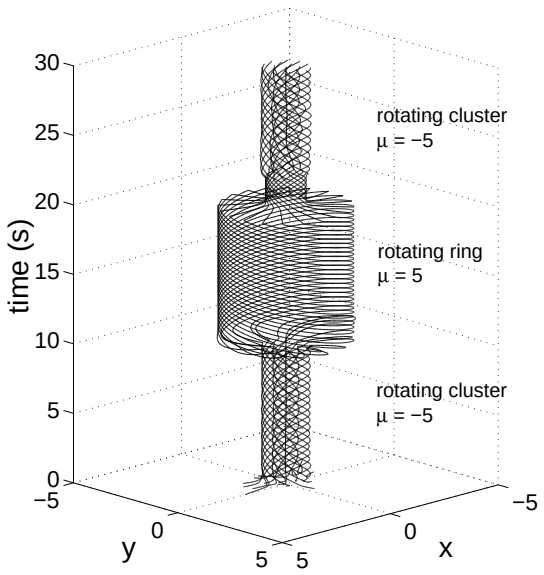

Figure 4.35: Evolution of the Hopf bifurcation

Figures 4.36 (i)-(vi) show the formation of the different autonomous patterns through the Hopf bifurcation. The initial pattern occurs when $\mu = -5$, as shown in Fig. 4.36 (ii), resulting in the rotating cluster pattern. Figure 4.36 (iv) shows the bifurcation of this pattern by making a simple parameter change so that $\mu = 5$. By doing so the system behaviour changes and a limit cycle motion is induced. Again the interaction with the repulsive potential results in an equally spaced rotating ring pattern. The final formation corresponds to again the case when $\mu = -5$ so that the rotating cluster pattern can be achieved again, as shown in Fig. 4.36 (vi).

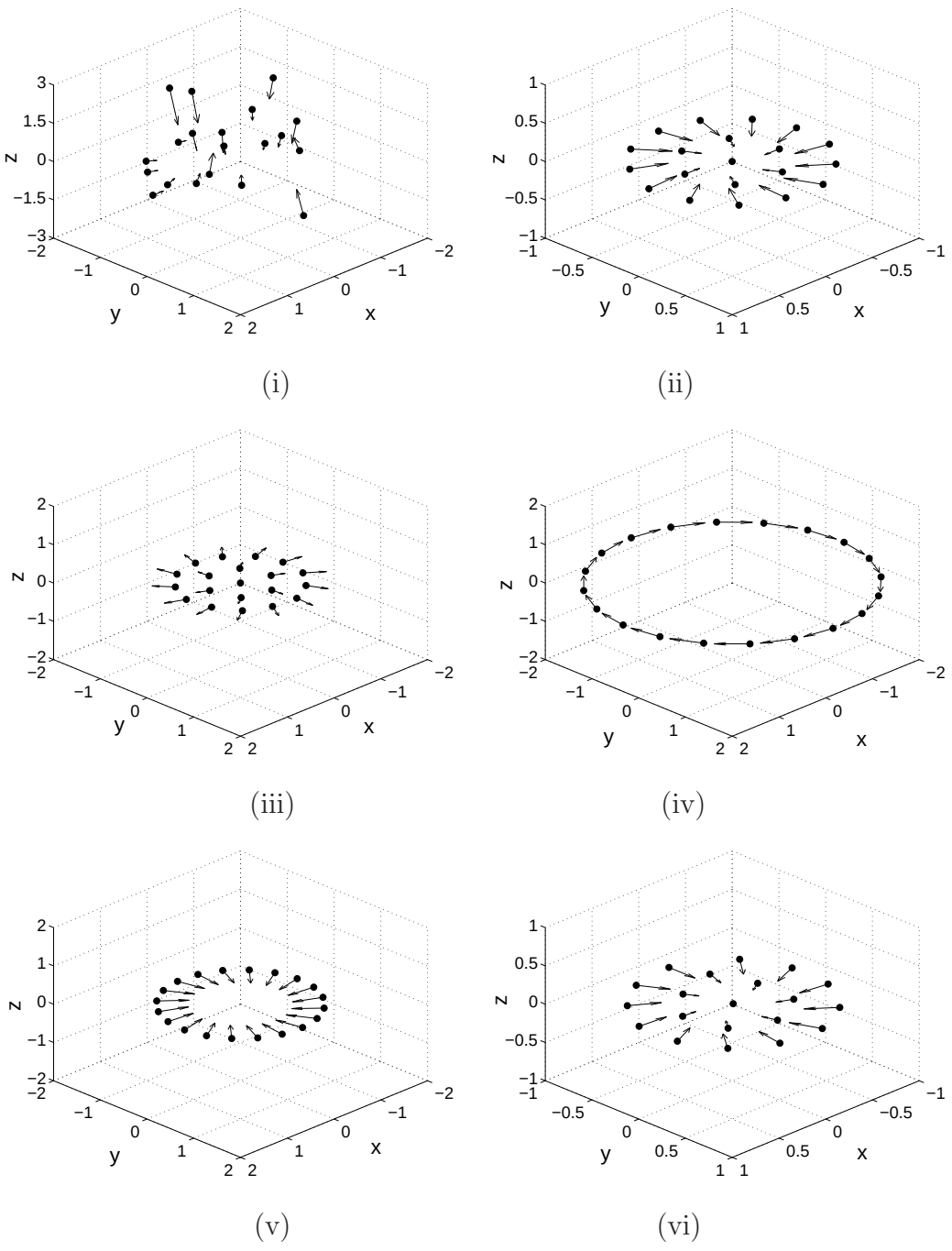

Figure 4.36: Hopf bifurcation (i) random initial conditions (ii) rotating cluster formation ($\mu = -5, t = 9s$) (iii) bifurcation of the system ($\mu = 5, t = 10s$) (iv) rotating ring formation ($t = 19s$) (v) bifurcation of the system ($\mu = -5, t = 20s$) (vi) rotating cluster formation ($t = 30s$)

4.3 Summary

This chapter has demonstrated the two swarming themes considered in this thesis; pattern formation and reconfigurability. It has been shown that through the new approach of bifurcating APFs, a verifiable swarming system will self-organise, capable of creating reconfigurable autonomous patterns. Using the potential field method the swarm system can be attracted to different states, with bifurcation theory providing a means of pattern formation once attracted to a particular state. In addition, it was also shown how other potentials can be used to form different swarm patterns. It was then demonstrated that by using bifurcation theory the swarm system can autonomously reconfigure between different patterns through simple parameter changes to the potential.

Chapter 5

Towards Real World Considerations

The work presented in earlier chapters has considered the ideal swarming scenario where it has been assumed that all *agents* are fully actuated and can communicate freely with each other. In real, safety or mission critical applications it is important to consider real world effects. As such, this chapter investigates the issue of actuator saturation and communication limitation to increase the fidelity of the swarm model. A new potential field inspired from the pitchfork bifurcation equation is developed based on hyperbolic-exponential potentials, addressing the issue of actuator saturation. Secondly, the assumption that every *agent* in the swarm can communicate with all other *agents* is unrealistic and limits the scalability of the model. As such this problem is addressed by adapting the repulsive potential field so that it only acts in a sensing region surrounding each *agent*. This new swarm model is then applied to both force and velocity field examples. In addition, the advantages of the new model are demonstrated indicating that the system is robust to *agent* failure, flexible and scalable. As part of future work, other real world effects will be investigated such as; consideration of computational load on each *agent*, communication time-delays, non-holonomic effects and robustness to partial *agent* failure.

5.1 Actuator Saturation

In **Chapter 4** it was shown that classical static bifurcations can be used to steer a swarm of *agents*, allowing for a simple transition between formations. Although

this form of autonomous control architecture has the advantages of being flexible and robust, the analysis considered the formation of patterns assuming ideal *agents*. In order to assure stability for real, safety or mission critical systems it is important to consider actuator saturation. From Eq. 3.2, the control force ($\mathbf{u}_i$) acting on each *agent* is shown in Eq. 5.1.

$$\mathbf{u}_i = \mathbf{u}^S + \mathbf{u}^R + \mathbf{u}^d \tag{5.1}$$

where,

$$\begin{pmatrix} \mathbf{u}^S \\ \mathbf{u}^R \\ \mathbf{u}^d \end{pmatrix} = \begin{pmatrix} -\nabla_i U^S(\mathbf{x}_i) \\ -\nabla_i U^R(\mathbf{x}_{ij}) \\ -\sigma \mathbf{v}_i \end{pmatrix} \tag{5.2}$$

Through the triangle inequality [125] the maximum control force must be;

$$|\mathbf{u}_i| \leqslant |\nabla_i U^S(\mathbf{x}_i)| + |\nabla_i U^R(\mathbf{x}_{ij})| + |\sigma \mathbf{v}_i| \tag{5.3}$$

The maximum control force that the system is required to produce will therefore be dependent upon the sum of the maximum gradient of the steering and repulsive potentials and the maximum speed that each *agent* can move.

Considering the classical pitchfork bifurcation as an example steering potential, referring back to Eq. 3.29, it can be seen that the control force is unbound as the distance ρ_i from the origin increases. Recently, work done by Badaway and McInnes devised a promising approach to overcome this unbound control force through the use of a hyperbolic potential function [98]. This function has a smooth shape at the goal state whilst becoming asymptotic with a constant gradient (thus bound control force) as the distance from origin increases. Equation 5.4 and Fig. 5.1 show the hyperbolic control potential, $U_h(\rho_i)$, that can be used as the steering potential to achieve a bound control force.

$$U_h(\rho_i) = C_h \left[(\rho_i - r)^2 + 1\right]^{0.5} \tag{5.4}$$

where the constant C_h controls the amplitude of the function.

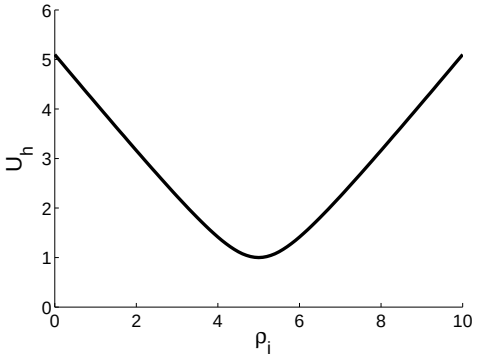

Figure 5.1: Hyperbolic potential function ($C_h = 1, r = 5$)

To make use of the principles demonstrated in the pitchfork bifurcation potential, an additional exponential potential function, $U_e(\rho_i)$, can be added as shown in Eq. 5.5 and Fig. 5.2.

$$U_e(\rho_i) = \mu C_e \exp^{-(\rho_i - r)^2 / L_e} \tag{5.5}$$

where C_e and L_e represent the amplitude and length scale of the function and μ is the bifurcation parameter.

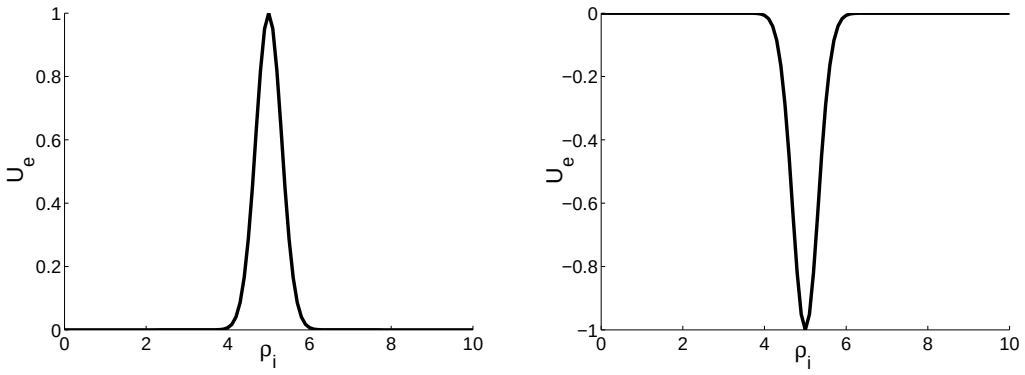

(i) (ii)

Figure 5.2: Exponential potential function ($C_e = 1, L_e = 0.2, r = 5$) (i) $\mu = 1$ (ii) $\mu = -1$

Combining Eq. 5.4 and 5.5, a new bound bifurcating steering potential equation can be achieved as shown in Eq. 5.6 and Fig. 5.3. If the bifurcation parameter $\mu < 0$ there is one goal state as shown in Fig. 5.3 (i). If however, the system bifurcates such that $\mu > 0$, two stable goal positions will emerge as shown in Fig. 5.3 (ii). The last term in Eq. 5.6 ensures that the formation is created in the $x - y$ plane.

$$\begin{aligned} U^S(\mathbf{x}_i) &= U_h(\rho_i) + U_e(\rho_i) + U_h(z_i) \\ &= C_h \left[(\rho_i - r)^2 + 1\right]^{0.5} + \mu C_e \exp^{-(\rho_i - r)^2/L_e} + C_z[z_i^2 + 1]^{0.5} \end{aligned} \quad (5.6)$$

where the constant C_z controls the amplitude of this bound hyperbolic potential function.

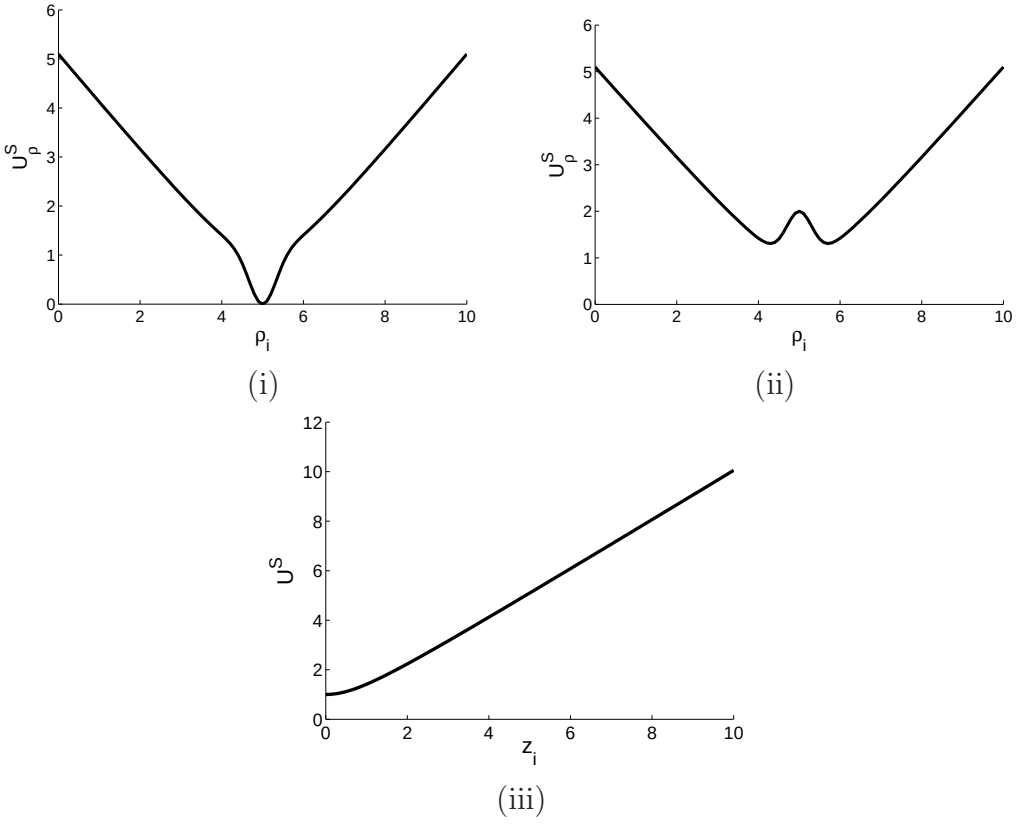

Figure 5.3: New bound steering potential ($C_h = 1, r = 5$) (i) U_ρ^S: $\mu = -1, C_e = 1, L_e = 0.2$ (ii) U_ρ^S: $\mu = 1, C_e = 1, L_e = 0.2$ (iii) U_z^S: $C_z = 1$

This new steering potential is then a bound control force, dependent upon the maximum gradient of the hyperbolic and exponential terms. Firstly, considering the hyperbolic function, the control force, $\mathbf{u}_h^S$, is shown in Eq. 5.7 and Fig. 5.4.

$$\mathbf{u}_h^S = -\nabla_i U_h(\rho_i, z_i) = [u_{h\rho}, u_{hz}]^T = \left[-\frac{C_h(\rho_i - r)}{[(\rho_i - r)^2 + 1]^{0.5}}, -\frac{C_z z_i}{(z_i^2 + 1)^{0.5}} \right]^T \quad (5.7)$$

Therefore, as $\rho_i \to \infty$, $u_h \to -C_h$; $\rho_i \to 0$, $u_h \to C_h$ and as $z_i \to \infty$, $u_z \to -C_z$

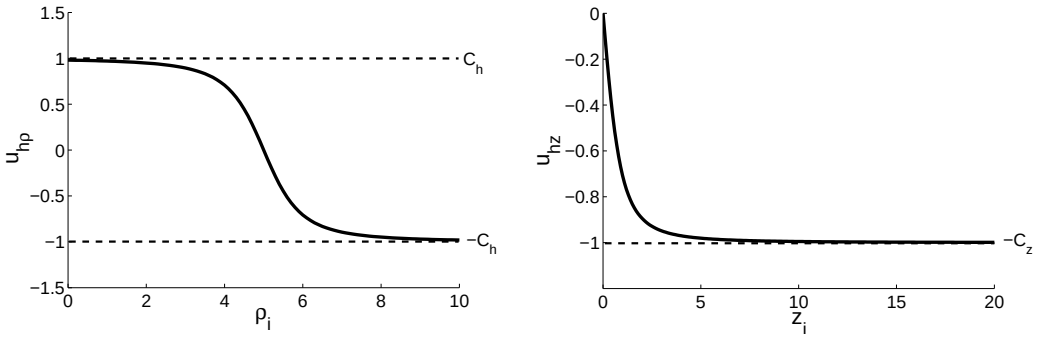

(i) (ii)

Figure 5.4: Hyperbolic control forces (i) $u_{h\rho_i}$: $C_h = 1, r = 5$ (ii) u_{hz}: $C_z = 1$

as shown in Fig. 5.4.

Similarly, the exponential control force is shown in Eq. 5.8.

$$\mathbf{u}_e^S = -\nabla_i U_e(\rho_i, z_i) = [u_{e\rho}, u_{ez}]^T = \left[2\mu \frac{C_e}{L_e}(\rho_i - r)\exp^{-(\rho_i - r)^2/L_e}, 0\right]^T \tag{5.8}$$

The maximum exponential control forces occurs when $\rho_i = r \pm \sqrt{\frac{L_e}{2}}$ giving the maximum control force, $u_{e\rho}$, equal to $\pm\sqrt{2}\mu \frac{C_e}{\sqrt{L_e}} \exp^{-0.5}$, as shown in Fig. 5.5.

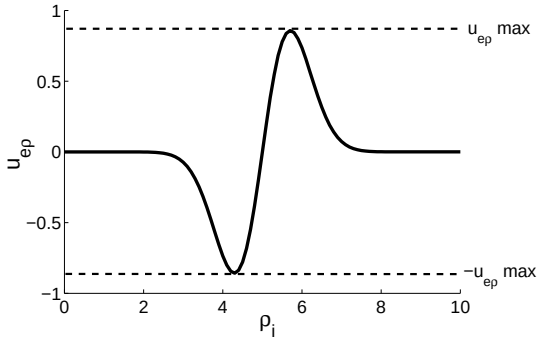

Figure 5.5: Exponential control force ($r = 5, C_e = 1, L_e = 1, \mu = 1$)

Therefore, depending upon the constants chosen in Eq. 5.6, the maximum bound control force in the ρ_i direction will either be controlled through the hyperbolic or exponential term in the steering potential equation. The equations have to be evaluated to determine if either the hyperbolic or exponential term dominates, as

shown in Fig. 5.6 (i) and (ii). Considering the case when $\mu > 0$, with constants choosen so that the hyperbolic term dominates, then $|u_\rho^S|_{max} = C_h$ as shown in Fig. 5.6 (i). If, however, the exponential term dominates, as shown in Fig. 5.6 (ii), then $|u_\rho^S|_{max}$ can be found numerically. In the z direction $|u_z^S|_{max} = C_z$, as shown in Fig. 5.4 (ii).

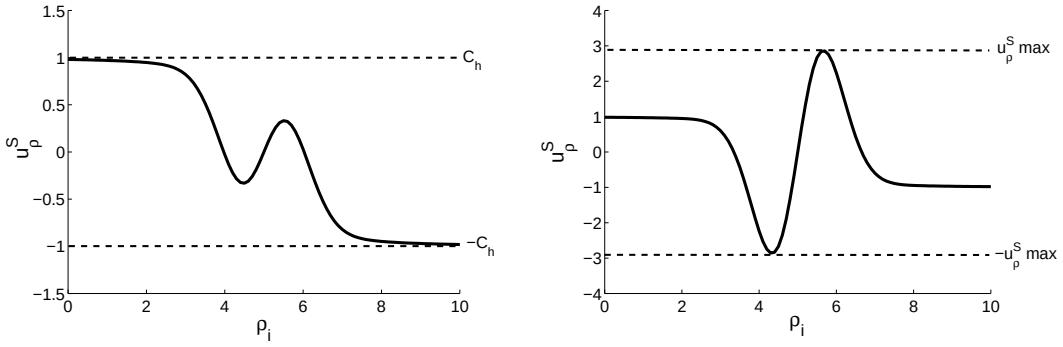

(i) (ii)

Figure 5.6: Steering potential control forces ($\mu = 1, C_h = 1, L_e = 1, r = 5$) (i) u_h^s dominating, $C_e = 1$ (ii) u_e^S dominating, $C_e = 4$

The bound steering potential control force is then;

$$|\mathbf{u}^S| = |\nabla_i U^S(\mathbf{x}_i)|_{max} \leq \left[\left(\nabla_i U^S(\rho_i)_{max}\right)^2 + \left(\nabla_i U^S(z_i)_{max}\right)^2\right]^{0.5} \tag{5.9}$$

The repulsive potential is a bound force that has a maximum value equal to C_R/L_R that occurs when $\mathbf{x}_{ij} = 0$. This would, however, occur when two *agents* are in the same position and therefore would have collided. The realistic maximum control force would therefore be $(\mathbf{u}_i^R)_{max} = C_R/L_R \exp^{-(|\mathbf{x}_{ij}|_{min}/L_R)}$ where, $|\mathbf{x}_{ij}|_{min} = |\mathbf{x}_i - \mathbf{x}_j|_{min}$, is the minimum separation distance between both *agents* without colliding, as shown in Fig. 5.7.

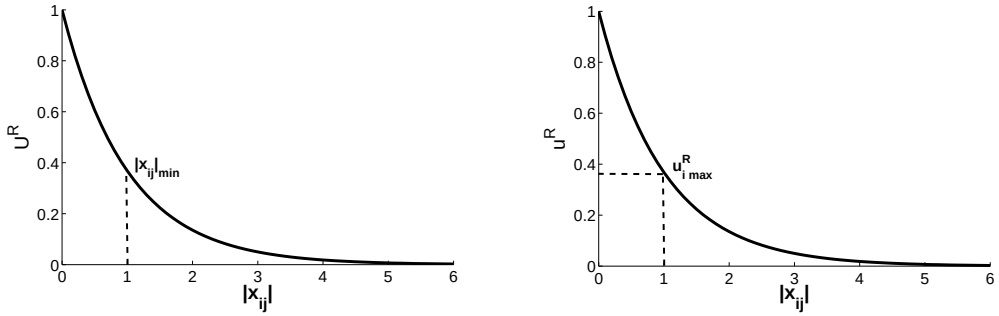

(i) (ii)

Figure 5.7: Repulsive potential ($C_r = 1, L_r = 1$) (i) U^R (ii) $\mathbf{u}^R$

The maximum control force is therefore;

$$|\mathbf{u}^R| = |\nabla_i U^R(\mathbf{x}_{ij})|_{max} = \frac{C_r}{L_r} \exp^{-|\mathbf{x}_{ij}|_{min}/L_r} \tag{5.10}$$

Referring back to **Section 3.2.1**, $|\mathbf{x}_{ij}|_{min}$ can be estimated by considering the case when one *agent* is moving at its maximum speed towards another *agent*. Assuming that the *agent* will brake to $V = 0$ at $\overline{S} = X_{min}/L_r$ then;

$$m \int_{V_m}^{0} V dV \;\; = \;\; C_r \int_{\infty}^{\overline{S}} \exp^{-\overline{S}} d\overline{S} \tag{5.11}$$

where V_m can assumed to be the initial speed of the *agent* if the dissipative constant σ is large.

It follows then that,

$$-\frac{1}{2} m V_m^2 \;\; = \;\; -C_r \left[\exp^{-\overline{S}} \right]_{\infty}^{\overline{S}} \tag{5.12}$$

The minimum separation is then estimated as;

$$X_{min} \;\; = \;\; L_r \ln \left(\frac{2C_r}{m V_m^2} \right) \tag{5.13}$$

Therefore, collision avoidance can be assured with the condition that $2Cr > mV_m^2$.

The dissipative force, $\mathbf{u}^d$ is bound by the maximum speed, V_m. Therefore;

$$|\mathbf{u}^d| = |\sigma \mathbf{v}_i|_{max} \leq \sigma V_m \tag{5.14}$$

The maximum total force that the actuator will generate is therefore;

$$|\mathbf{u}_i| \leqslant |\nabla_i U^S(\mathbf{x}_i)| + |\nabla_i U^R(\mathbf{x}_{ij})| + |\sigma \mathbf{v}_i| \tag{5.15}$$

If the steering potential is dominated by the hyperbolic term, the maximum control force is;

$$\begin{aligned} |\mathbf{u}_i| &\leqslant |\nabla_i U^S(\mathbf{x}_i)| + |\nabla_i U^R(\mathbf{x}_{ij})| + |\sigma \mathbf{v}_i| \\ &\leqslant \sqrt{C_h^2 + C_z^2} + \frac{C_r}{L_r} \exp^{-|\mathbf{x}_{ij}|_{min}/L_r} + \sigma V_m \end{aligned} \tag{5.16}$$

If, however, the steering potential is dominated by the exponential term, $|\nabla_i U^S(\mathbf{x}_i)|$ will have to be evaluated, with $|\nabla_i U^S(z_i)_{max}| = C_z$, $|\nabla_i U^R(\mathbf{x}_{ij})| = \frac{C_r}{L_r} \exp^{-|\mathbf{x}_{ij}|_{min}/L_r}$ and $|\sigma \mathbf{v}_i| = \sigma V_m$.

Therefore, it has been shown how to overcome the problem of actuator saturation in the swarm force model, developing a new bound bifurcating potential. This model can be easily extended to the first order velocity field case, placing bounds on the maximum velocity experienced.

5.2 Sensing Region

Although the artificial potential function method is theoretically elegant, Sigurd points out that the assumption that all *agents* in a swarm have information on all other *agents* is unrealistic as the number of *agents* increase [129]. To address this disadvantage in the APF method, the requirement of global knowledge will be removed and each *agent* will now have a sensing region [72, 77, 92], as shown in Eq. 5.17 and Fig. 5.8, that will still ensure collision avoidance and an equally spaced final formation.

$$U_{ij}^{R} = \left\{ \begin{array}{ll} \sum_{j,j\neq i} C_r \exp^{-|\mathbf{x}_{ij}|/L_r} & \text{if } |\mathbf{x}_{ij}| \leq Z_r \\ 0 & \text{if } |\mathbf{x}_{ij}| > Z_r \end{array} \right\} \tag{5.17}$$

where Z_r is the radius of repulsive zone of influence.

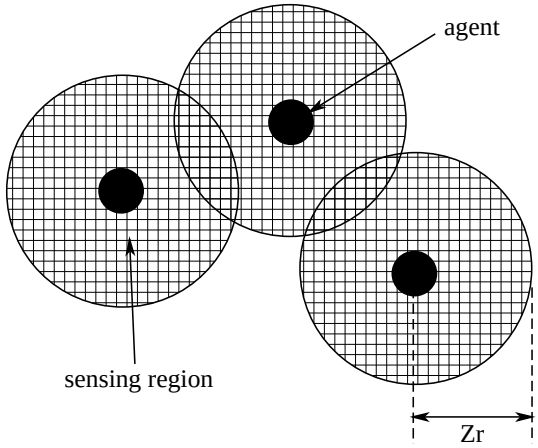

Figure 5.8: *Agent* repulsive potential sensing region

Therefore, as the repulsive potential only acts in a region surrounding each *agent*, scale separation will still hold true so that the system will move under the influence of a long-range steering potential but with short-range collision avoidance. While not a rigorous proof, related work by Tanner has shown that, by using graph theory, if the communication network between *agents* remains connected for all time the system is guaranteed to relax into the minimum of the potential [112].

5.3 Second Order Swarm

To demonstrate the use of the new bound control laws with local communication, consider a swarm of 20 *agents* that have mass of 10 kg, required to form three different formations; ring (diameter 50 m), cluster (diameter 16 m) and double ring (inner and outer diameters of 10 m and 20 m respectively). Each *agent* is given random initial conditions, with an initial speed equal to 0.1 ms^{-1} and $Z_r = 10$ m. The results are shown in Fig. 5.9, with Table 5.1 noting the value of the parameters during each stage.

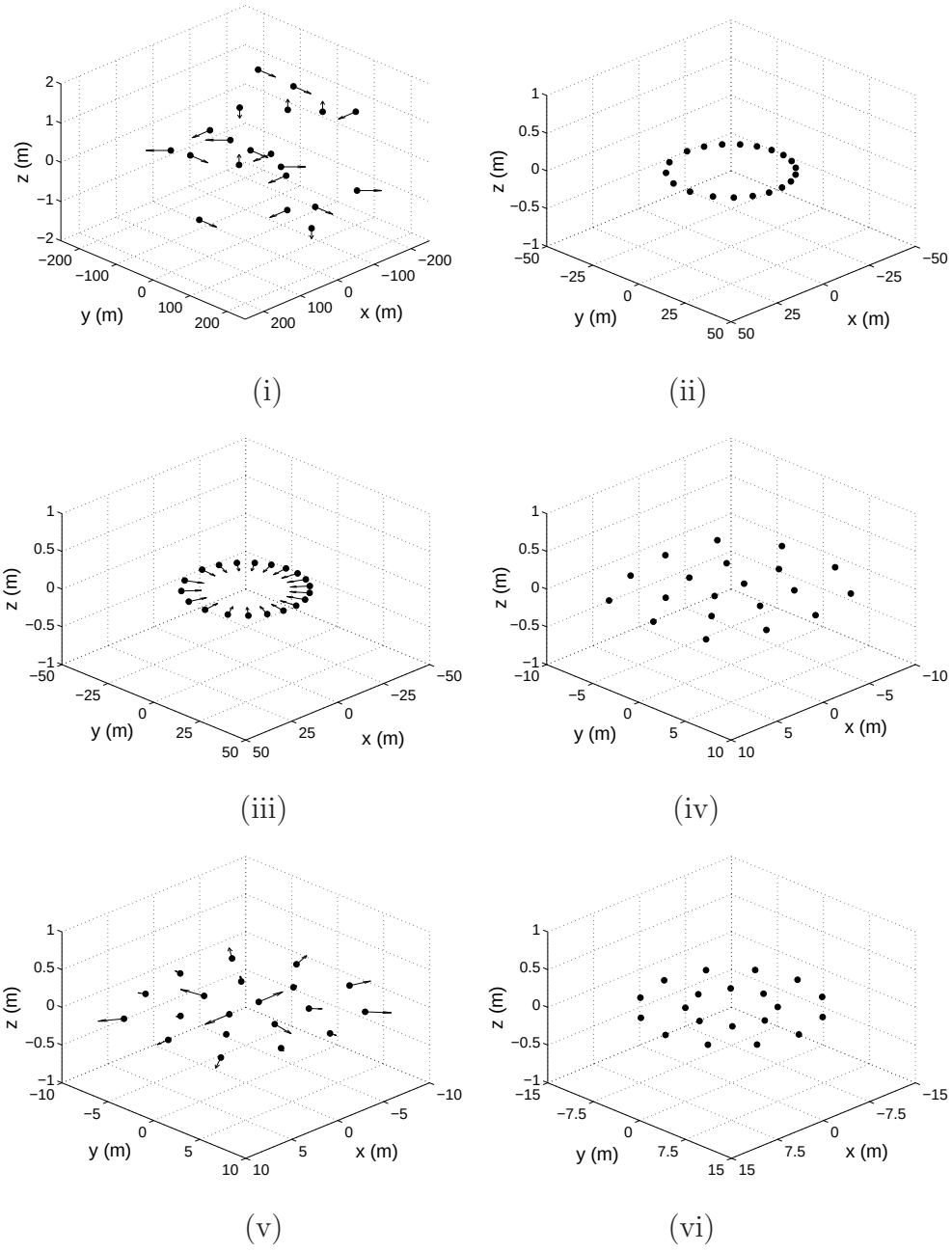

Figure 5.9: Second order swarm (i) initial conditions (ii) ring (iii) bifurcation (iv) cluster (v) bifurcation (vi) double ring

Table 5.1: Bound control constants

Formation	μ	r	C_h	C_e	L_e	C_z	C_r	L_r	σ
Ring	0	25	0.05	-	-	0.01	1	1	0.5
Cluster	0	0	0.02	-	-	0.05	1	1	0.5
Two rings	4	8	0.1	0.1	5	0.05	1	1	1

From the results shown in Fig. 5.9 it can be seen that the desired formations are achieved during the simulation. Figure 5.10 shows the separation distance between the *agents* indicating that they do not collide during the simulation, satisfying the assumption made regarding the minimum separation distance (estimated by $X_{min} = L_r \ln\left(\frac{2C_r}{mV_m^2}\right) = 3$ m).

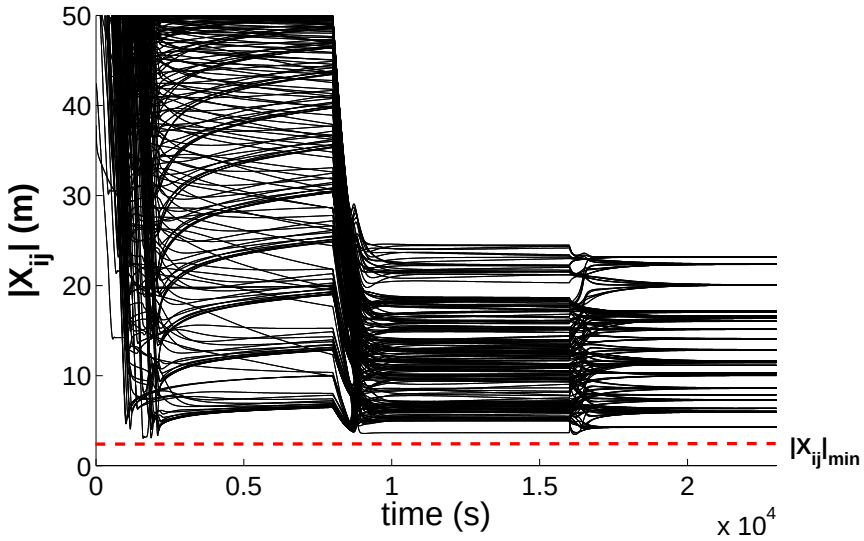

Figure 5.10: Second order swarm *agent* separation distance

During the formation of the first two stages, the maximum bound control force is equal to that given in Eq. 5.16. Similarly, in the formation of the double ring state when the steering potential is influenced by both the hyperbolic and exponential term, as the hyperbolic term dominates the maximum bound control force is also given by Eq. 5.16. The control force calculated from the simulation is shown in Fig. 5.11 (i)-(iii) and summarised in Table 5.2 with a comparison made to the analytical upper bound.

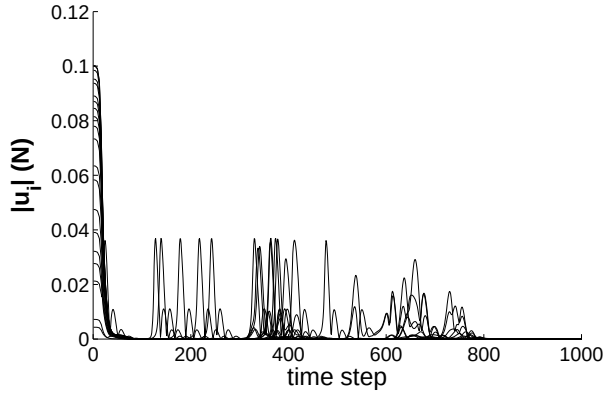

(i)

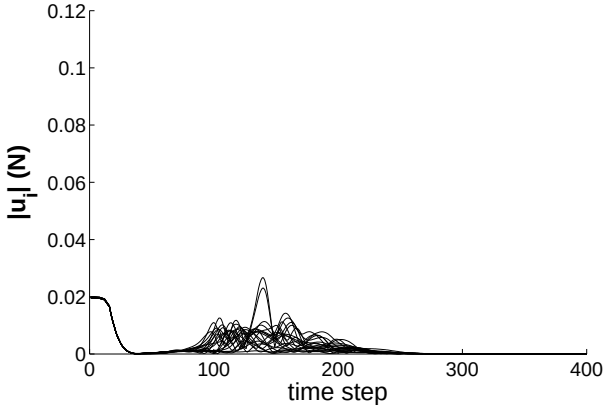

(ii)

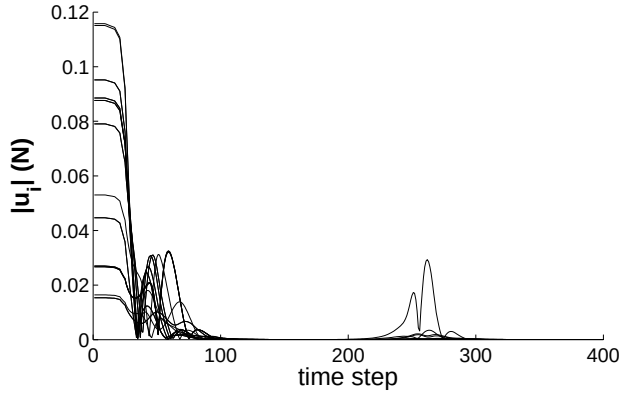

(iii)

Figure 5.11: Control force (i) ring (ii) cluster (iii) double ring

Table 5.2: Control force

Formation	Analytical $\|\mathbf{u}_i\|_{max}$ (N)	Simulated $\|\mathbf{u}_i\|_{max}$ (N)
Ring	0.15	0.1
Cluster	0.15	0.02
Two rings	0.26	0.115

From the results shown in Fig. 5.11 (i)-(iii), it can be seen that the maximum control force was found to occur at the start of the simulation of each formation, as at this point each *agent* will be moving at their maximum velocity. It can be seen that as each *agent* is driven to the equilibrium position, short range repulsion occurs as they interact, agreeing well with the scale separation explained in **Section 3.2.1**. From Table 5.2 it can also be seen that the maximum simulated control force during each formation is less than the maximum analytical bound control force. A real system could therefore be designed in such a way that actuator saturation can be avoided so that the desired patterns will form.

5.4 First Order Swarm

The new bound potential field is now demonstrated in a first order swarm system, where 10 *agents* are desired to form three formation patterns; double ring, ring and cluster, traveling at a constant final forward speed equal to 2 ms^{-1}. A swarm of 10 *agents* are considered to move in the $x-y$ plane. The desired bound velocity field acting in the $x-y$ plane will be transformed into a desired heading and velocity command, as described by Eq. 2.8 and 2.9. It will be assumed that the maximum speed of the *agents* is 3 ms^{-1}, with a maximum turning rate and acceleration defined as 90 $^o\text{s}^{-1}$ and 0.981 ms^{-2} respectively. Therefore, the desired velocity field is as follows;

$$\begin{aligned} \dot{x}_{desired} &= -\left[\frac{C_h(\rho_n - r)}{[(\rho_n - r)^2 + 1]^{0.5}} + 2\mu\frac{C_e}{L_e}(\rho_n - r)\exp^{-(\rho_n - r)^2/L_e}\right]\frac{x_n}{\rho_n} \\ &\quad + \sum_{j,j\neq i}\frac{C_r}{L_r}\frac{x_{ij}}{|\mathbf{x}_{ij}|}\exp^{-|\mathbf{x}_{ij}|/L_r} + u_c \end{aligned} \tag{5.18}$$

$$\begin{aligned}\dot{y}_{desired} &= -\left[\frac{C_h(\rho_n - r)}{[(\rho_n - r)^2 + 1]^{0.5}} + 2\mu\frac{C_e}{L_e}(\rho_n - r)\exp^{-(\rho_n - r)^2/L_e}\right]\frac{y_n}{\rho_n} \\ &\quad + \sum_{j,j\neq i}\frac{C_r}{L_r}\frac{y_{ij}}{|\mathbf{x}_{ij}|}\exp^{-|\mathbf{x}_{ij}|/L_r} \end{aligned} \tag{5.19}$$

where, as the *agents* are desired to move at a constant forward speed equal to u_c, x_i is replaced with $x_n = x_i - u_c t$ and ρ_i with $\rho_n = (x_n^2 + y_i^2)^{0.5}$ in the steering potential terms.

The desired command speed ($V_{desired}$) and heading angle ($\psi_{desired}$) are therefore;

$$V_{desired} = (\dot{x}_{desired}^2 + \dot{y}_{desired}^2)^{0.5} \tag{5.20}$$

$$\psi_{desired} = \arctan\left(\frac{\dot{y}_{desired}}{\dot{x}_{desired}}\right) \tag{5.21}$$

The state variables for the system are then defined as;

$$\begin{pmatrix} x_1 \\ x_2 \\ x_3 \\ x_4 \end{pmatrix} = \begin{pmatrix} V_i \\ \psi_i \\ x_i \\ y_i \end{pmatrix} \tag{5.22}$$

A system of first order equations of motion are then solved resulting in a commanded speed and heading angle that can be used to control each *agent*, as shown in Eq. 5.23.

$$\begin{pmatrix} \dot{x}_1 \\ \dot{x}_2 \\ \dot{x}_3 \\ \dot{x}_4 \end{pmatrix} = \begin{pmatrix} -\lambda_v(V_i - V_{desired}) & \text{if } |\dot{V}_i| \leq \dot{V}_{max} \\ -\lambda_\psi(\psi_i - \psi_{desired}) & \text{if } |\dot{\psi}_i| \leq \dot{\psi}_{max} \\ V_i\cos(\psi_i) & \\ V_i\sin(\psi_i) & \end{pmatrix} \tag{5.23}$$

where λ_v and λ_ψ are inverse time constants.

In addition as there is a bound on the maximum turning rate and speed there is turning circle associated with each *agent*. The radius of the turning circle is defined in Eq. 5.24, so that if the maximum speed and turning rate are 3

ms^{-1} and 90 ^{o} s^{-1} respectively, then the maximum turning radius, $R_{turning}$, is approximately 1.9 m.

$$R_{turning} = \frac{V_{max}}{\dot{\psi}_{max}} \tag{5.24}$$

In order to estimate that size of the repulsive free parameters, C_r and L_r, consider the case of 2 *agents* interacting through the repulsive potential only. Considering a simple 1-dimensional system with position coordinate, X, with $\frac{dX}{dt} \approx V_{max}$ for $X >> 0$. Therefore, assuming that at close separation distances the repulsive potential only acts, the dynamics of each *agent* is;

$$\frac{dX}{dt} = V_{max} - \frac{C_r}{L_r} \exp^{-\frac{X}{L_r}} \tag{5.25}$$

The minimum separation distance, X_{min}, will therefore be estimated by setting $\frac{dX}{dt} = 0$ so that,

$$X_{min} = L_r \ln\left(\frac{C_r}{V_{max} L_r}\right) \tag{5.26}$$

In order to ensure collision avoidance, the minimum separation distance between the *agents* in the formation must be $2 \times R_{turning} = 3.8$ m. The repulsive potential constants, C_r and L_r, are therefore chosen to ensure that the minimum separation, X_{min}, is greater than this value. Each *agent* is given random initial conditions in the $x - y$ plane, random initial heading angles and an initial speed of 2 ms^{-1}, with $Z_r = 10$ m. The free parameter values are summarised in Table 5.3.

Table 5.3: 1 parameter static bifurcation free parameters

$formation$	C_h	r	μ	C_e	L_e	C_r	L_r	λ_v	λ_ψ
double ring	1	15	5	1	6	34	5	0.5	0.5
ring	1	25	0	-	-	34	5	0.5	0.5
cluster	1	0	0	-	-	34	5	0.5	0.5

From the results shown in Fig. 5.12 (i)-(iv) it can be seen that the swarm successfully creates the desired formations, with Fig. 5.13 showing that no collisions occur during the simulation.

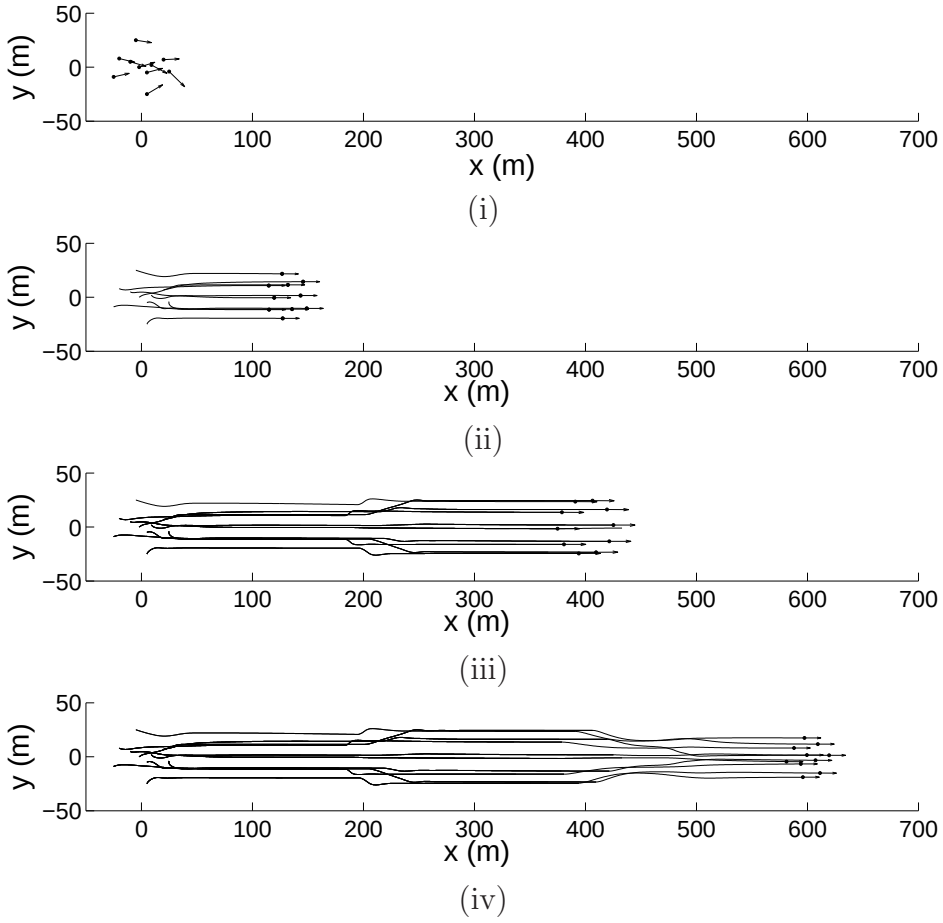

Figure 5.12: First order swarm (i) initial conditions (ii) double ring ($r_o = 18$ m, $r_i = 12$ m) (iii) ring ($r = 25$ m) (iv) cluster ($r = 20$ m)

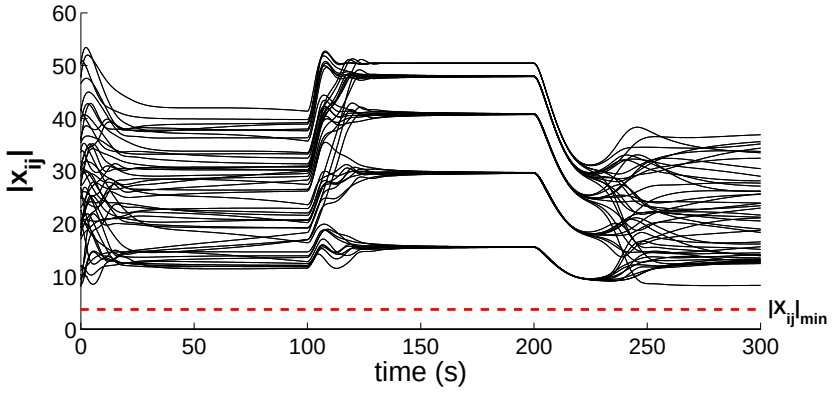

Figure 5.13: First order swarm *agent* separation distance

5.5 Advantages of Swarm System

5.5.1 Robustness of the Model

As one of the desirable characteristics of the model developed is that the swarm of *agents* are robust to failures, Fig. 5.14 demonstrate this for a swarm of 30 *agents*.

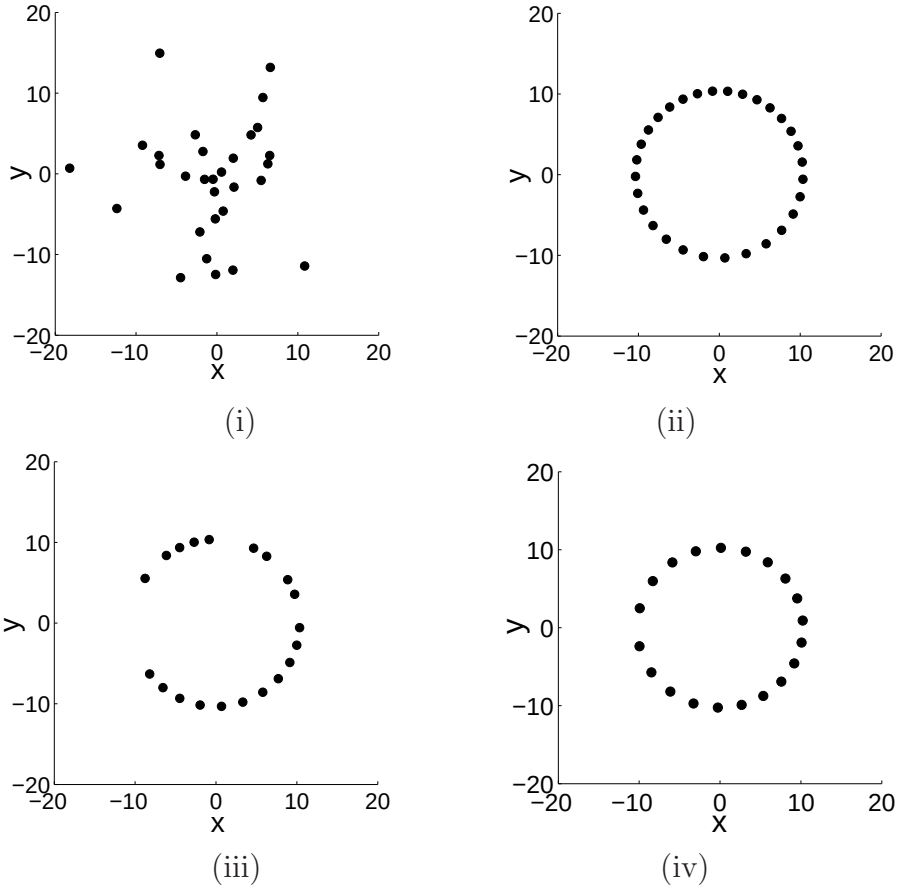

Figure 5.14: Robustness of the model (i) random initial conditions for 30 *agents* (ii) ring formation ($\mu = -2$, $r = 10$, $C_r = 3$, $L_r = 5$) (iii) failure of 10 *agents* (iv) reconfiguration of the formation

As can be seen from the results the swarm successfully falls into a ring pattern with radius 10 m. Figure 5.14 (iii) shows the random failure of 10 *agents* with the assumption that once they fail they are completely removed from the system. The system will then autonomously reconfigure to a new ring configuration, as shown in Fig. 5.14 (iv). To further improve this, future work will consider the case when the *agents* cannot be assumed to be removed or have partial failure.

5.5.2 Scalable Formation

Another advantage of the model developed is that the system scales well as the number of *agents* increase, as shown in Fig. 5.15.

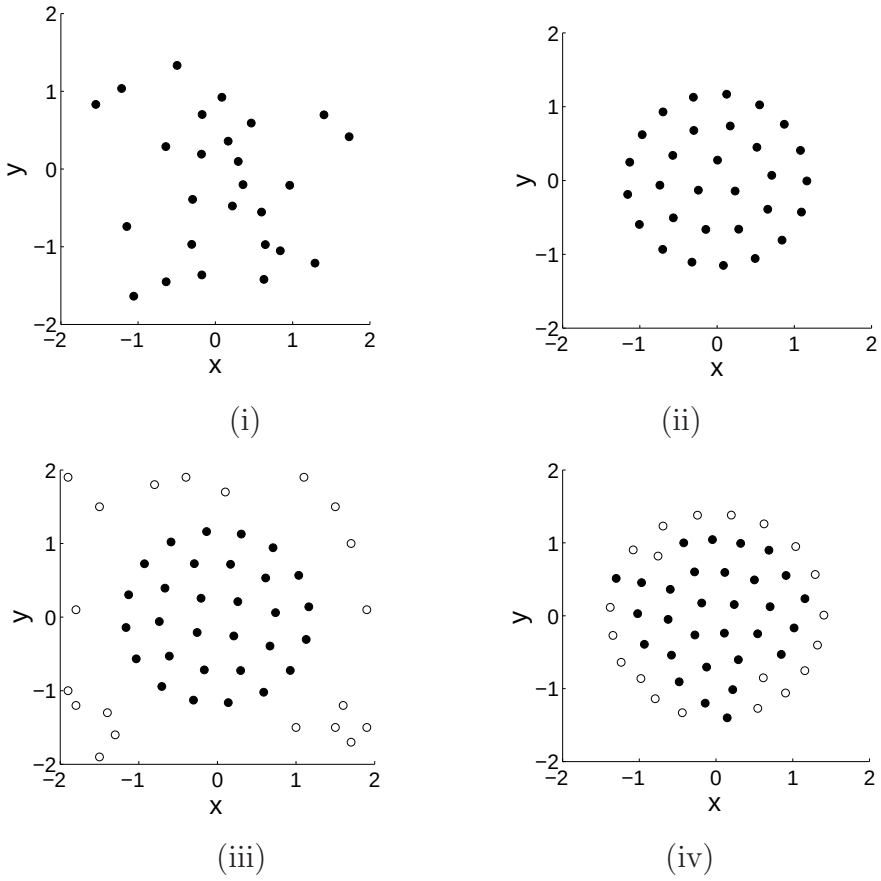

Figure 5.15: Scalable formation (i) random initial conditions for 30 *agents* (ii) cluster formation, $\mu = -2$, $r = 0$, $C_r = 1$ and $L_r = 0.5$ (iii) addition of 20 *agents* (iv) reconfiguration of the cluster formation

As can be seen from the results the system will autonomously reconfigure with the addition of new *agents*. In addition, as the swarm can be based on local communication, the control required by each *agent* will not alter significantly with the addition of more *agents*, allowing the swarm model to be considered scalable.

5.5.3 Flexible Formations

The final advantage of the model is that the swarm can be shown to avoid obstacles and also alter its pattern through a simple parameter change. As an example, consider the case when 30 *agents* are desired to form a cluster pattern, autonomously manoeuver to avoid circular obstacles (represented by the obstacle potential function shown in Eq. 2.22) and then form a ring pattern.

From the results, shown in Fig. 5.16, it can be seen that from random initial conditions the swarm successfully forms the cluster pattern. It then approaches the obstacles and autonomously manoeuvres to avoid them and then finally bifurcates to forms the desired ring pattern.

As discussed previously, the stability of the system has been investigated so that desired patterns are achieved. Each *agent* moves under the influence of the long-range steering potential with short-range collision avoidance, effectively treating other *agents* in the swarm as obstacles and moving to avoid them. In the case shown here, although there is no guarantee provided that *agents* will avoid the obstacles, if the *agents* are able to sense other objects (either stationary or moving), they will be dominated by the repulsive collision avoidance potential created by the obstacle until that term is negligible, assuming that they can manoeuvre around the obstacle. Once this occurs the *agents* will again act under the influence of the formation dynamics and create the desired formation, as shown in Fig. 5.16.

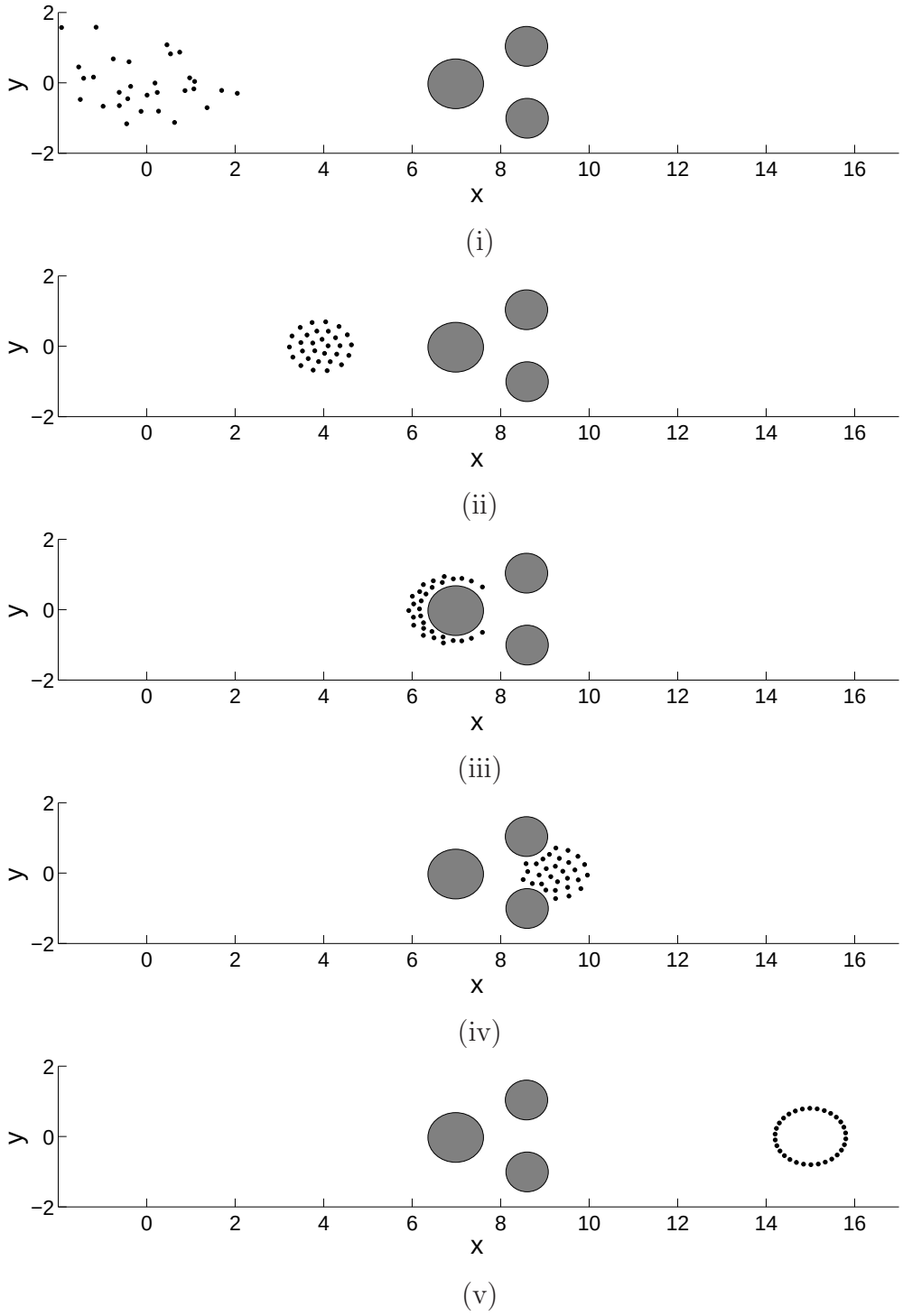

Figure 5.16: Flexible formation (i) random initial conditions (ii) cluster (iii) obstacle avoidance (iv) obstacle avoidance (v) ring

5.6 Summary

This chapter has considered two ways in which the utility of the proposed swarming model can be improved. Firstly, the issue of actuator saturation was addressed, giving an example how a combined hyperbolic-exponential potential can be used to achieve a bound bifurcating potential field. The issue of communication constraints was also addressed by assuming that the repulsive potential can now only act in a region close to each *agent*. To demonstrate this both a second and first order system were considered. Finally, the advantages of the model were demonstrated showing that the system is robust, scalable and flexible. Future work will investigate other real world effects such as; consideration of computational load on each *agent*, communication time-delays, non-holonomic effects and robustness to partial *agent* failure.

Chapter 6

Spacecraft Formation Flying

This chapter considers the implementation of the proposed second order force swarm model, as discussed in **Chapter 5**, for spacecraft formation flying missions. Firstly, there is a brief overview of spacecraft formation flying, describing why the swarming model is useful. Spacecraft formation flying in both Low-Earth-Orbit (LEO) and deep-space are considered in **Sections 6.2** and **6.3** respectively. For LEO, the swarm model is adapted considering the two-body problem, whereas for deep-space missions the swarm of spacecraft are developed based on the three-body problem, operating at the Sun-Earth L_2 position.

6.1 Introduction

Many future spacecraft missions may consist of multiple, autonomous spacecraft flying in formation, driven by commercial, military and scientific requirements [55]. A distributed satellite system in LEO could be used to improve communication capabilities on Earth, with advantages such as fault tolerance as individual spacecraft failure does not necessarily imply mission failure. In addition, there is increased mission flexibility as the formation can autonomously reconfigure, as well as the potential for mass production of small, identical spacecraft, reducing manufacturing and launch costs. The challenging aspects include the development of reliable, autonomous control laws that can ensure collision avoidance, as well technologically meeting the requirements associated with such systems. This may include accurate sensors required for precise determination of the state of the system or new forms of propulsion.

The field of distributed spacecraft systems can be divided into three areas; constellation, cluster or leader-follower. In the constellation case, the spacecraft are positioned relative to an object (such as the Earth), whereas a cluster formation is positioned relative to each other. The leader-follower case considers two spacecraft, where the follower spacecraft tracks the leader, maintaining a formation.

At present there are several current and future planned SFF missions. These missions can be split into those that will operate in LEO or deep-space. Although a small number of spacecraft in LEO could be controlled separately by a ground station on Earth, as the operational distance from the Earth increases, spacecraft formation flying becomes a more viable option. Examples of current LEO SFF missions include the leader-follower EO-1 and Landsat 7 mission, as discussed in **Section 1.3.2**. Also, COSMIC/FORMOSAT-3, launched in 2006, is a joint Taiwan/US science constellation mission consisting of six LEO satellites that are used for space weather monitoring, global weather and climate change research [130], as shown in Fig. 6.1 (i). For deep-space SFF many missions are based around the deployment of the formation at Lagrange points, which are equilibrium positions where the gravitational and centrifugal forces of two massive bodies balance. Examples of future missions are DARWIN that would consist of 4 spacecraft located at the Sun-Earth L_2 position, as discussed in **Section 1.3**. The Terrestrial Planet Finder Interferometer (TPF-I) is an example of a cluster formation of 4 spacecraft in a halo orbit about the Sun-Earth L_2 position, that will be used to study all aspects of planets outside of our solar system, as shown in Fig. 6.1 (ii).

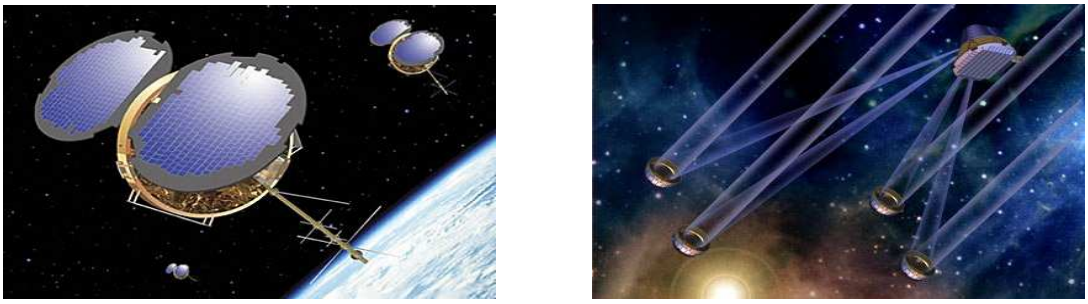

(i) (ii)

Figure 6.1: Spacecraft formation flying missions (i) COSMIC/FORMOSAT-3 constellation (NASA) (ii) TPF-I cluster (NASA)

This chapter aims to demonstrate that the swarm control model can be adapted

to allow spacecraft formation flying in both LEO and deep-space. To demonstrate this, linear equations of motion for both the two-body and three-body problem are discussed, with higher fidelity models considered as part of future work.

6.2 Two Body Problem

The two-body problem is concerned with the motion of two bodies that interact under their mutual gravitation. For a spacecraft orbiting the Earth it is assumed that both the spacecraft and Earth can be modelled as point masses and also perturbation forces, such as aerodynamic effects, can be ignored. Under these assumptions, the spacecraft and Earth system is shown in Fig. 6.2.

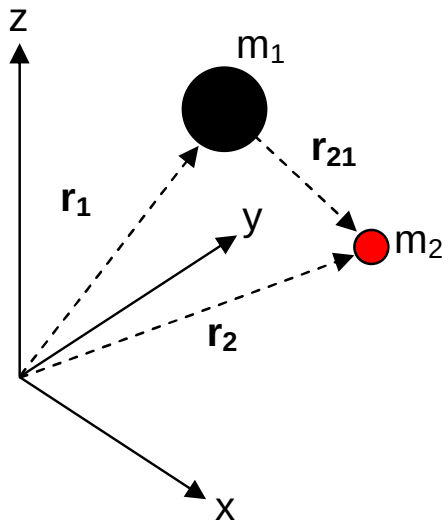

Figure 6.2: Two-body problem

From Fig. 6.2, the Earth and spacecraft are defined with mass, m_1 and m_2 at a position vector, $\mathbf{r}_1$ and $\mathbf{r}_2$ respectively. The inertial equations of motion of each mass can be expressed as;

$$m_1\ddot{\mathbf{r}}_1 = \frac{Gm_1m_2}{|\mathbf{r}_{21}|^3}\mathbf{r}_{21} \tag{6.1}$$

$$m_2\ddot{\mathbf{r}}_2 = -\frac{Gm_1m_2}{|\mathbf{r}_{21}|^3}\mathbf{r}_{21} \tag{6.2}$$

where, $\mathbf{r}_{21} = \mathbf{r}_2 - \mathbf{r}_1$ is position vector of the spacecraft relative to the Earth and G is the universal gravitational constant ($6.673 \times 10^{-11}\text{m}^3\text{kg}^{-1}\text{s}^{-2}$).

A gravitational coefficient μ_g is defined as;

$$\mu_g = G(m_1 + m_2) \tag{6.3}$$

It will be assumed that the mass of the Earth is much greater than the spacecraft ($m_1 >> m_2$), so that Eq. 6.4 can be approximated by;

$$\mu_g \approx Gm_1 \tag{6.4}$$

where, the mass of the Earth is assumed to be 5.9742×10^{24} kg [131].

Taking the difference between Eq. 6.1 and 6.2, the equation of motion of m_2 relative to m_1 is;

$$\ddot{\mathbf{r}}_{21} = -\frac{\mu_g}{|\mathbf{r}_{21}|^3}\mathbf{r}_{21} \tag{6.5}$$

Under the assumption of a spherical Earth, initial conditions are choosen such that a circular orbit is achieved [121], as shown in Fig. 6.3. The initial conditions are; $[x_o, y_o, z_o]^T = [r_o, 0, 0]^T$ and $[v_{xo}, v_{yo}, v_{zo}]^T = [0, \sqrt{\frac{\mu_g}{r_o}}, 0]^T$, where $r_o = r_{earth} + r_{sc}$ is the initial radius of the spacecraft from the centre of the Earth, with assumed radius of the Earth $r_{earth} = 6371$ km [121] and initial altitude $r_{sc} = 1000$ km.

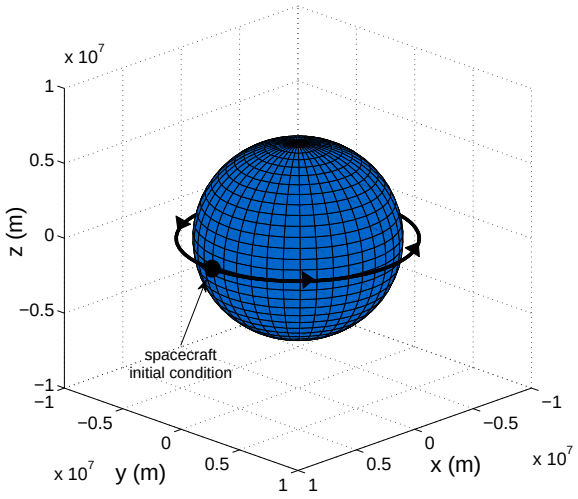

Figure 6.3: Relative dynamics in an inertial coordinate frame

6.2.1 Relative Motion Dynamics

In this section the relative dynamics of two spacecraft, in close proximity, traveling around a spherical Earth are considered. It is assumed that the target spacecraft is in a circular orbit around the Earth with an orbital radius R_t and orbital rate $\omega_e = \sqrt{\mu_g/R_t^3}$. A reference frame with (x, y, z) coordinates with basis vector $(\vec{i}, \vec{j}, \vec{k})$ is attached to the centre of mass of the target vehicle that orbits with an angular velocity, $\vec{\omega} = \omega_e \vec{K}$ with respect to the inertial frame of reference [126], as summarised in Fig. 6.4.

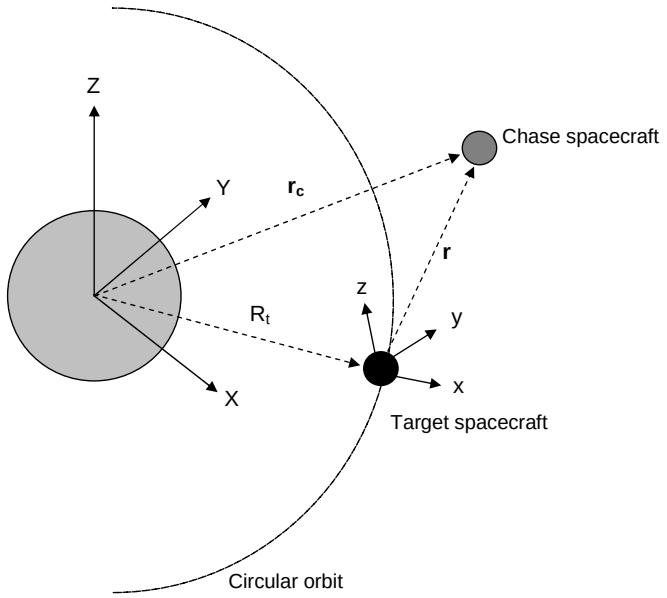

Figure 6.4: Motion of spacecraft orbiting the Earth

Assuming that there are no external forces or disturbances acting on each spacecraft and letting the position of the chase vehicle relative to the target vehicle be $\mathbf{r}$, then the motion relative to the Earth's centre for the target and chase spacecraft are given by Eq. 6.6 and 6.7 respectively [132];

$$\ddot{\mathbf{r}}_t + \frac{\mu}{|\mathbf{r}_t|^3}\mathbf{r}_t = 0 \tag{6.6}$$

$$\ddot{\mathbf{r}}_c + \frac{\mu}{|\mathbf{r}_c|^3}\mathbf{r}_c = 0 \tag{6.7}$$

where, $|\mathbf{r}_t| = R_t$ and $|\mathbf{r}_c| = [(R_t + x)^2 + y^2 + z^2]^{0.5}$.

Taking the difference between the equations of motion of the chase and target spacecraft results in;

$$\ddot{\mathbf{r}} + \frac{\mu}{|\mathbf{r}_t + \mathbf{r}|^3}(\mathbf{r}_t + \mathbf{r}) - \frac{\mu}{|\mathbf{r}_t|^3}\mathbf{r}_t = 0 \tag{6.8}$$

where, $\mathbf{r} = \mathbf{r}_c - \mathbf{r}_t$.

Assuming that the orbital radius of the target spacecraft is much larger than the relative distance between the spacecraft ($|\mathbf{r}_t| >> |\mathbf{r}|$), the non-linear relative equations of motion can be linearised to form the Clohessy-Wiltshire or Hill's (HCW) relative equations of motion as follows;

$$\ddot{x} - 2\omega_e\dot{y} - 3\omega_e^2 x = 0 \tag{6.9}$$

$$\ddot{y} + 2\omega_e\dot{x} = 0 \tag{6.10}$$

$$\ddot{z} + \omega_e^2 z = 0 \tag{6.11}$$

The closed form solutions of the HCW equations are given by Eq. 6.12-6.14 [132].

$$x(t) = \frac{\dot{x}_0}{\omega_e}\sin(\omega_e t) - \left(3x_0 + \frac{2\dot{y}_0}{\omega_e}\right)\cos(\omega_e t) + \left(4x_0 + \frac{2\dot{y}_0}{\omega_e}\right) \tag{6.12}$$

$$y(t) = \frac{2\dot{x}_0}{\omega_e}\cos(\omega_e t) + \left(6x_0 + \frac{4\dot{y}_0}{\omega_e}\right)\sin(\omega_e t) - (6\omega_e x_0 + 3\dot{y}_0)t - \frac{2\dot{x}_0}{\omega_e} + y_0 \tag{6.13}$$

$$z(t) = \frac{\dot{z}_0}{\omega_e}\sin(\omega_e t) + z_0\cos(\omega_e t) \tag{6.14}$$

where, $[x_o, y_o, z_o]^T$ and $[\dot{x}_o, \dot{y}_o, \dot{z}_o]^T$ are the position and velocity initial conditions at $t = 0$ respectively.

From Eq. 6.13 it can be seen that the 3rd term of $y(t)$ becomes unbound with time, so that if the constraint $2\omega_e x_0 + \dot{y}_0 = 0$ is satisfied, it will ensure that the chase spacecraft does not drift away from the leader. Using this constraint the HCW admit periodic solutions given by Eq. 6.15-6.20 [133];

$$x = \frac{c_1}{2}\sin(\omega_e t + \alpha_o) \tag{6.15}$$

$$y = c_1\cos(\omega_e t + \alpha_0) + c_3 \tag{6.16}$$

$$z = c_2\sin(\omega_e t + \beta_0) \tag{6.17}$$

$$\dot{x} = \frac{c_1}{2}\omega_e\cos(\omega_e t + \alpha_o) \tag{6.18}$$

$$\dot{y} = -c_1\omega_e\sin(\omega_e t + \alpha_0) \tag{6.19}$$

$$\dot{z} = c_2\omega_e\cos(\omega_e t + \beta_0) \tag{6.20}$$

where, $c_1, c_2, c_3, c_4, \alpha_0$ and β_0 are constant, determined from the initial conditions.

The initial conditions that satisfy Eq. 6.15-6.20 at time, $t = 0$, are given by Eq. 6.21-6.26;

$$x_0 = \frac{c_1}{2}\sin(\alpha_o) \tag{6.21}$$

$$y_0 = c_1\cos(\alpha_0) + c_3 \tag{6.22}$$

$$z_0 = c_2\sin(\beta_0) \tag{6.23}$$

$$\dot{x}_0 = \frac{c_1}{2}\omega_e\cos(\alpha_o) \tag{6.24}$$

$$\dot{y}_0 = -c_1\omega_e\sin(\alpha_0) \tag{6.25}$$

$$\dot{z}_0 = c_2\omega_e\cos(\beta_0) \tag{6.26}$$

Depending upon the choice of free-parameters, c_1, c_2, c_3, α_0 and β_0, a variety of bounded relative orbits can be achieved. Orbits known as projected circular orbits

(PCO) can be achieved by choosing $c_1, c_2 = \rho_c$, $c_3 = 0$ and $\alpha_0 = \beta_0$ so that the relative orbit of the chase spacecraft in the $y - z$ plane is circular with radius, ρ_c. The initial conditions are then;

$$x_0 = \frac{\rho_c}{2}\sin(\alpha_0) \tag{6.27}$$

$$y_0 = \rho_c \cos(\alpha_0) \tag{6.28}$$

$$z_0 = \rho_c \sin(\alpha_0) \tag{6.29}$$

$$\dot{x}_0 = \frac{\rho_c}{2}\omega_e \cos(\alpha_0) \tag{6.30}$$

$$\dot{y}_0 = -\rho_c \omega_e \sin(\alpha_0) \tag{6.31}$$

$$\dot{z}_0 = \rho_c \omega_e \cos(\alpha_0) \tag{6.32}$$

so that,

$$y^2 + z^2 = \rho_c^2 \tag{6.33}$$

As an example, consider the case where it is desired that the chase spacecraft be in a PCO, $\rho_c = 1000$ m in the $y - z$ plane, about the target spacecraft orbiting at a radius, $R_t = 6671$ km (300 km above the Earth's surface). Therefore, the initial conditions for the chase spacecraft are as follows;

$$\begin{bmatrix} x_o \\ y_o \\ z_o \\ \dot{x}_o \\ \dot{y}_o \\ \dot{z}_o \end{bmatrix} = \begin{bmatrix} 0 \\ -1000 \text{ m} \\ 0 \\ -0.5795 \text{ ms}^{-1} \\ 0 \\ -1.1590 \text{ ms}^{-1} \end{bmatrix} \tag{6.34}$$

where, $\alpha_0 = 180^o$.

Figure 6.5 shows the motion of the chase spacecraft relative to the target spacecraft, with Fig. 6.6 showing the projection of the orbit onto the $y-z$ plane. As can be seen from the results, the chase spacecraft achieves the desired bound circular periodic orbit in the $y-z$ plane with radius, $\rho_c = 1000$ m.

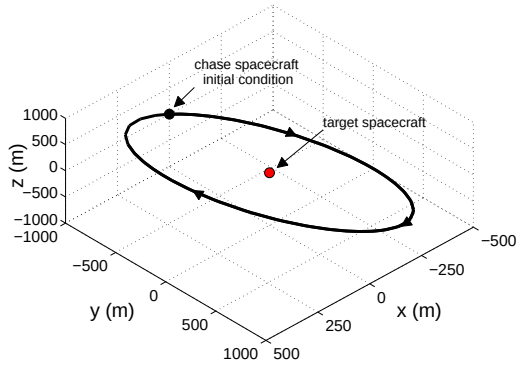

Figure 6.5: Motion of the chase spacecraft relative to the target spacecraft

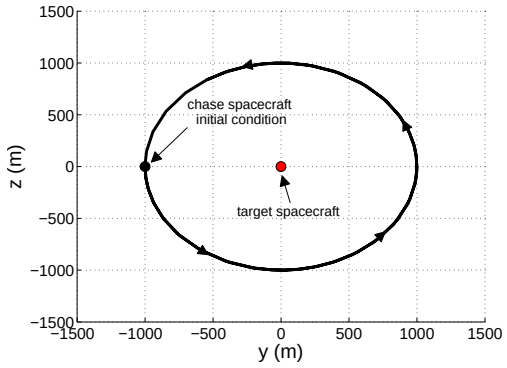

Figure 6.6: Motion of the chase spacecraft relative to the target spacecraft projected in $y-z$ plane

Therefore, it has been shown that if the initial conditions of a spacecraft are choosen to satisfy the PCO initial conditions, then a spacecraft can follow a circular periodic orbit about a target spacecraft. The bifurcating potential field will now be used to force a swarm of spacecraft onto a desired equally spaced PCO from arbitrary initial conditions and then bifurcate to a different equally spaced periodic orbit. To force the spacecraft onto a desired orbit with radius, ρ_c, in the $y-z$ plane, the following steering potential, shown in Eq. 6.35, will be used;

$$U^S(\mathbf{x}_i) = C_x \left[(x_i - \frac{\rho_c}{2})^2 + 1\right]^{0.5} + C_h \left[(\rho_{yz} - \rho_c)^2 + 1\right]^{0.5} + \mu C_e \exp^{-(\rho_{yz}-\rho_c)^2/L_e} \tag{6.35}$$

where, $\rho_{yz} = (y_i^2 + z_i^2)^{0.5}$.

From Eq. 6.30-6.32 it is known that the desired velocity of the spacecraft to orbit on the PCO is a function of α_0, ρ_c and ω_e, so that if the spacecraft were to start far from the desired PCO, a simple first order controller could be used to drive the system to the desired velocity, with the steering potential forcing the system to the desired orbit. The HCW equations of motion given in Eq. 6.9-6.11 are re-cast into the swarm model, including the new forcing terms;

$$\ddot{x}_i - 2\omega_e \dot{y}_i - 3\omega_e^2 x_i = -\frac{\partial U^R}{\partial x_i} - \frac{\partial U^S}{\partial x_i} - \lambda_v (\dot{x}_i - \dot{x}_d) \tag{6.36}$$

$$\ddot{y}_i + 2\omega_e \dot{x}_i = -\frac{\partial U^R}{\partial y_i} - \frac{\partial U^S}{\partial y_i} - \lambda_v (\dot{y}_i - \dot{y}_d) \tag{6.37}$$

$$\ddot{z}_i + \omega_e^2 z_i = -\frac{\partial U^R}{\partial z_i} - \frac{\partial U^S}{\partial z_i} - \lambda_v (\dot{z}_i - \dot{z}_d) \tag{6.38}$$

where, $\dot{x}_d = \frac{\rho_c}{2}\omega_e \cos(\alpha_0)$, $\dot{y}_d = -\rho_c \omega_e \sin(\alpha_0)$, $\dot{z}_d = \rho_c \omega_e \cos(\alpha_0)$ and λ_v is an inverse time constant determining the response of the system.

Consider a formation of 5 spacecraft that have mass 10 kg and minimum separation distance, $|\mathbf{x}_{ij}|_{min} = 3$ m, that are required to achieve three different PCOs with radius of 5 m, 10 m and 15 m. Each spacecraft are given random initial positions (satisfying the constraint that $|\mathbf{x}_{ij}|_{initial} > 3$ m), with an initial maximum speed of 0.1 ms^{-1}, sensing radius, $Z_r = 10$ m and maximum actuator force of 2 N. To satisfy these conditions, Table 6.1 summarises the bound potential constants used in each formation.

Table 6.1: LEO SFF bound constants

Formation	μ	ρ_c	C_h	C_x	C_e	L_e	C_r	L_r	λ_v
A	0	5	0.3	0.3	-	-	4	0.8	10
B	0	10	0.3	0.3	-	-	4	2	10
C	0	15	0.3	0.3	-	-	4	3	10

From **Section 5.1**, the maximum bound control force from Eq. 6.36-6.38 can be estimated as follows;

$$|\mathbf{u}^S| = |\nabla_i U^S(\mathbf{x}_i)|_{max} = \sqrt{(C_x^2 + C_h^2)} \tag{6.39}$$

$$|\mathbf{u}^R| = |\nabla_i U^R(\mathbf{x}_{ij})|_{max} = \frac{C_r}{L_r} \exp^{-|\mathbf{x}_{ij}|_{min}/L_r} \tag{6.40}$$

$$|\mathbf{u}^d| = |\lambda_v(\dot{\mathbf{x}}_i - \dot{\mathbf{x}}_d)|_{max} = \lambda_v(|\dot{\mathbf{x}}|_{max} - |\dot{\mathbf{x}}_d|_{min}) = \lambda_v(|\dot{\mathbf{x}}|_{max} - \rho_c\omega_e) \tag{6.41}$$

The results of the simulation are shown in Fig. 6.7-6.9 indicating that the formation of spacecraft can successfully create desired patterns and autonomously reconfigure between them.

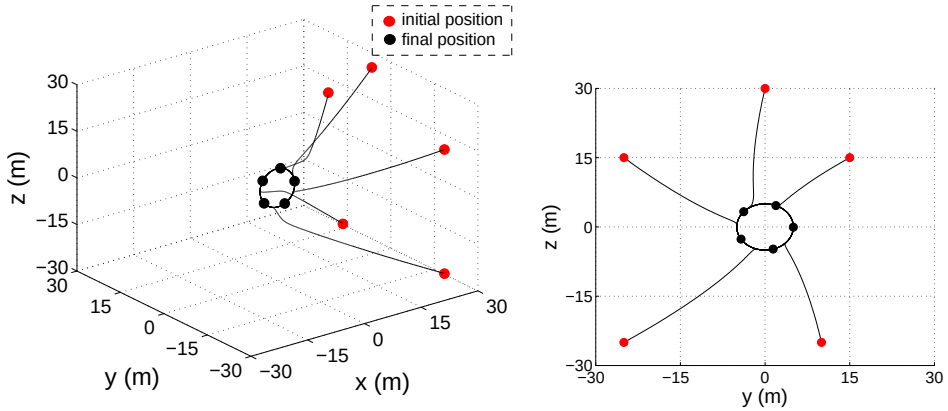

(i) (ii)

Figure 6.7: Formation A - $\rho_{ca} = 5$ m (i) $x - y - z$ plane (ii) $y - z$ plane

Figure 6.10 confirms that the desired PCO are achieved in each formation and that collision avoidance is ensured throughout the simulation.

Figure 6.11 shows the velocity profile of each spacecraft in the x, y and z directions, with the results showing that the swarm of spacecraft are successfully driven to the desired velocity once in the equilibrium formation.

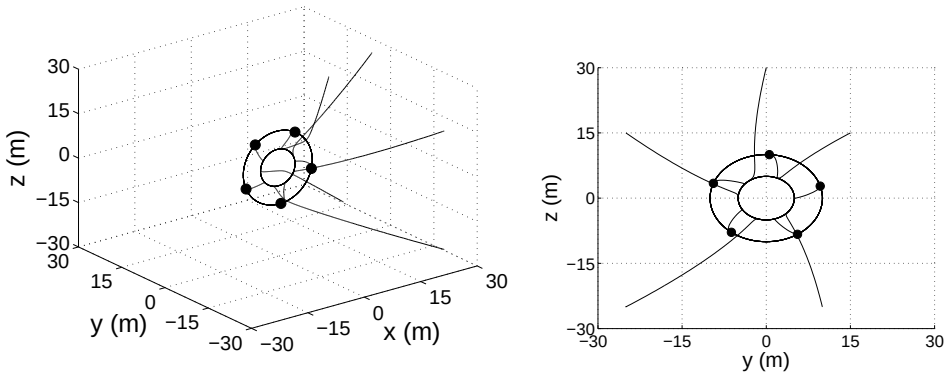

(i) (ii)

Figure 6.8: Formation B - $\rho_{cb} = 10$ m (i) $x-y-z$ plane (ii) $y-z$ plane

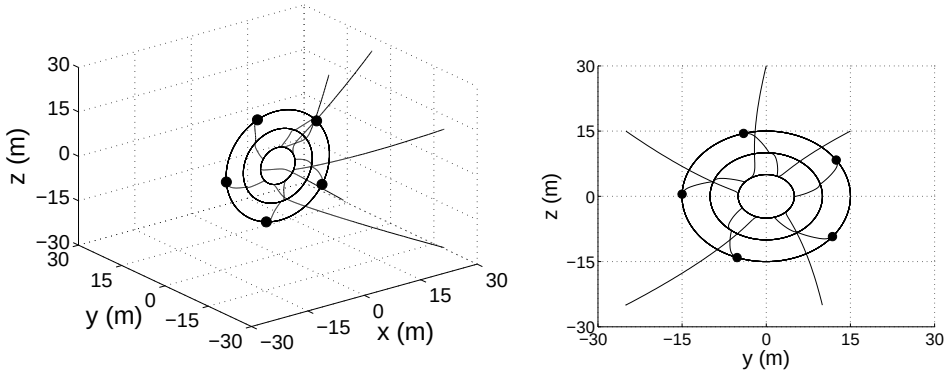

(i) (ii)

Figure 6.9: Formation C - $\rho_{cc} = 15$ m (i) $x-y-z$ plane (ii) $y-z$ plane

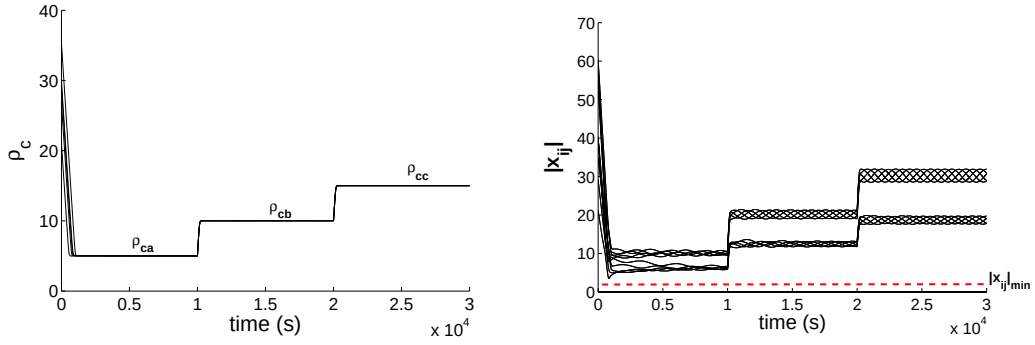

(i) (ii)

Figure 6.10: Formation A, B and C (i) relative orbit radius (ii) separation distance

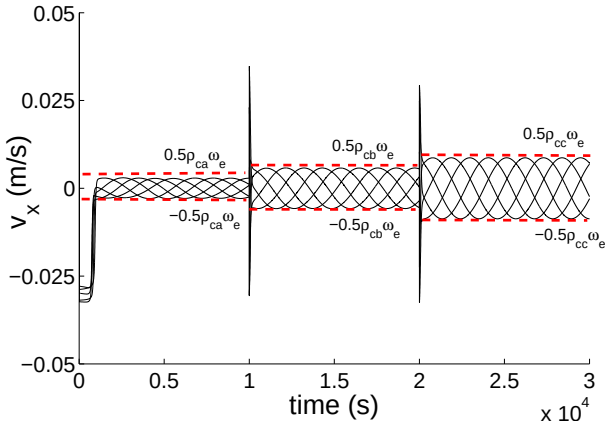

(i)

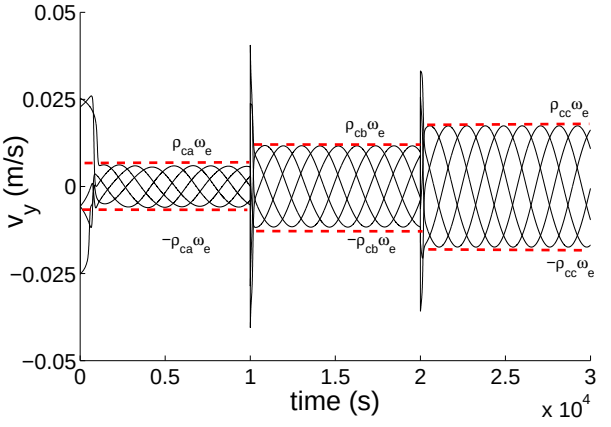

(ii)

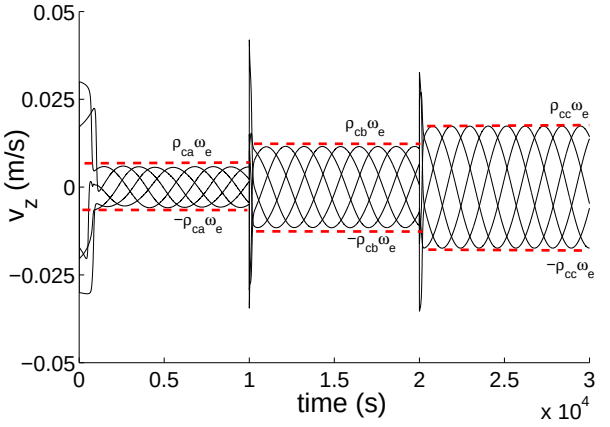

(iii)

Figure 6.11: Formation velocity (i) v_x (ii) v_y (iii) v_z

Figure 6.12 shows the actuator force acting on each spacecraft. As expected the largest force occurs at the beginning of each formation, driving each spacecraft to the desired PCO. Once in this condition the actuator force decays to zero and the swarm of spacecraft follows an equally spaced periodic orbit. Table 6.2 shows that the simulated swarm actuator force is lower than the analytical bound force satisfying the constraint that the actuator force should be less than 2 N.

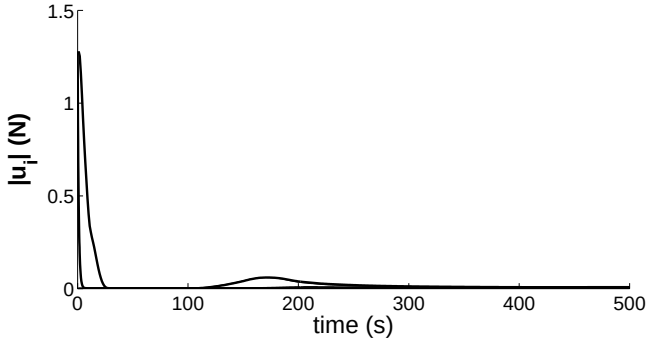

(i)

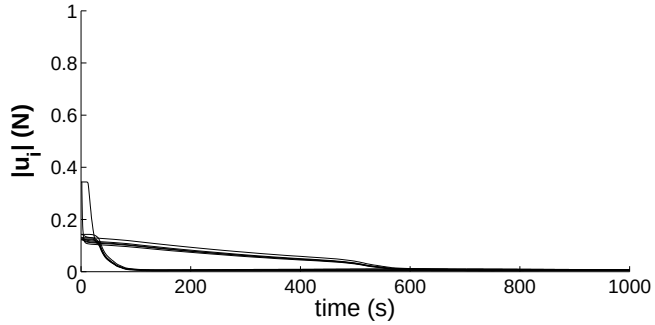

(ii)

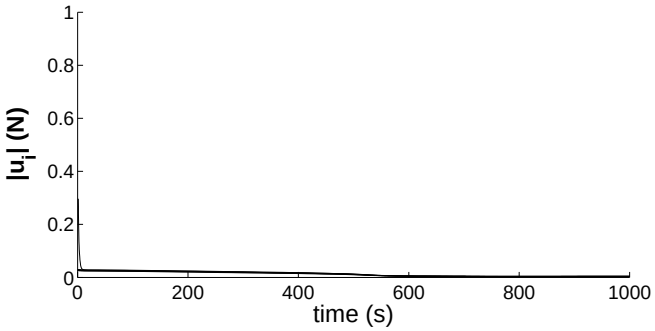

(iii)

Figure 6.12: Actuator force (i) formation A (ii) formation B (iii) formation C

Table 6.2: LEO SFF control force

Formation	Analytical $\|\mathbf{u}_i\|_{max}$ (N)	Simulated $\|\mathbf{u}_i\|_{max}$ (N)
A	1.4	1.3
B	1.3	0.3
C	1.2	0.3

This section has considered the implementation of the bifurcating swarm system in LEO orbit, taking advantage of the HCW linear, unperturbed equations of relative motion that yield closed periodic solutions. It was shown that using the bound bifurcating swarm potentials, that a swarm of spacecraft can be driven safely towards a desired periodic orbit, relaxing into an equally spaced rotating ring formation about a target spacecraft. Potential applications of these formations include simultaneous scientific data gathering that could be used to forecast weather or make gravity field measurements, with the swarm being able to reconfigure to meet different mission requirements.

The linear, unperturbed HCW equations of motion provide a starting point to illustrate the implementation of the swarm model for space formation flying in LEO. There are several real world, non-linear effects that can be considered to improve the model. For example, higher order orbital dynamics will include significant perturbations such as the Earth gravity harmonics. The largest of these is the second zonal harmonic J_2 perturbation, which is caused by the oblateness of the Earth [134]. Other perturbations include drag, solar radiation and the eccentricity of the reference orbit [135, 136]. Also, there was no consideration to the form of propulsion used and it was assumed that the spacecraft could move instantaneously in all degrees-of-freedom. As such these effects on the SFF model can all be viewed as part of future work.

6.3 Three Body Problem

The three-body problem is concerned with the motion of an infinitesimal body that interacts with the gravitational field of two massive primary bodies. In particular, the circular restricted three-body problem (CRTBP) considers the case when the motion of the primary bodies are constrained to circular orbits about their common centre of mass, rotating with constant angular velocity, ω. Figure 6.13 considers the case when the primary bodies are the Sun and the Earth.

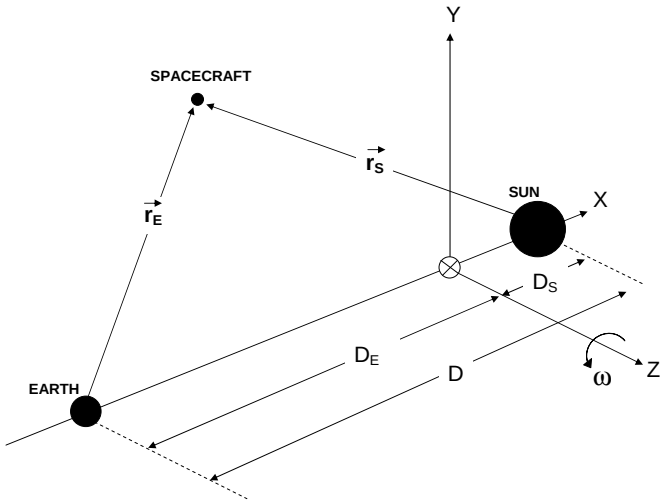

Figure 6.13: Sun-Earth restricted three-body problem

Using a similar convention to that set out by Wie [126], the dynamics of a spacecraft in Sun-Earth CRTBP are shown in Eq. 6.42-6.44.

$$\ddot{X} - 2\omega\dot{Y} - \omega^2 X = -\frac{\mu_S(X - D_S)}{|\mathbf{r}_S|^3} - \frac{\mu_E(X + D_E)}{|\mathbf{r}_E|^3} \tag{6.42}$$

$$\ddot{Y} + 2\omega\dot{X} - \omega^2 Y = -\frac{\mu_S Y}{|\mathbf{r}_S|^3} - \frac{\mu_E Y}{|\mathbf{r}_E|^3} \tag{6.43}$$

$$\ddot{Z} = -\frac{\mu_S Z}{|\mathbf{r}_S|^3} - \frac{\mu_E Z}{|\mathbf{r}_E|^3} \tag{6.44}$$

where,

$$|\mathbf{r}_S| = \left[(X - D_S)^2 + Y^2 + Z^2\right]^{0.5} \tag{6.45}$$

$$|\mathbf{r}_E| = \left[(X + D_E)^2 + Y^2 + Z^2\right]^{0.5} \tag{6.46}$$

and M_S, M_E are the mass of the Sun and the Earth respectively and $\mu_S = GM_S$, $\mu_E = GM_E$.

By setting all the time derivatives in Eq. 6.42-6.44 to zero, five equilibrium points are found, know as the Lagrange or libration points, where the gravitational and centrifugal forces of the two primary bodies balance. Euler discovered three collinear unstable equilibrium points that lie on the X-axis (L_1, L_2 and L_3), with Lagrange discovering two other stable equilibrium points that form an equilateral triangle with the primary bodies (L_4 and L_5) [126], as shown in Fig. 6.14.

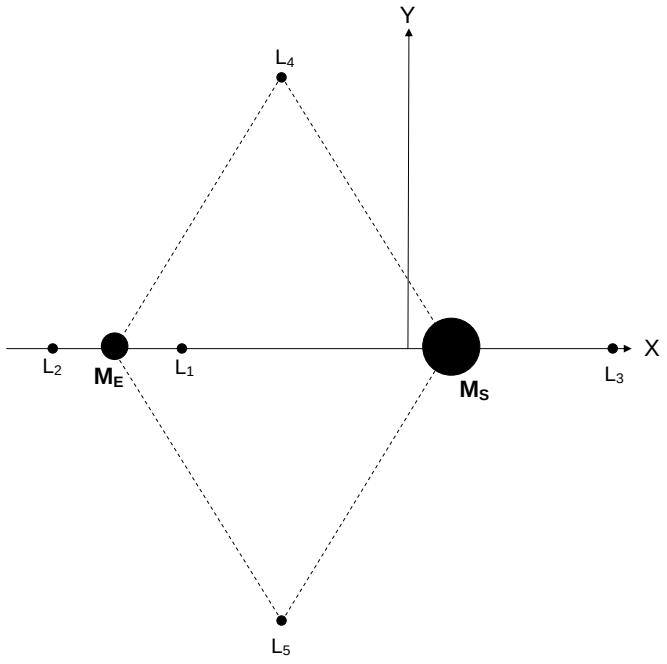

Figure 6.14: Libration points

The motion of spacecraft near the libration points can be accurately described by the linearised equations of motion [131, 137, 138].

$$\ddot{x} - 2\omega\dot{y} - (\omega^2 + 2\mu_o^2)x = 0 \tag{6.47}$$

$$\ddot{y} + 2\omega\dot{x} + (\mu_o^2 - \omega^2)y = 0 \tag{6.48}$$

$$\ddot{z} + \mu_o^2 z = 0 \tag{6.49}$$

where,

$$\mu_o^2 = \frac{\mu_E}{|R_{EL2}|^3} + \frac{\mu_S}{|R_{SL2}|^3} \tag{6.50}$$

and $[x, y, z]^T$ represents the position coordinate of a spacecraft relative to libration points and $|R_{EL2}|$ and $|R_{SL2}|$ are the distance from the Earth and the Sun to the Sun-Earth L_2 point respectively.

Using these linearised equations of motion, a swarm of spacecraft will be desired to form patterns about the Sun-Earth L_2 point. This libration point offers a good location to observe the Universe and is currently the home to several satellites such as the Wilkinson Microwave Anisotropy Probe[1] and Herschel[2]. Setting all the time derivatives in Eq. 6.42-6.44 to zero, the Sun-Earth L_2 position is located at -1.01D m (assuming that $D_S = 4.54841 \times 10^5$ m, $D_E = 1.495891 \times 10^{11}$ m, $M_E = 5.9742 \times 10^{24}$ m, $M_S = 1.981 \times 10^{30}$ m [131]). It should be noted that although the Sun-Earth L_2 position was choosen any of the other libration points could have been equally used to demonstrate spacecraft formation flying.

Consider a swarm of 10 spacecraft that are desired to form an equally spaced ring formation, with radius, $r = 25$ m, in the $y - z$ plane pointing towards the Sun and Earth. Formation reconfiguration is particularly important in spacecraft formation flying as it allows a change in mission type [139] and is demonstrated by the addition of a further 5 spacecraft that are desired to form a double ring formation with inner radius, $r_i = 15.5$ m and outer radius, $r_o = 28.5$ m. As it is desirable that the formation of spacecraft can point in an arbitrary direction, the swarm is then desired to form a ring formation with radius, $r = 35$ m at an angle of $\phi = 45^o$ and $\theta = 45^o$, as explained in **Section 4.1.3**. It will be assumed that each spacecraft has a mass of 10 kg, sensing radius, $Z_R = 25$ m, maximum speed, 0.1 ms^{-1}, minimum separation distance, $|\mathbf{x}_{ij}|_{min} = 5$ m and maximum actuator force of 0.5 N.

[1] http://map.gsfc.nasa.gov/, accessed 14/10/09
[2] sci.esa.int/herschel/, accessed 14/10/09

To satisfy these constraints, Table 6.3 summarises the parameters choosen for each formation.

Table 6.3: Deep-space SFF bound constants

Formation	μ	r	C_h	C_e	L_e	C_z	C_r	L_r	σ
A	0	25	0.03	-	-	0.03	3	2	1
B	3	22	0.03	0.2	15	0.03	3	2	1
C	0	35	0.02	-	-	0.02	3	2	1.5

For *formation A* the spacecraft are given random initial conditions, satisfying the constraint that $|\mathbf{x}_{ij}|_{initial} > 5$ m, with an initial speed of 0.1 ms^{-1}. For *formation B*, the five additional spacecraft are desired to form the inner ring with radius, $r_i = 15.5$ m. Their initial conditions are chosen randomly within the bound of $-r < y_i, z_i < r$ and constraint $|\mathbf{x}_{ij}|_{initial} > 5$ m, with an initial speed of 0.1 ms^{-1}. The initial conditions for *formation C* are the final conditions of *formation B*.

The results of the simulation are shown in Fig. 6.15, indicating that the spacecraft formation successfully creates a ring, double ring and orientated ring formation as desired.

In addition, Fig. 6.16 shows that the spacecraft are driven to the desired radius for each formation, with 6.17 showing that they achieve this without colliding.

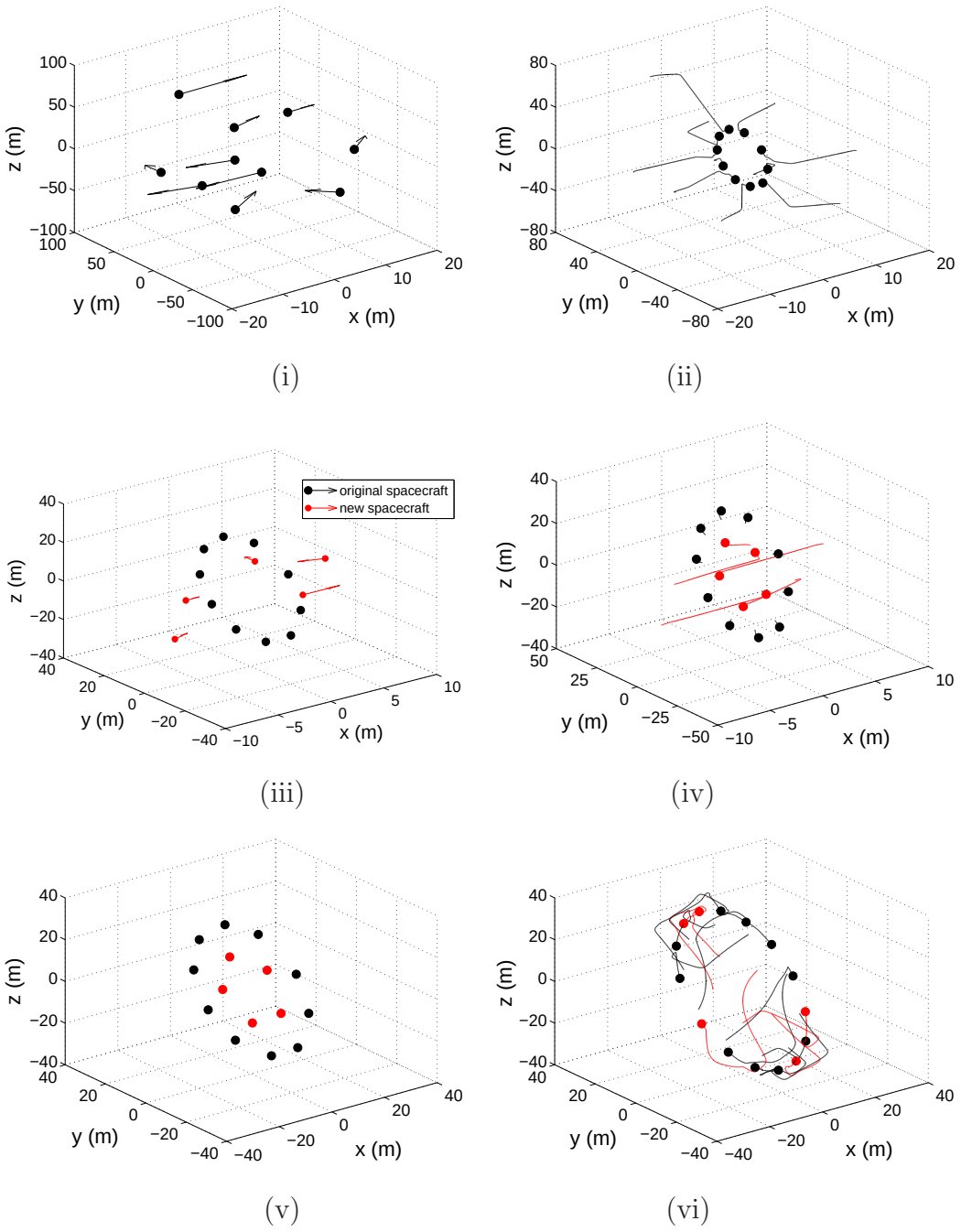

Figure 6.15: Spacecraft formation flying at L_2 (i) initial conditions (ii) formation A (iii) 5 additional spacecraft (iv) formation B (v) initial conditions formation C (vi) formation C

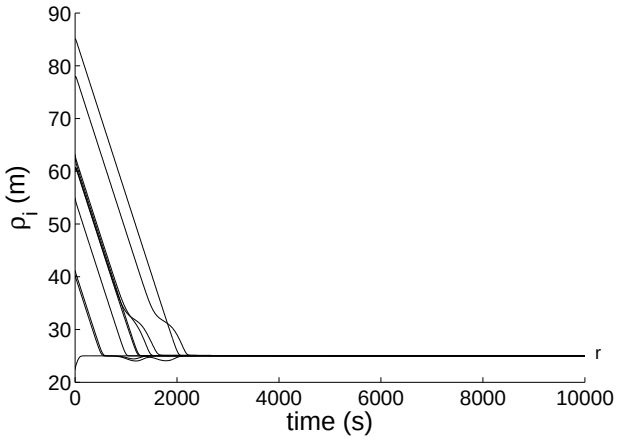

(i)

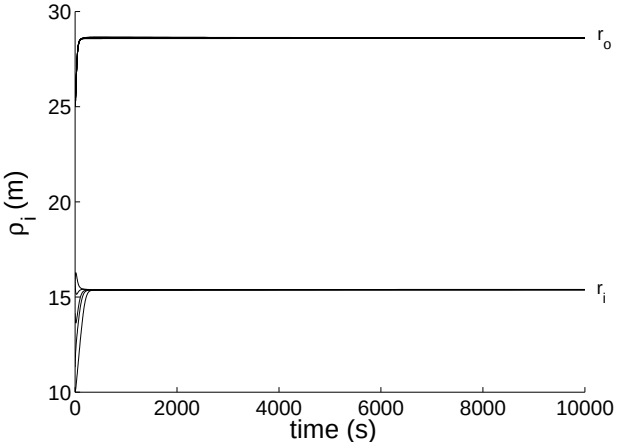

(ii)

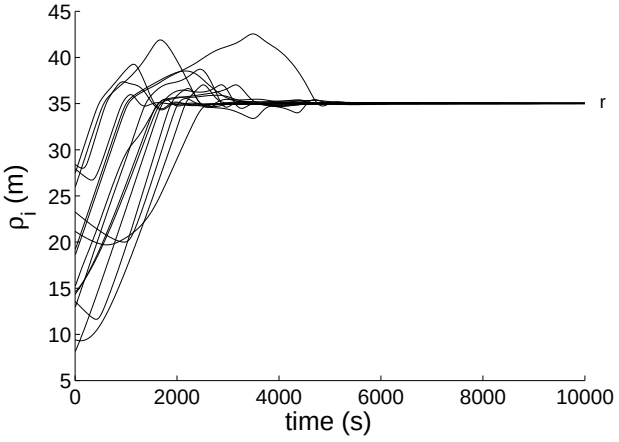

(iii)

Figure 6.16: Formation radius (i) formation A (ii) formation B (iii) formation C

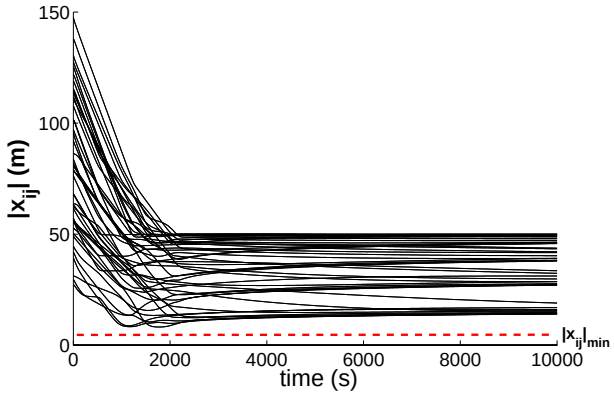

(i)

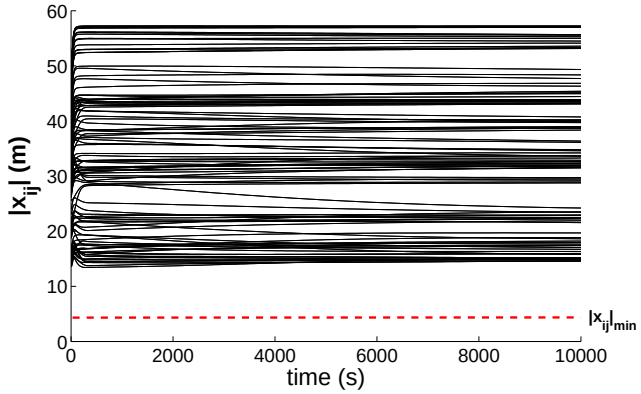

(ii)

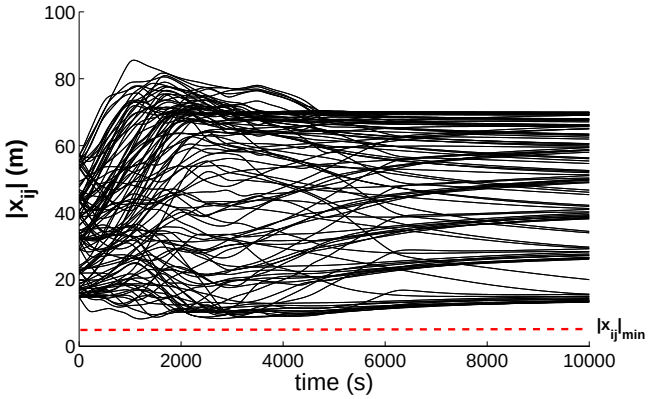

(iii)

Figure 6.17: Formation separation distance (i) formation A (ii) formation B (iii) formation C

Figure 6.18 shows the actuator force acting on each spacecraft during each formation. Table 6.4 shows a comparison between the maximum analytical control force and the maximum simulated control force, indicating that actuator saturation can be avoided, satisfying the constraint that the maximum actuator force be less than 0.5 N. Figure 6.18 indicates that as the spacecraft are driven towards their desired formation, collision avoidance occurs, again agreeing well with the scale-separation assumption made in **Section 3.2.1**.

Table 6.4: Deep-space SFF control force

Formation	Analytical $\|\mathbf{u}_i\|_{max}$ (N)	Simulated $\|\mathbf{u}_i\|_{max}$ (N)
A	0.17	0.14
B	0.23	0.13
C	0.2	0.03

From the results it can be seen that the swarm of spacecraft can successful form the desired patterns at the Sun-Earth L_2 position based on the linearised equations of motion. As the distance of the spacecraft from the Sun-Earth L_2 position was small in comparison with the distances between L_2 and the Earth and Sun, the linearised equations are valid under the assumptions made regarding the CRTBP.

To further improve the model perturbations at the Sun-Earth L_2 position can be considered. For example, lunar and other planetary perturbations can be included, as well as considering the effects of solar radiation pressure. In addition, the CRTBP can be altered to consider the elliptical motion of the Sun and Earth about their barycenter. Similarly with LEO SFF, there was no consideration to the form of propulsion and it was assumed that the spacecraft could move instantaneously in all degrees-of-freedom. As such these effects on the SFF model can all be viewed as part of future work.

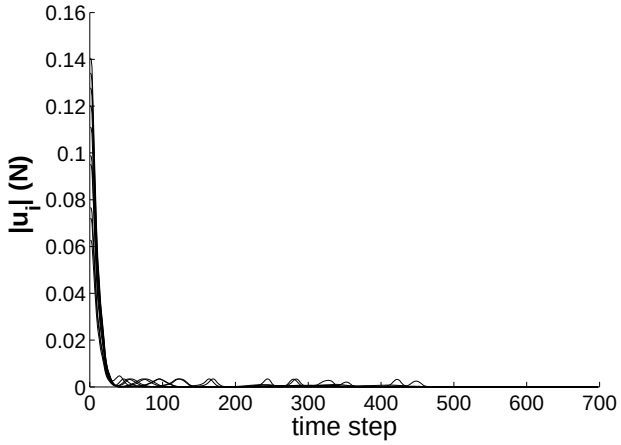

(i)

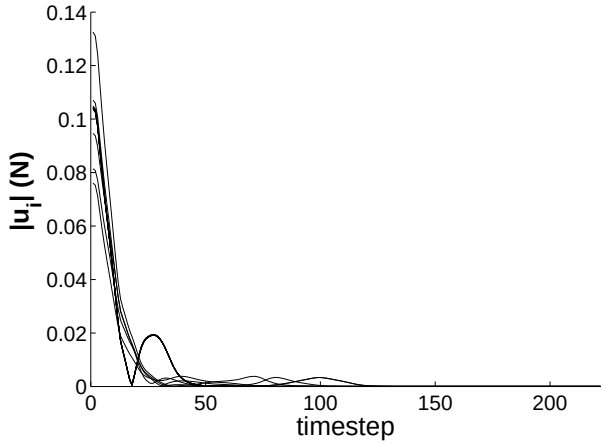

(ii)

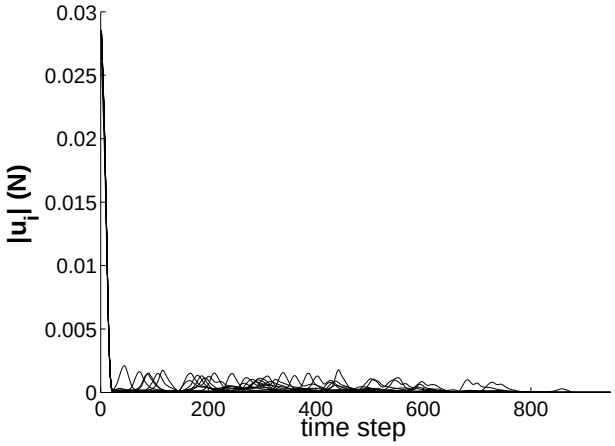

(iii)

Figure 6.18: Formation actuator force (i) formation A (ii) formation B (iii) formation C

6.4 Summary

This chapter has demonstrated SFF using the proposed swarm model. Firstly, SFF in LEO was considered with the orbital dynamics of the spacecraft modelled using HCW relative linearised equations of motions. Under the assumption of a spherical Earth and neglecting perturbations in the two-body problem, it was shown that the swarm model could be used to drive a formation of spacecraft safely onto an equally spaced relative PCO about a target spacecraft. It was also shown that the formation could autonomously reconfigure, through a simple parameter change, to a new PCO satisfying constraints associated with each spacecraft. Deep-space SFF was then considered at the Sun-Earth L_2 position. Under the assumption that the Sun and Earth rotate about their barycenter in a circular orbit, the linearised CRTBP equations of motion where used to model the orbital dynamics of the spacecraft at L_2. The swarm model was then used to form three different formations again demonstrating pattern formation and reconfigurability. As part of future work, these models can both be improved by including higher order effects, as well as considering practical constraints associated with the spacecraft.

Chapter 7

Unmanned Aerial Vehicles

This chapter considers the implementation of the first order velocity field swarm model, as discussed on **Chapter 5**, in a linearised 6 DOF guidance and control model for a formation of 3 UAVs. Through the control of forward speed and roll, pitch and yaw angles, it is shown that 3 UAVs can safely form three triangular patterns, whilst satisfying the saturation limits of the UAV control surfaces.

7.1 Introduction

As well as many future spacecraft missions consisting of multiple spacecraft, the near future may also see the deployment of swarms of UAVs, again driven by commercial, military and scientific requirements [37]. For distributed sensing missions, that may be repetitive or dangerous, this is particulary suitable as the swarm is autonomous. In addition, it has been shown that by flying multiple UAVs in formation, fuel consumption can be reduced by a reduction in induced drag [140].

In the dynamic modelling of UAVs, the equations of motion can take five different forms; (i) non-linear fully coupled, (ii) non-linear semi-coupled, (iii) non-linear decoupled, (iv) linear coupled and (v) linear decoupled. Each of these models has advantages and disadvantages, such as precision, accuracy, complexity and credibility [141]. As the purpose of this chapter is to demonstrate that the swarm model can be applied to a formation of UAVs, the linear decoupled equations of motion are considered, with higher order models viewed as part of future work.

The block diagram of the guidance and control system for a formation of UAVs is shown in Fig. 7.1. For the guidance system, the first order swarm control discussed in **Section 5.4** is used. As 6 DOF linear decoupled equations of motion are considered, a robust linear time-invariant control system is used to ensure that the system can follow the guidance algorithm, assuming that the UAV roll (ϕ), pitch (θ) and yaw (ψ) angles can be measured, as well as the UAV forward speed (u) and position $(x, y, z)^T$.

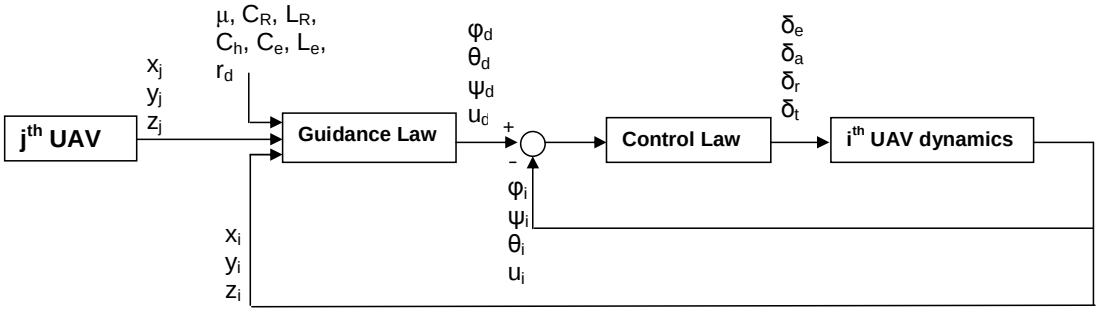

Figure 7.1: UAV control block diagram

7.2 UAV Dynamics

To simulate each UAV, the linear decoupled equations of motion that describe small deviations from constant speed, straight and level flight, can be split into two uncoupled sets of longitudinal and lateral directions, as shown in Eq. 7.1 and 7.2 respectively [141].

$$\begin{bmatrix} \dot{u} \\ \dot{w} \\ \dot{q} \\ \dot{\theta} \end{bmatrix} = \begin{bmatrix} X_u & X_w & 0 & -g\cos\theta_0 \\ Z_u & Z_w & u_0 + z_q & -g\sin\theta_0 \\ M_u & M_w & M_q & 0 \\ 0 & 0 & 1 & 0 \end{bmatrix} \begin{bmatrix} u \\ w \\ q \\ \theta \end{bmatrix} + \begin{bmatrix} X_{\delta e} & X_{\delta th} \\ Z_{\delta e} & Z_{\delta th} \\ M_{\delta e} & M_{\delta th} \\ 0 & 0 \end{bmatrix} \begin{bmatrix} \delta_e \\ \delta_{th} \end{bmatrix} \tag{7.1}$$

$$\begin{bmatrix} \dot{v} \\ \dot{p} \\ \dot{r} \\ \dot{\phi} \\ \dot{\psi} \end{bmatrix} = \begin{bmatrix} Y_v & Y_p & Y_r - u_0 & g\cos\theta_0 & 0 \\ L_v & L_p & L_r & 0 & 0 \\ N_v & N_p & N_r & 0 & 0 \\ 0 & 1 & \tan\theta_0 & 0 & 0 \\ 0 & 0 & 1 & 0 & 0 \end{bmatrix} \begin{bmatrix} v \\ p \\ r \\ \phi \\ \psi \end{bmatrix} + \begin{bmatrix} Y_{\delta a} & Y_{\delta r} \\ L_{\delta a} & L_{\delta r} \\ N_{\delta a} & N_{\delta r} \\ 0 & 0 \\ 0 & 0 \end{bmatrix} \begin{bmatrix} \delta_a \\ \delta_r \end{bmatrix} \tag{7.2}$$

where, $(u, v, w)^T$ represent the forward, side and vertical velocity, $(\phi, \theta, \psi)^T$ represent the roll, pitch and yaw angle, $(p, q, r)^T$ represent the roll, pitch and yaw rate respectively and $(\delta_a,\ \delta_r,\ \delta_e,\ \delta_t)^T$ represent the aileron, rudder, elevator deflection and thrust offset, as shown in Fig. 7.2. All of these state variables represent the deviation from the trim flight conditions.

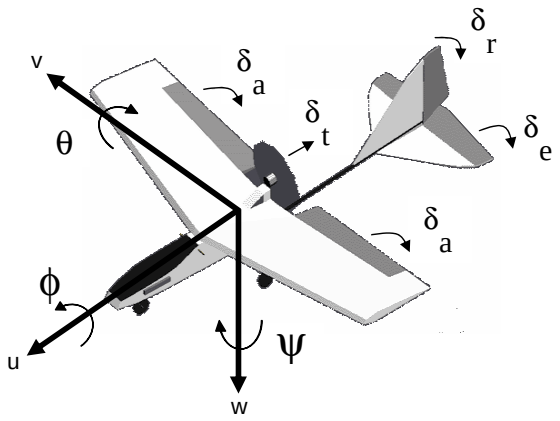

Figure 7.2: UAV state variable definition

The UAV model is based on a low-speed fixed wing UAV, that has a steady forward speed, $u_0 = 12.5$ ms^{-1}, mass of 430 g and 1 m wingspan. The stability derivatives for both longitudinal and lateral motion are summarised in Table 7.1 and 7.2 [142].

Table 7.1: Longitudinal linearised stability derivatives

X_u	$[s^{-1}]$	-0.13
X_w	$[s^{-1}]$	0.14
Z_u	$[s^{-1}]$	-3.17
Z_w	$[s^{-1}]$	-13.06
z_q	$[ms^{-1}]$	-1.37
u_o	$[m^{-1}s^{-1}]$	12.5
M_u	$[ms^{-1}]$	-1.95
M_w	$[m^{-1}s^{-1}]$	-17.41
M_q	$[s^{-1}]$	-21.86
X_{δ_e}	$[ms^{-2}]$	0
X_{δ_t}	$[kg^{-1}]$	2.32
Z_{δ_e}	$[ms^{-2}]$	-7.73
Z_{δ_t}	$[kg^{-1}]$	0
M_{δ_e}	$[s^{-2}]$	-205.25
M_{δ_t}	$[s^{-2}]$	0
θ_o	[rad]	-0.0078

Table 7.2: Lateral linearised stability derivatives

Y_v	$[s^{-1}]$	-0.68
Y_p	$[ms^{-1}]$	-0.11
Y_r	$[ms^{-1}]$	-12.20
L_v	$[m^{-}1s^{-1}]$	-32.17
L_p	$[s^{-1}]$	-56.38
L_r	$[s^{-1}]$	19.30
N_v	$[m^{-}1s^{-1}]$	7.89
N_p	$[s^{-1}]$	-3.13
N_r	$[s^{-1}]$	-4.00
$Y_{\delta a}$	$[ms^{-2}]$	-3.34
$Y_{\delta r}$	$[kg^{-2}]$	22.99
$L_{\delta a}$	$[s^{-2}]$	-26.88
$L_{\delta r}$	$[s^{-2}]$	-6.80
$N_{\delta a}$	$[s^{-2}]$	58.54
$N_{\delta r}$	$[s^{-2}]$	-226.79

7.3 UAV Guidance and Control

The guidance algorithm for the UAVs is based on the first order swarm model described by Eq. 5.18 and 5.19. From this model, the desired forward speed, u_d, and desired yaw angle, ψ_d, can be calculated, as shown in Eq. 7.3 and 7.4.

$$u_d = (\dot{x}^2_{desired} + \dot{y}^2_{desired})^{0.5} \tag{7.3}$$

$$\psi_d = \arctan\left(\frac{\dot{y}_{desired}}{\dot{x}_{desired}}\right) \tag{7.4}$$

To control the UAVs and achieve straight and level flight, a robust controller for a linear time-invariant multi-variable system is used [143], as shown in Fig. 7.3.

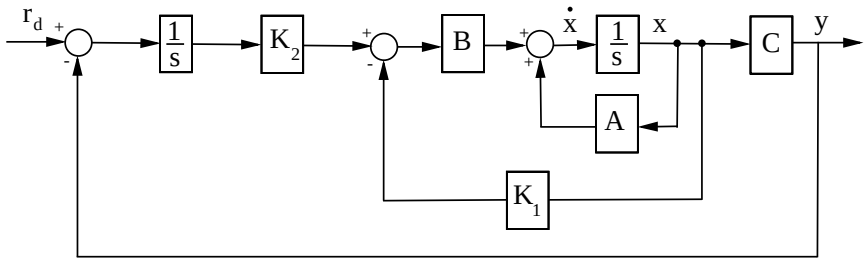

Figure 7.3: Block diagram of robust linear time-invariant multi-variable control system

Both the longitudinal and lateral linearised equations of motion can be expressed in the state space form as;

$$\dot{\mathbf{x}} = \mathbf{A}\mathbf{x} + \mathbf{B}\mathbf{u} \tag{7.5}$$

$$\mathbf{y} = \mathbf{C}\mathbf{x} \tag{7.6}$$

where, $\mathbf{x}_{longitudinal} = [u, w, q, \theta]^T$, $\mathbf{x}_{lateral} = [v, p, r, \phi, \psi]^T$ are the state variables of the system, $\mathbf{u}_{longitudinal} = [\delta_e, \delta_t]^T$, $\mathbf{u}_{lateral} = [\delta_a, \delta_r]^T$ are the inputs and $\mathbf{y}$ is the output of the system.

The error, $\mathbf{e}$ in the system is defined as;

$$\mathbf{e} = \mathbf{y} - \mathbf{r}_d \tag{7.7}$$

where, $\mathbf{r}_d$ is the desired state of the system.

From Eq. 7.5, it is known that;

$$\frac{d}{dt}\dot{\mathbf{x}} = \mathbf{A}\dot{\mathbf{x}} + \mathbf{B}\dot{\mathbf{u}} \tag{7.8}$$

and assuming that $\dot{\mathbf{r}}_d = 0$, then;

$$\frac{d}{dt}\mathbf{e} = \mathbf{C}\dot{\mathbf{x}} \tag{7.9}$$

Combining Eq. 7.8 and 7.9 results in;

$$\frac{d}{dt}\begin{bmatrix} \dot{\mathbf{x}}(t) \\ \mathbf{e}(t) \end{bmatrix} = \begin{bmatrix} \mathbf{A} & 0 \\ \mathbf{C} & 0 \end{bmatrix}\begin{bmatrix} \dot{\mathbf{x}}(t) \\ \mathbf{e}(t) \end{bmatrix} + \begin{bmatrix} \mathbf{B} \\ 0 \end{bmatrix}\dot{\mathbf{u}}(t) \tag{7.10}$$

To ensure the controllability of the system, the rank of the following matrix should be considered [144];

$$rank\begin{bmatrix} \mathbf{A} & \mathbf{B} \\ \mathbf{C} & 0 \end{bmatrix} = n + p \tag{7.11}$$

where, n is the order of the $\mathbf{A}$ matrix and p is the order of the $\mathbf{C}$ matrix.

Accordingly, it is found that only two state variables for both the longitudinal and lateral equations of motion can be controlled. Therefore, controlling both forward speed and attitude and meeting the requirements of guidance algorithm, u and θ are choosen for longitudinal motion control, with ϕ and ψ choosen for lateral motion control.

The input, $\mathbf{u}$, for both longitudinal and lateral motions of the controller is;

$$\mathbf{u}(t) = -\mathbf{K}_1\mathbf{x}(t) - \mathbf{K}_2\int_0^t \mathbf{e}(t)dt \tag{7.12}$$

where, $\mathbf{K}_1$ and $\mathbf{K}_2$ are feedback gains of the controller, selected using the pole placement method.

7.4 Formation of UAVs

Using the guidance and control system discussed in **Section 7.3**, a formation of 3 UAVs are desired to travel at three different equally spaced triangular patterns, traveling at constant forward speed of 12.5 ms^{-1}, at constant altitude.

From the guidance algorithm, u_d and ψ_d are calculated, with $\theta_d = 0^o$ and $\phi_d = 0^o$ in order to achieve fixed attitude flight. It is assumed that each UAV has a maximum turning rate of 30 $^o\text{s}^{-1}$ and forward speed of 15 ms^{-1}. From Eq. 5.24 it is known that the turning circle associated with each UAV is approximately 29 m, so that the system should be designed such that the minimum separation distance between UAVs is 58 m. To satisfy these constraints Table 7.3 summarises the free parameters and random initial conditions (ensuring $|\mathbf{x}_{ij}|_{initial} > 58$ m) for each UAV, with $Z_R = 125$ m.

Table 7.3: Static bifurcation free parameters

time (s)	μ	r	C_r	L_r	C_h	$x_{initial}$ (m)	$y_{initial}$ (m)
0-1000	0	50	335	40	0.2	-50	15
1000-2000	0	70	335	40	0.2	0	-60
2000-3000	0	50	335	40	0.2	30	70

The results of the simulation are shown in Fig. 7.4-7.14. Figures 7.4 and 7.5 show the UAVs flight path and patterns, indicating that the UAVs can safely form three equally spaced triangular patterns. Figures 7.6-7.9 show a comparison between the desired and actual controlled variables about the trim condition. It can be seen from Fig. 7.6 and 7.7 that each UAV can follow the desired speed and yaw angle provided by the guidance algorithm, traveling at constant speed of 12.5 ms^{-1}, with $\psi = 0^o$ once in equilibrium.

In addition, Fig. 7.8 and 7.9 show that the UAVs achieve level flight, with both ϕ and θ changing as the guidance commands change, again reaching the desired value once in equilibrium. Although only 4 state variables are controlled, Fig. 7.10 and 7.11 confirm that the side and vertical velocity, as well as the angular rates are zero once in the final equilibrium state.

The saturation limits of the aircraft control surfaces are $\delta_e \pm 0.35$ rad, $\delta_a, \delta_r =$

± 0.79 rad and thrust $-0.35 < \delta_t < 5.45$ N. Figures 7.12-7.14 confirm that the system can operate within these limits, with no collisions.

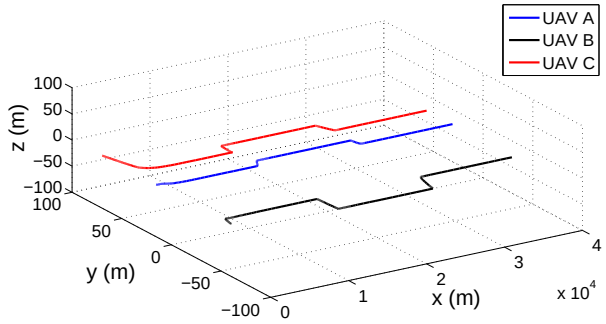

Figure 7.4: UAV flight path

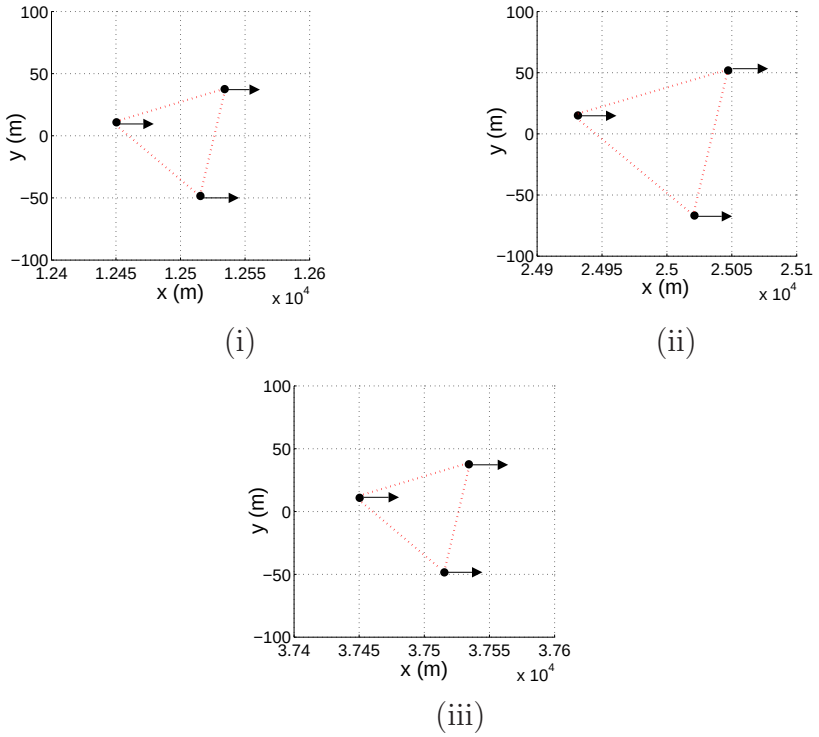

Figure 7.5: UAV formations (i) pattern A (ii) pattern B (iii) pattern C

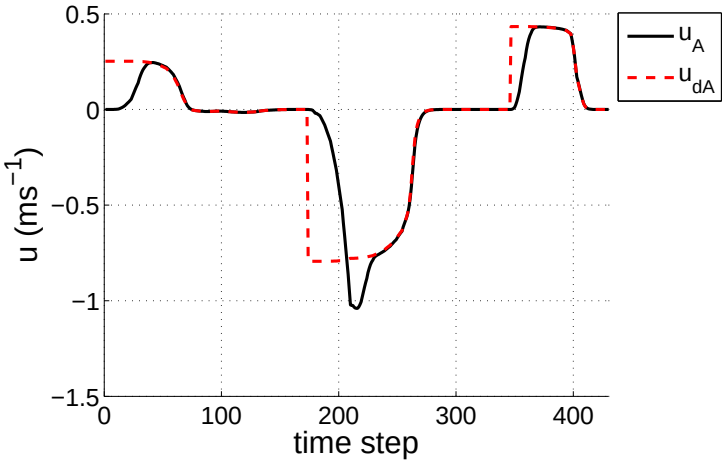

(i)

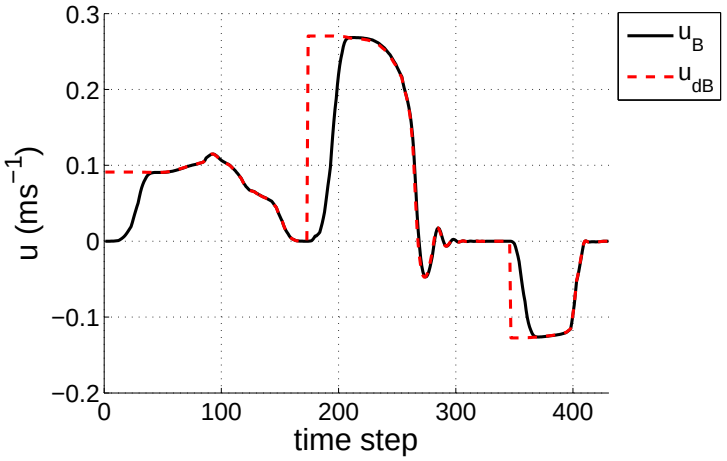

(ii)

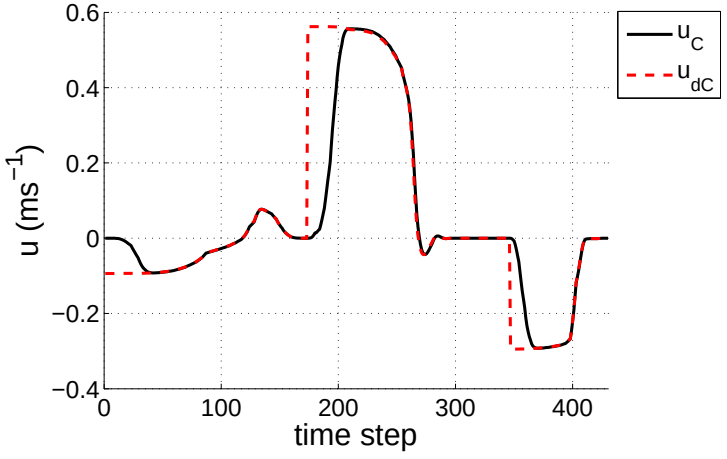

(iii)

Figure 7.6: Comparison between actual and desired UAV forward speed about trim (i) UAV A (ii) UAV B (iii) UAV C

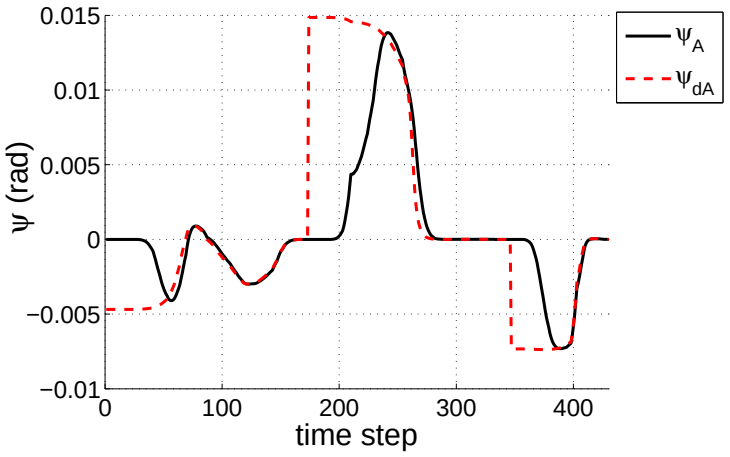

(i)

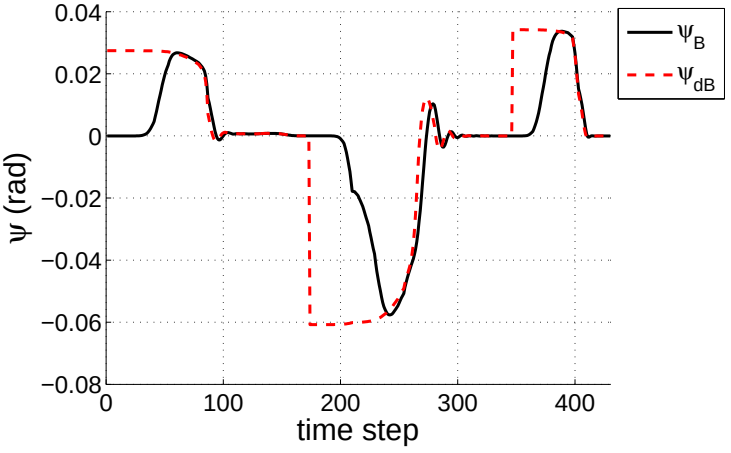

(ii)

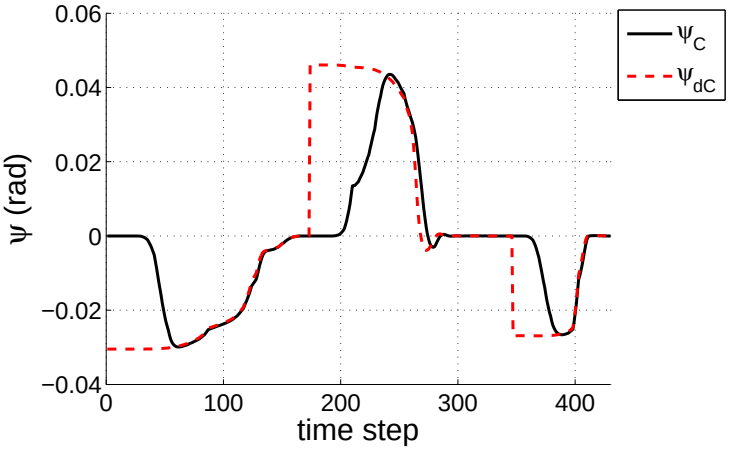

(iii)

Figure 7.7: Comparison between actual and desired yaw angle about trim (i) UAV A (ii) UAV B (iii) UAV C

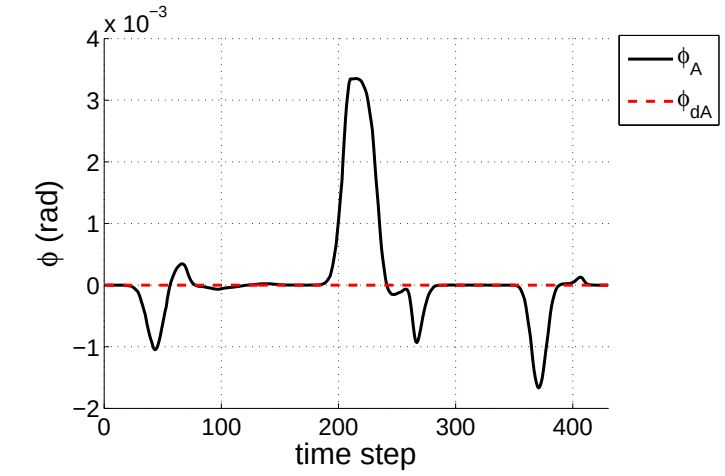

(i)

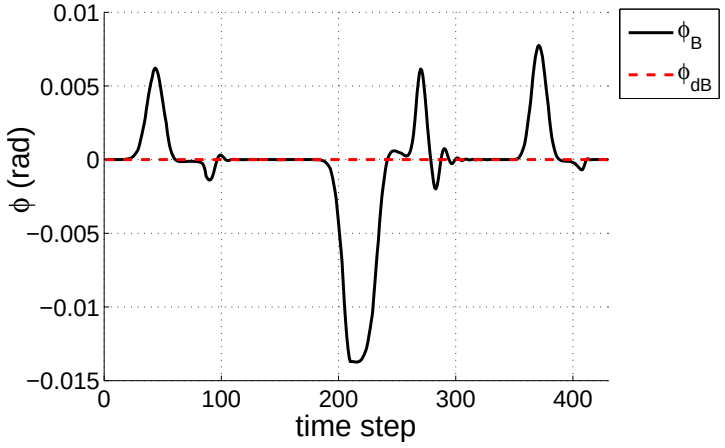

(ii)

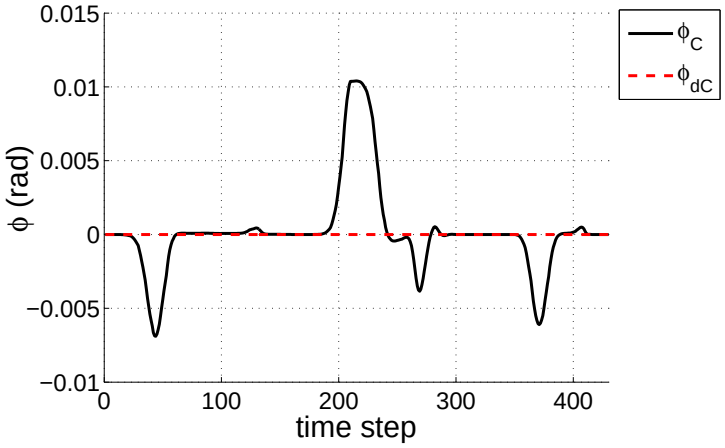

(iii)

Figure 7.8: Comparison between actual and desired UAV roll angle about trim (i) UAV A (ii) UAV B (iii) UAV C

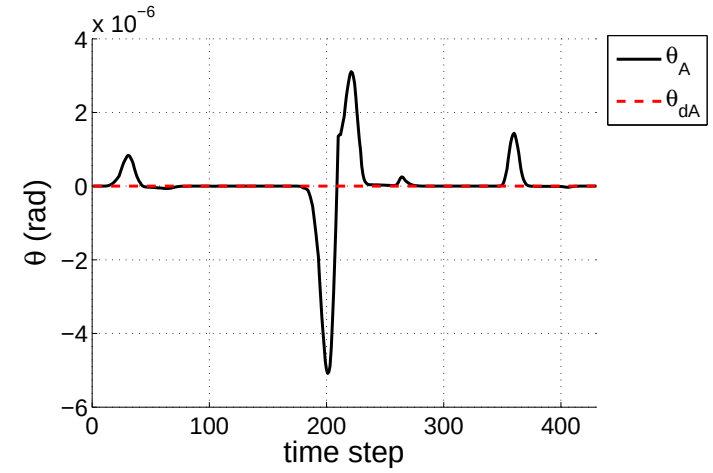

(i)

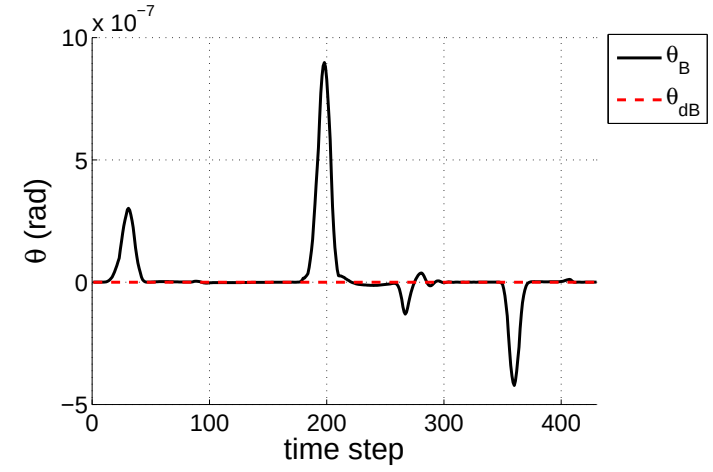

(ii)

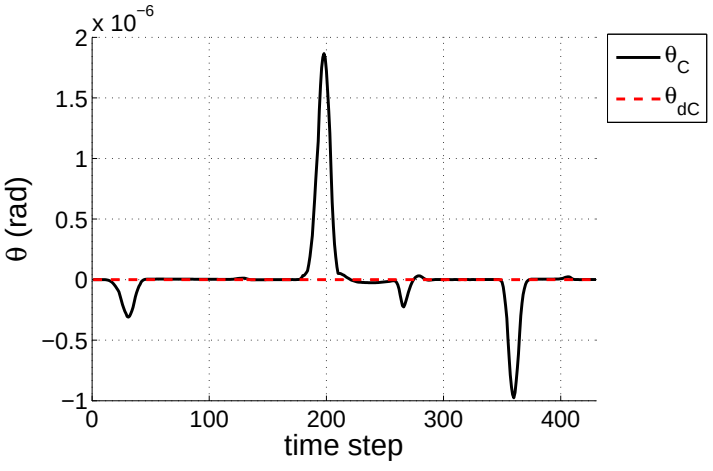

(iii)

Figure 7.9: Comparison between actual and desired UAV pitch angle about trim (i) UAV A (ii) UAV B (iii) UAV C

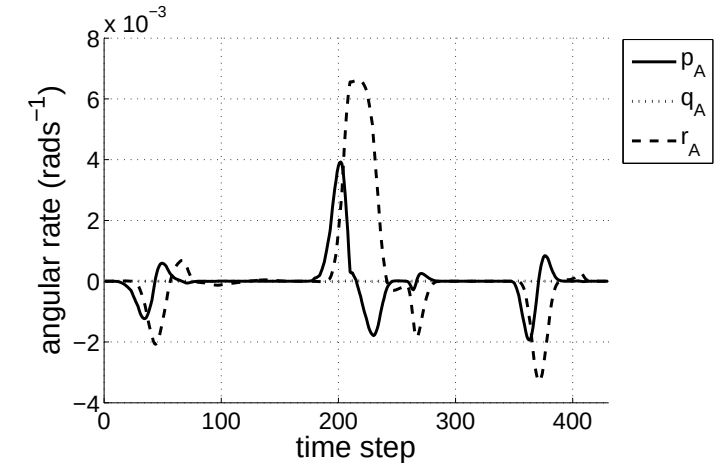

(i)

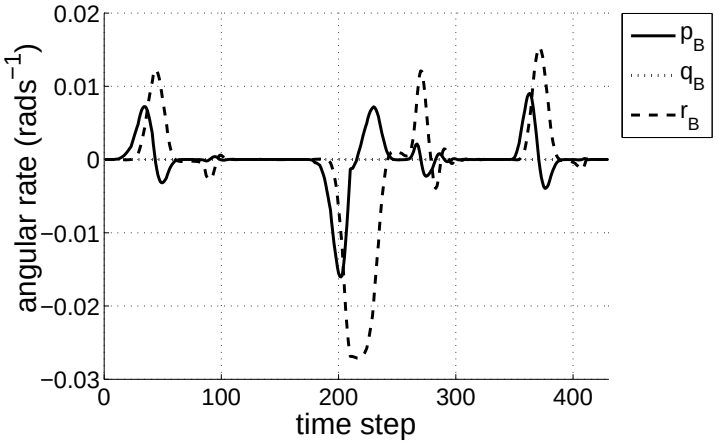

(ii)

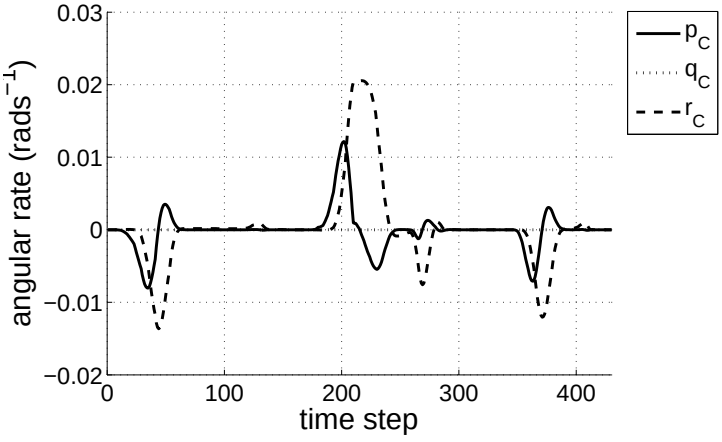

(iii)

Figure 7.10: UAV angular rate about trim (i) UAV A (ii) UAV B (iii) UAV C

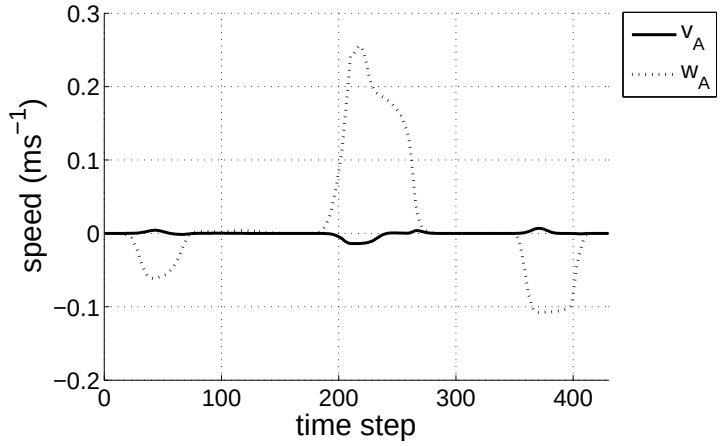

(i)

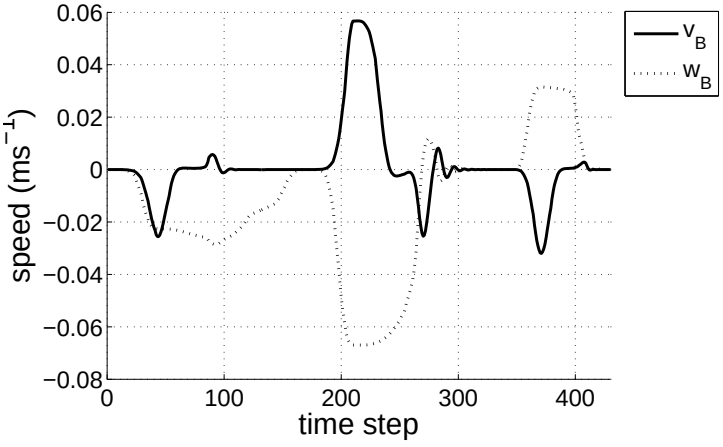

(ii)

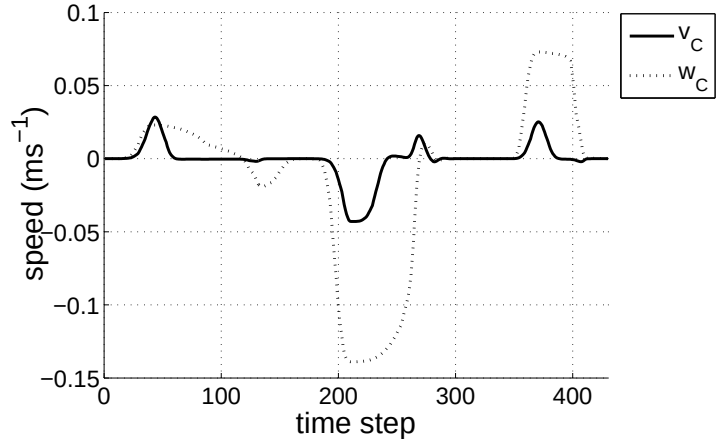

(iii)

Figure 7.11: UAV side and vertical speed about trim (i) UAV A (ii) UAV B (iii) UAV C

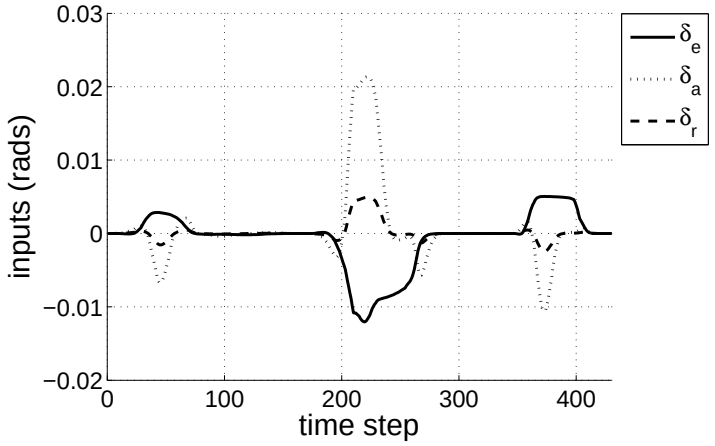

(i)

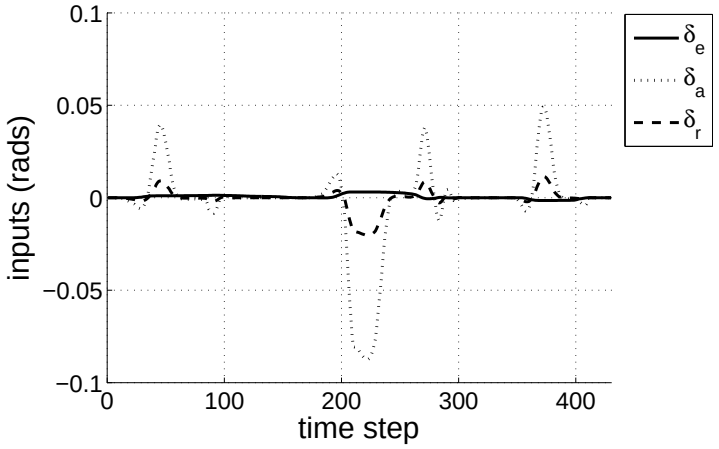

(ii)

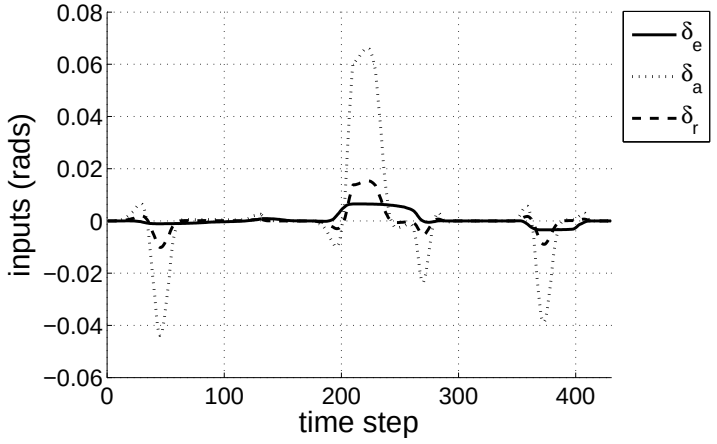

(iii)

Figure 7.12: UAV elevator, aileron and rudder inputs about trim (i) UAV A (ii) UAV B (iii) UAV C

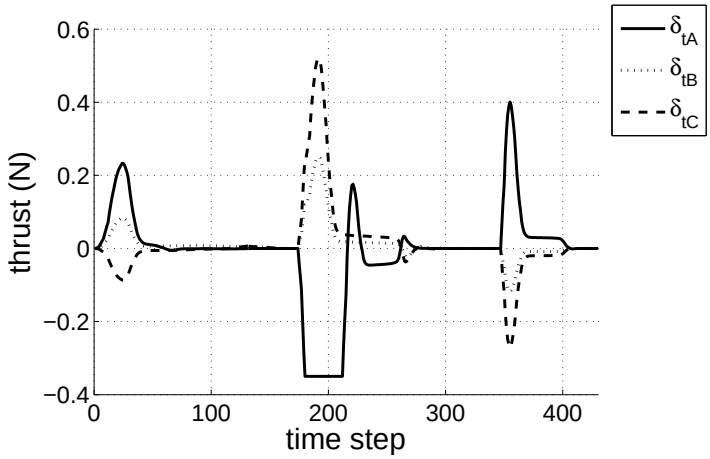

Figure 7.13: UAV thrust input about trim condition

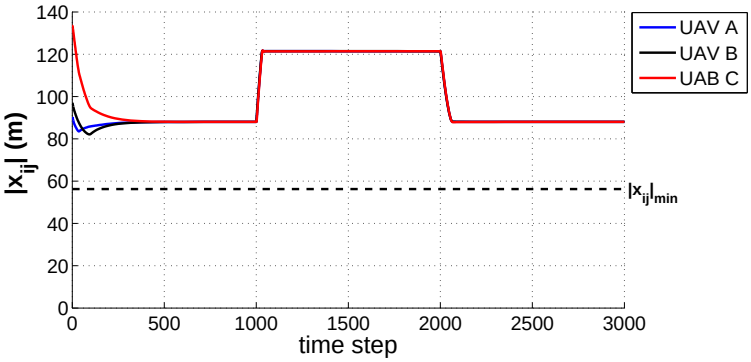

Figure 7.14: UAV separation distance

Therefore, from the results shown it can be seen that a formation of UAVs can safely form different patterns, satisfying the assumptions made regarding the model. To further improve the model, higher order models of the UAV dynamics can be considered. In addition, when simulating the UAV system all aspects of the UAV dynamics could be considered. This may include the UAV structure, propulsion system, sensors and consideration of the atmospheric flight conditions [141]. For example, an important perturbation when dealing with small UAVs is to consider the effect of wind on the system. All of these improvements can be considered as part of future work.

7.5 Summary

This chapter has considered the implementation of the first order swarm model in a guidance and control model of a formation of 3 UAVs. A 6 DOF simulation, based on the linear decoupled equations of motion, was developed considering the trim conditions of a real UAV, traveling in straight and level flight, with forward speed of 12.5 ms^{-1}. Using a robust linear time-invariant controller it was shown that by using state feedback of forward speed and roll, pitch and yaw angles, a formation of 3 UAVs can safely form 3 triangular patterns.

Chapter 8

Conclusions and Future Work

8.1 Conclusions

This thesis has addressed the following areas of work;

1. Development of new methodologies for verifiable swarming systems, replacing traditional heuristic methods with a more rigorous analytical approach.
2. Investigation of two areas of generic swarming systems; pattern formation and reconfigurability.
3. Implementation of these methodologies in engineering systems.

Firstly, **Chapter 1** provided an overview of swarming systems, highlighting that many future engineering systems may consist of multiple, mobile autonomous *agents*, that must operate in a coordinated and safe manner. The advantages of such systems are the potential for system robustness, scalability and increased flexibility. They are desirable, from an engineering point of view, as engineers are often driven by the need to solve problems in new and efficient ways. Much of the research into swarming is motivated by the *swarm intelligence* paradigm, and as such there are a wide variety of methods to control a swarm system, such as the APF method. This approach was identified as the control method of choice as it allows for a simple, verifiable approach to swarming systems. In addition, as the APF is based on dynamical systems theory, there are an array of tools that can be utilised to develop new ways in which to approach swarming.

In **Chapter 2**, concepts from dynamical systems theory used in this thesis were discussed. Firstly, the APF methodology was considered, showing that it can be applied to both first order velocity field and second order force controllers. The advantage of using the APF method is that the stability of the system can be proven analytically, therefore addressing the first aim of the work, so that traditional heuristic methods can be replaced with a more analytical approach. Using Lyapunov stability theory, the stability of a non-linear system can be investigated. Lyapunov's second method allows the determination of the stability of the system without requiring a solution, with Lyapunov's indirect method investigating the local stability of the system through linearisation techniques. To allow reconfigurability in the swarm model, bifurcation theory was discussed, describing ways in which the artificial potential field can be manipulated through a simple parameter change. Both static and dynamic bifurcations were considered allowing a transition between both fixed point and periodic attractors.

The main contribution to knowledge presented in this thesis was discussed in **Chapters 3** and **4** and can be summarised in the following statement;

> *Through the new approach of bifurcating APFs, a verifiable swarming system will self-organise, capable of creating reconfigurable, autonomous patterns.*

The swarm model for both first and second order systems was introduced in **Chapter 3**, consisting of a steering and repulsive potential. The steering potential, based bifurcating APFs, was used to control the swarm, with the repulsive potential ensuring collision avoidance between *agents*. Before considering this model further, a pair-wise potential field was discussed, identifying useful properties of a swarm system. The stability of the swarm model was then considered, showing that there exists a scale separation between the steering and repulsive potentials, such that each *agent* in the swarm moves under the influence of a long-range steering potential, but with short range collision avoidance. This allows for collisions to be treated separately in the Lyapunov stability analysis, with both Lyapunov's second and indirect method being used to show that the behaviour of the swarm system is verifiable.

To address aim 2, **Chapter 4** considers pattern formation and reconfigurability. It was shown that a swarm of *agents* can be attracted to different states

depending on the form of the potential. Pattern formation using the bifurcation potentials, discussed in **Chapter 2**, was then demonstrated, indicating that a variety of different patterns can be achieved. For example, the static pitchfork bifurcation can lead to ring, line or cluster patterns. It was also shown that the dynamic Hopf bifurcation can lead to rotating ring and cluster patterns. In addition to the bifurcation potential patterns, other potentials were developed allowing for patterns such as a swarm grid and multiple ring configurations. It was also shown that the patterns can be arbitrarily orientated through a coordinate transformation. Reconfigurability using the bifurcating potential field was then demonstrated for both the static and dynamic bifurcations, showing that through a simple parameter change, the swarm model can autonomously reconfigure.

In **Chapter 1** swarm robotics was identified as one of the major research fields investigating swarming. The key issues to consider in the development of real swarms of robots are; how can the control laws be developed such that the safety of the system is ensured and how can real practical and technological constraints be overcome? Using the bifurcating APF, **Chapter 5** considers two approaches to these issues. Firstly, to assure stability for real, safety critical systems it is important to consider actuator saturation. Using the pitchfork bifurcating potential as an example, it is known that the control force from this potential is unbound as distance from the origin increases. To overcome this, a hyperbolic-exponential bifurcating potential was developed, allowing for a bound steering potential, therefore overcoming the issue of actuator saturation. The second real world consideration is that of communication. The assumption that all *agents* have global knowledge of all other *agents* is unrealistic as the number of *agents* increases, so the repulsive potential was altered such that it only acts in a region surrounding each *agent*. These considerations were demonstrated in both first and second order swarm examples, with the final section of the chapter illustrating that the swarm model can be robust to individual failure, scalable and flexible to obstacles.

The final objective of the work was to demonstrate the swarm model in engineering systems. In **Chapter 1**, SFF and UAVs were identified as two swarm robot applications. **Chapters 6** and **7** consider these applications with use of the second order force and first order velocity field methods for SFF and UAVs

respectively.

SFF missions are desirable as they can improve mission capabilities, as well as being more fault tolerant in comparison to single spacecraft missions. **Chapter 6** considers SFF in LEO and in deep space. Taking advantage of linear, unperturbed equations of relative motion that yield closed periodic solutions in LEO, it was shown that a formation of spacecraft can form an equally spaced rotating ring pattern about a target spacecraft. Using the new bound bifurcating potentials and communication constraints, it was also shown that the formation can reconfigure to a new bound equally spaced periodic orbit, satisfying assumptions made regarding the actuators. The second example considers a formation of spacecraft in deep-space. Using the circular restricted three-body problem, it was shown that SFF can be achieved at the Sun-Earth L_2 position. Using the linearised equations of motion at L_2, and assuming that the distance from L_2 is small, a formation of spacecraft were shown to form several different patterns, that could be used to meet different mission requirements.

For swarms of UAVs, **Chapter 7** develops a guidance and control algorithm for 3 UAVs, based on the linearised 6 DOF equations of motion of a real UAV about straight and level flight. Using a robust linear time-invariant controller it was shown that by using state feedback of forward speed and roll, pitch and yaw angles, a formation of 3 UAVs can safely form 3 triangular patterns.

8.2 Future Work

The work presented in this thesis has addressed the objectives stated in **Chapter 1**, developing a new verifiable swarming model, allowing for pattern formation and reconfigurability. Although the work addressed the objectives, there is scope to expand and further improve the research in the following ways;

- In **Chapters 3** and **4** bifurcation theory was discussed, showing that a swarm of *agents* could bifurcate from a single pattern and double pattern. It was noted that balance between *agents* during the split is largely uncontrolled, so as part of future work it would be interesting to investigate analytically the probability of the split and its sensitivity to initial conditions.

- It was also shown analytically that each *agent* would be driven to desired equilibrium positions, however, there was no discussion on how long this would take. In the development of real engineered systems this will be very important and can therefore also be considered as part of future work.

- In **Chapter 5** two real world effects were considered. There are, of course, many other real world effects that could be taken into consideration to further improve the model. For example, in mobile robots an important consideration is non-holonomic effects. Other effects would be to consider sensor and actuator inaccuracy in the model, consideration of computational load on each *agent*, communication time-delays and robustness to partial *agent* failure.

- These real world effects all have an influence on the stability of the system. **Chapter 5** considered the implementation of a limited sensing region, although no analytical proof was provided that the stability of the system can be assured. Future work could therefore consider this further, considering similar work carried out using a graph theory approach.

- Both the LEO and deep-space SFF flying models illustrated simple ways in which the swarm formation could be applied to space applications. As such, the linearised equations of motion in the two and three-body problems were considered. This could be extended by considering higher order models on the effects of the swarm formation, as well as considering other dynamic complexities of the formation. For example, no consideration was given to the specific form of propulsion. In deep-space missions, it may be desirable to have a form of propulsion that will allow the mission to operate for an indefinite duration. In this case the swarm model could be adapted to consider the effect of using solar sails as the form of propulsion.

- For swarms of UAVs, the full non-linear equations of motion should be considered to increase the fidelity of the model. In addition, the aircraft structure, propulsion system and avionics could be included in the modeling. For small UAVs, an important perturbation to consider is wind, so the development of a controller to account for this could be carried out.

- Investigation of other areas of generic swarming systems; for example, single robot path planning has been studied extensively, although there has

been little work been carried out on swarm path planning. Other areas include swarm avoidance of arbitrary shaped obstacles, avoidance of moving obstacles, optimal swarm path planning and swarm foraging.

- The swarm considered in this thesis was homogeneous. In order to meet different system requirements it would be interesting to consider heterogeneous swarms. Swarms could therefore meet different engineering requirements, although still operate together and ensure collision avoidance.

- Other areas of dynamical systems theory could be investigated; for example, complexity theory is a new, rapidly growing scientific field that could be used to investigate the control of a very large number of *agents*. Scale-free networks, for example, have been suggested as a way of maximising the effectiveness of controlling a large group of interacting components [145].

- The end goal would be to implement the swarm model in a formation of real robots. By validating the swarm theory in one application, such as UAVs, it allows for a starting point in the justification for more ambitious applications, such as SFF.

It is clear that there is large scope for future work. The end goal is to develop swarms of robots that can be used to solve engineering problems in new and efficient ways. Figure 8.1 summarises these aims with a possible future space exploration mission. By developing the technology required to achieve swarming, swarms of spacecraft, robots and UAVs could all work together in the not so distant future.

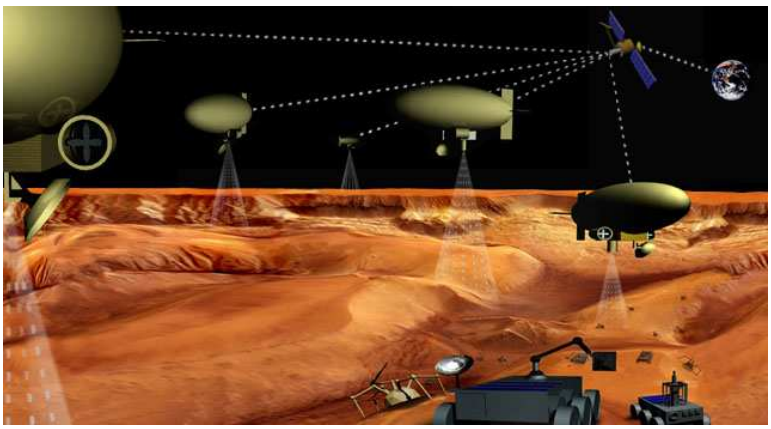

Figure 8.1: Future swarm system (JPL, CALTECH)

Bibliography

[1] Y. Chuang, Y.R. Huang, M.R. D'Orsogna, and A.L. Bertozzi. Multi-vehicle flocking: Scalability of cooperative control algorithms using pair-wise potentials. In *IEEE International Conference on Robotics and Automation*, pages 2292–2299, Roma, Italy, 10-14 April 2007.

[2] L. Bayindir and E. Sahin. A review of studies in swarm robotics. *Turkish Journal of Electrical Engineering and Computer Sciences*, 15(2):115–147, 2007.

[3] P. Romanczuk, I.D. Couzin, and L. Schimansky-Geier. Collective motion due to individual escape and pursuit response. *Physical Review Letters*, 102(1):010602, 2009.

[4] N. Correll and A. Martinoli. A challenging application in swarm robotics: The autonomous inspection of complex engineered structures. *Bulletin of the Swiss Society for Automatic Control*, 46:15–19, 2007.

[5] C.R. McInnes. Velocity field path-planning for single and multiple unmanned aerial vehicles. *The Aeronautical Journal*, 107(1073):419–426, 2003.

[6] D. Kingston, R. Beard, T. McLain, M. Larsen, and W. Ren. Autonomous vehicle technologies for small fixed wing UAVs. In *2nd AIAA Unmanned Unlimited Systems, Technologies, and Operations*, San Diego, California, USA, 15 - 18 September 2003.

[7] E.W. Frew, D.A. Lawrence, and S. Morris. Coordinated stand-off tracking of moving targets using Lyapunov guidance vector fields. *Journal of Guidance, Control and Dynamics*, 31(2):290–306, 2008.

[8] M. Quigley, M.A. Goodrich, S. Griffiths, A. Eldredge, and R.W. Beard. Target acquisition, localization, and surveillance using a fixed-wing mini-

UAV and gimbaled camera. In *IEEE International Conference on Robotics and Automation*, pages 2600–2605, Barcelona, Spain, 18-22 April 2005.

[9] A. Ollero and L. Merino. Control and perception techniques for aerial robotics. *Annual Reviews in Control*, 28(2):167–178, 2004.

[10] K. Carpenter, C.J. Schrijver, R.J. Allen, A. Brown, D. Chenette, W.C. Danchi, M. Karovska, S. Kilston, R.G. Lyon, J. Marzouk, L.M. Mazzuca, R.V. Moe, F. Walter, and N. Murphy. The stellar imager (SI): a revolutionary large-baseline imaging interferometer at the Sun-Earth L_2 point. *New Frontiers in Stellar Interferometry*, 5491(1):243–254, 2004.

[11] O. Wallner. Darwin system assessment study. *Astrium Summary Report, European Space Agency*, 1:1–18, 12 December 2006.

[12] A. Mogilner, L. Edelstein-Keshet, L. Bent, and A. Spiros. Mutual interactions, potentials, and individual distance in social aggregation. *Journal of Mathematical Biology*, 47(4):353–359, 2003.

[13] R.S. Miller and W. Stephen. Spatial relationships in flocks of sandhill cranes. *Ecology*, 47(2):323–327, 1966.

[14] A. Ilachinski. Land warfare and complexity, part I: Mathematical background and technical sourcebook. *Report: Center for Naval Analyses, Alexandria, Virginia*, pages 1–202, 1996.

[15] H.V.D. Parunak and S.A. Brueckner. Engineering swarming systems. In F. Bergenti, M.P. Gleizes, and F. Zambonelli, editors, *Methodologies and Software Engineering for Agent Systems*. Springer US, 2004.

[16] M. Ayre, L. Pettazzi, and D. Izzo. Self-assembly in space using behaviour-based intelligent components. *European Space Agency internal report*, 1:1–91, June 2005.

[17] R.A. Brooks. The robust layered control system for a mobile robot. *IEEE Transactions of Robotics and Automation*, 2(1):14–23, 1986.

[18] M.J. Mataric. Designing emergent behaviors: From local interactions to collective intelligence. In *Proceedings of the 2nd International Conference on: From animals to animats 2: simulation of adaptive behavior*, pages 432–441, Honolulu, Hawai, USA, August 1993.

[19] L. Zhou, Z. Qidan, Y. Dongmei, and Z. Xiuping. Research on subsumption architecture and application in dynamic programming of robot. In *Proceedings of the International Conference on Intelligent Mechatronics and Automation*, pages 522–526, Chengdu, China, 26-31 August 2004.

[20] A.R. Neto, G.A. Campos, J.T. Souza, M. Roisenberg, and V.X. Marques. Autonomous agents and subsumption models for simulation of population dynamics. In *Proceedings of the 7th International Conference on Machine Learning and Cybernetics*, pages 2400–2445, Kunming, China, 12-15 July 2008.

[21] G. Beni. The concept of cellular robotic system. In *Proceedings of IEEE International Symposium on Intelligent Control*, pages 57–62, Arlington, Virginia, USA, 24-26 Aug 1988.

[22] J. von Neumann. The general and logical theory of automata. In L.A. Jeffress, editor, *Cerebral Mechanisms in Behavior - The Hixon Symposium*, pages 1–31. Hafner, New York, 1967.

[23] G. Beni and J. Wang. Swarm intelligence in cellular robotic systems. In *Proceedings NATO Advanced Workshop on Robots and Biological Systems*, Tuscany, Italy, 26-30 June 1989.

[24] A. Winfield, C. Harper, and J. Nembrini. Towards dependable swarms and a new discipline of swarm engineering. In E. Sahin and W. Spears, editors, *SAB'04 Swarm Robotics workshop*, pages 126–142. Springer-Verlag, 2005.

[25] E. Bonabeau, M. Dorigo, and G. Theraulaz. *Swarm intelligence: from natural to artificial systems*. Oxford, New York, USA, 1999.

[26] L. Bai, M. Eyiyurekli, and D.E. Breen. An emergent system for self-aligning and self-organizing shape primitives. In *2nd IEEE International Conference on Self-Adaptive and Self-Organising Systems*, pages 445–454, Venice, Italy, 20-24 October 2008.

[27] J. Gravner and D. Griffeath. Modeling snow-crystal growth: A three-dimensional meso-scopic approach. *Physical Review E: Statistical, Nonlinear, and Soft Matter Physics*, 79(1):011601, 2009.

[28] F. Heylighen. The science of self-organization and adaptivity. In L.D. Kiel, editor, *The Encyclopedia of Life Support Systems (EOLSS)*, pages 253–280. Eolss Publishers, Oxford, 2001.

[29] R. Beckers, J.L. Deneubourg, and S. Goss. Trails and U-turns in the selection of a path by the ant lasius niger. *Journal of Theoretical Biology*, 159(4):397–415, 1992.

[30] Y. Sallez, T. Berger, and D. Trenesaux. A stigmergic approach for dynamic routing of active products in FMS. *Computers in Industry*, 60(3):204 – 216, 2009.

[31] M. Gardner. Mathematical games: The fantastic combinations of John Conway's new solitaire game "life". *Scientific America*, 223:120–123, 1970.

[32] D.A. Wolf-Gladrow. *Lattice-Gas Cellular Automata and Lattice Boltzmann Models - An Introduction*. Springer, 2000.

[33] I.G. Georgoudas. Modelling earthquake activity features using cellular automata. *Mathematical and Computer Modelling*, 46(1-2):124 – 137, 2007.

[34] Z.Y. Billings and A.F. Routh. Identification of the belousov-zhabotinskii reaction using cellular automata models. *International Journal of Bifurcation and Chaos in Applied Sciences and Engineering*, 17(5):1687–1701, 2007.

[35] C. Reynolds. Flocks, herds and schools: a distributed behavioural model. *Computer Graphics*, 21(4):25–34, 1987.

[36] F. Heppner and U. Grenander. A stochastic non-linear model for coordinated bird flocks. In S. Krasner, editor, *The Ubiquity of Chaos*, pages 233–238. Washington AAAS Publications, 1990.

[37] W.J. Crowther. Flocking of autonomous unmanned air vehicles. *Aeronautical Journal*, 107(1068):99–110, 2003.

[38] W.J. Crowther. Rule-based guidance for flight vehicle flocking. *Proceedings of the Institution of Mechanical Engineers - Part G: Journal of Aerospace Engineering*, 218(2):111–124, 2004.

[39] M. Dorigo. *Optimization, Learning and Natural Algorithms*. PhD thesis, Politecnico di Milano, 1992.

[40] M. Dorigo and L.M. Gambardella. Ant colonies for the travelling salesman problem. *BioSystems*, 43(2):73 – 81, 1997.

[41] A.E. Rizzoli, R. Montemanni, E. Lucibello, and L.M. Gambardella. Ant colony optimization for real-world vehicle routing problems: from theory to applications. *Swarm Intelligence*, 1(2):135 – 151, 2007.

[42] K.M. Sim and W.H. Sun. Multiple ant-colony optimization for network routing. In *Proceedings of 1st International Symposium on Cyber Worlds*, pages 277–281, Tokyo, Japan, 6-8 November 2002.

[43] A. Shmygelska, R. Aguirre-Hernndez, and H.H. Hoos. An ant colony optimization algorithm for the 2D HP protein folding problem. In *Book Series Lecture Notes in Computer Science*, pages 40–52. Springer Berlin/Heidelberg, 2001.

[44] J. Kennedy and R. Eberhart. Particle swarm optimization. In *Proceedings of the IEEE International Conference on Neural Networks*, pages 1942–1948, Piscataway, NJ, USA, 27 November - 1 December 1995.

[45] H. Yoshida, K. Kawata, Y. Fukuyama, S. Takayama, and Y. Nakanishi. Particle swarm optimization for reactive power and voltage control in electric power systems considering voltage security assessment. *IEEE Trans. on Power Systems*, 15(4), 2000.

[46] J. Ciurana, A. Arias, and T. Ozel. Neural network modeling and particle swarm optimization (PSO) of process parameters in pulsed laser micromachining of hardened AISI H13 steel. *Materials and Manufacturing Processes*, 24(3):358–368, 2009.

[47] R.C. Arkin. *Behaviour-Based Robotics*. MIT Press, 1998.

[48] R. Gross, M. Bonani, F. Mondada, and M. Dorigo. Autonomous self-assembly in a swarm-bot. *IEEE Transactions on Robotics*, 22(6):1115–1130, 2006.

[49] V. Trianni and M. Dorigo. Emergent collective decisions in a swarm of robots. In *Proceedings of the IEEE Swarm Intelligence Symposium*, pages 241–248, Pasadena, California, USA, 8-10 June 2005.

[50] A.L. Christensen, R. O'Grady, and M. Dorigo. Morphology control in a multi-robot system. *IEEE Robotics and Automation Magazine*, 14(4):18–25, 2007.

[51] M.A. Montes de Oca and T. Stuetzle. Towards incremental social learning in optimization and multi-agent systems. In W. Rand, S.G. Ficici, and R. Riolo, editors, *Proceedings of the Evolutionary Computation and Multi-Agent Systems and Simulation (ECoMASS) Workshop*, pages 1939–1944, New York, NY, USA, 2008. ACM Press.

[52] F. Schlachter, E. Meister, S. Kernbach, and P. Levi. Evolve-ability of the robot platform in the symbrion project. In *IEEE International Conference on Self-Adaptive and Self-Organizing Systems Workshops*, pages 144–149, Venice, Italy, 20-24 October 2008.

[53] M. Szymanski, L. Winkler, D. Laneri, F. Schlachter, A.C. van Rossum, T. Schmickl, and R. Thenius. SymbricatorRTOS: A flexible and dynamic framework for bio-inspired robot control systems and evolution. In *Proceedings of the IEEE Congress on Evolutionary Computation*, Trondheim, Norway, 18-21 May 2009.

[54] S.J.A. Edwards. *Swarming on the Battlefield: past, present and future*. RAND, 2000.

[55] J.A. Roberts. *Satellite formation flying for an interferometry mission*. PhD thesis, Cranfield University, 2005.

[56] T. Prince. LISA: Probing the universe with gravitational waves. *LISA Mission Science Office*, LISA Project internal report number LISA-LIST-RP-436, March 2007.

[57] J.T. Koo and M.S. Shahruz. Formation of a group of unmanned aerial vehicles. In *Proceedings of the American Control Conference*, pages 69–74, Arlington, USA, 25-27 June 2001.

[58] P. Parjanian. Behaviour coordination mechanisms - state of the art. *University of Southern California, Institute of Robotics and Intelligent Systems IRIS Technical Report IRIS99-375*, pages 1–49, 1999.

[59] M.J. Mataric. Integration of representation in goal-driven behaviour-based robots. *IEEE Transactions of Robotics and Automation*, 8(3):304–312, 1992.

[60] L. Parker. Designing control laws for cooperative agent teams. In *Proceedings of the IEEE International Conference on Robotics and Automation*, pages 582–587, Atlanta, Geogia, USA, 26 May 1993.

[61] T. Balch and R.C. Arkin. Behavior-based formation control for multi-robot teams. *IEEE Transactions on Robotics and Automation*, 14(6):926–939, 1998.

[62] X.T. Liu and J. Baltes. An intuitive and flexible architecture for intelligent mobile robots. In *2nd International Conference on Autonomous Robots and Agents*, Palmerston North, New Zealand, 13-15 December 2004.

[63] K. Lerman, A. Martinoli, and A. Galstyan. A review of probabilistic macroscopic models for swarm robotic systems. In E. Sahin and W. Spears, editors, *Swarm Robotics Workshop: State-of-the-art Survey*, pages 143–152. Springer Berlin/Verlag, 2005.

[64] W. Lui, A. Winfield, and J. Sa. Modelling swarm robotic systems: A case study in collective foraging. In *Proceeding of Towards Autonomous Robotic Systems*, pages 25 – 32, Aberystwyth, UK, 3-5 September 2007.

[65] E. Bonabeau, A. Sobkowski, G. Theraulaz, and J. Deneubourg. Adaptive task allocation inspired by a model of division of labor in social insects. In *Proceedings of BCEC97 Biocomputing and emergent computation*, pages 36–45, Skovde, Sweden, 1-2 September 1997.

[66] O. Soysal, E. Bahceci, and E. Sahin. Aggregation in swarm robotic systems: Evolution and probabilistic control. *Turkish Journal of Electrical Engineering and Computer Sciences*, 15:199–225, 2007.

[67] O. Khatib. Real-time obstacle avoidance for manipulators and mobile robots. *The International Journal of Robotics Research*, 5(1):90–98, 1986.

[68] W.H. Huang, B.R. Fajen, J.R. Fink, and W.H. Warren. Visual navigation and obstacle avoidance using a steering potential function. *Robotics and Autonomous Systems*, 54(4):288 – 299, 2006.

[69] C.W. Warren. Global path planning using artificial potential fields. In *Proceedings of IEEE International Conference on Robotics and Automation*, pages 316–321, Scottsdale, AZ, USA, May 1989.

[70] J. Borenstein and Y. Koren. Real-time obstacle avoidance for fast mobile robots. *IEEE Transactions on System, Man and Cybernetics*, 19(5):1179–1187, 1989.

[71] R. Volpe and P. Khosla. Manipulator control with superquadric artificial potential functions: Theory and experiments. *IEEE Transactions on Systems, Man and Cybernetics*, 20(6):1423–1436, 1990.

[72] S.S. Ge and Y.J Cui. Dynamic motion planning for mobile robots using potential field method. *Autonomous Robots*, 13(3):207–222, 2002.

[73] B.Q. Nguyen, Y-L. Chuang, D. Tung, C. Hsieh, Z. Jin, L. Shi, D. Marthaler, A. Bertozzi, and R.M. Murray. Virtual attractive-repulsive potentials for cooperative control of second order dynamic vehicles on the caltech MVWT. In *Proceedings of American Control Conference*, pages 1084–1089, Portland, USA, 8-10 June 2005.

[74] J.H. Reif and H. Wang. Social potential fields: A distributed behavioral control for autonomous robots. *Robots and Autonomous Systems*, 27(3):171–194, 1999.

[75] V. Gazi and K.M. Passino. A class of attraction/repulsion functions for stable swarm aggregations. In *Proceedings of the 41st IEEE Conference on Decision and Control*, volume 3, pages 2842–2847, Las Vegas, Nevada, USA, December 2002.

[76] D.E. Chang, S.C. Shadden, J.E. Marsden, and R. Olfati-Saber. Collision avoidance for multiple agent systems. In *Proceedings of 42nd IEEE Conference on Decision and Control*, volume 1, pages 539–543, Maui, Hawaii, USA, December 2003.

[77] P. Ogren, E. Fiorelli, and N.E. Leonard. Cooperative control of mobile sensor networks: Adaptive gradient climbing in a distributed environment. *IEEE Transactions on Automatic Control*, 49(8):1292–1302, 2004.

[78] M.R. D'Orsogna, Y.L. Chuang, A.L. Bertozzi, and S. Chayes. The road to catastrophe: Stability and collapse in 2D driven particle systems. In *Hawaii International Conference on Statistics, Mathematics and Related Fields*, Honolulu, Hawaii, USA, 16-18 January 2006.

[79] D.H. Kim, H. Wang, and S. Shin. Decentralized control of autonomous swarm systems using artificial potential functions: Analytical design guidelines. *Journal of Intelligent and Robotic Systems*, 45(4):369–394, 2006.

[80] Z. Qidan, Y. Yongjie, and X. Zhuoyi. Robot path planning based on artificial potential field approach with simulated annealing. In *Proceedings of the 6th International Conference on Intelligent Systems Design and Applications*, pages 622–627, Jinan, China, 16-18 October 2006.

[81] K.M. Krishna and P.K. Kalra. Solving the local minima problem for a mobile robot by classification of spatio-temporal sensory sequences. *Journal of Robotic Systems*, 17(10):549–564, 2000.

[82] M.H. Mabrouk and C.R. McInnes. An emergent wall following behaviour to escape local minima for swarms of agents. *International Journal of Computer Science*, 35(4):IJCS–35–4–3, 2008.

[83] L.S. Marcolino and L. Chaimowicz. No robot left behind: Coordination to overcome local minima in swarm navigation. In *Proceedings of IEEE International Conference on Robotics and Automation*, Pasadena, California, 19-23 May 2008.

[84] A. Badawy. *On-Orbit Manoeuvring Using Superquadric Potential Fields*. PhD thesis, University of Strathclyde, 2007.

[85] S. Keisuke. Deadlock-free motion planning using the Laplace potential field. *Advanced Robotics*, 7(5):449–461, 1992.

[86] J. Guldner and V.I. Utlun. Sliding mode control for gradient tracking and robot navigation using artificial potential fields. *IEEE Transactions on Robotics and Automation*, 11(2):247–254, 1995.

[87] M.R. D'Orsogna, Y.L. Chuang, A.L. Bertozzi, and S. Chayes. Self-propelled particles with soft-core interactions: Patterns, stability and collapse. *Physical Review Letters*, 96(10):104302, 2006.

[88] S.W. Ekanayake and P.N. Pathirana. Formations of robotic swarm: An artificial force based approach. *International Journal of Advanced Robotic Systems*, 6(1), 2009.

[89] K.J. Kyriakopoulos, P. Kakambouras, and N.J. Krikelis. Potential fields for non-holonomic vehicles. In *Proceedings of the IEEE International Symposium on Intelligent Control*, pages 461–465, Monterey, California, USA, 27-29 August 1995.

[90] V. Gazi, B. Fidan, Y.S. Hanay, and M.I. Kksal. Aggregation, foraging, and formation control of swarms with non-holonomic agents using potential functions and sliding mode techniques. *Turkish Journal of Electrical Engineering and Computer Sciences*, 15(2):149–168, 2007.

[91] W.M. Spears, D.F. Spears, R. Heil, W. Kerr, and S. Hettiarachchi. An overview of physicomimetics. In *Lecture Notes in Computer Science, State of the Art Series*, pages 84–97. Springer Berlin/Heidelberg, 2005.

[92] N.E. Leonard and E. Fiorelli. Virtual leaders, artificial potentials and coordinated control of groups. In *Proceedings of the 40th IEEE Conference on Decision and Control*, volume 3, pages 2968–2973, Orlando, FL, USA, 2001.

[93] M.R. D'Orsogna, Y. Chuang, A.L. Bertozzi, and L.S. Chayes. Pattern formation, stability and collapse in 2D driven particle systems. In *Device Applications of Non-linear Dynamics*, pages 103–133. Springer Berlin/Heidelberg, 2007.

[94] C.R. McInnes. Autonomous path planning for on-orbit servicing vehicles. *Journal of the British Interplanetary Society*, 53(1/2):26–38, 2000.

[95] S.J. Schwartz, A. Balogh, P. Cargull, A.N. Fazakerley, and A.J. Coates. SWARM: a fleet of microsatellites to explore the magnetosphere. In *Proceedings of the Workshop held at Imperial College: Cluster-II: Multiscale/Multipoint Plasma Measurements*, London, UK, 22-24 September 1999.

[96] S.A. Curtis, M.L. Rilee, P.E. Clark, and G.C. Marr. Use of swarm intelligence in spacecraft constellations for the resource exploration of the asteroid belt. In *3rd International Workshop on Satellite Constellations and Formation Flying*, Pisa, Italy, 2003.

[97] F. McQuade, F. Ward, and C.R. McInnes. The autonomous configuration of satellite formations using generic potential functions. In *International symposium, Formation Flying, Mission and Technologies*, Toulouse, France, 29-31 October 2002.

[98] A. Badawy and C.R. McInnes. On-orbit assembly using superquadric potential fields. *Journal of Guidance, Control, and Dynamics*, 31(1):30–43, 2008.

[99] O. Ilaya, C. Bil, and M. Evans. Control design for unmanned aerial vehicle swarming. *Proceedings of IMeche Part G: Journal of Aerospace Engineering*, 222(4):549–567, 2008.

[100] K. Han, J. Lee, and K. Kim. Unmanned aerial vehicle swarm control using potential functions and sliding mode control. *Proceedings of IMechE Part G: J. Aerospace Engineering*, 222(6):721–730, 2008.

[101] D.P. Scharf, F.Y. Hadaegh, and S.R. Ploen. A survey of spacecraft formation flying guidance and control (Part II): Control. In *American Control Conference*, pages 2976–2985, Colorado, US, 4-6 June 2003.

[102] J.R.T Lawton. *A behavior-based approach to multiple spacecraft formation flying*. PhD thesis, Brigham Young University, 2000.

[103] D.P. Scharf, F.Y. Hadaegh, and S.R. Ploen. Precision formation delta-v requirements for distributed platforms in Earth orbit. In *SPIE Remote Sensing of the Atmosphere, Ocean, Environment, and Space Conference*, Honolul, Hawaii, USA, 8-11 November 2004.

[104] P.B. Jones, M.A. Blake, and J.K. Archibald. A real-time algorithm for task allocation. In *International Symposium on Intelligent Control*, pages 672–677, Vancouver, Canada, 27-30 October 2002.

[105] W. Ren and R.W. Beard. A decentralized scheme for spacecraft formation flying via the virtual structure approach. In *Proceedings of the American*

Control Conference, pages 1747–1751, Denver, Colorado, USA, 4-6 June 2003.

[106] K.D. Do and J. Pan. Non-linear formation control of unicycle-type mobile robots. *Robotics and Autonomous Systems*, 55(3):191–204, 2007.

[107] P.K.C Wang and F.Y. Hadaegh. Coordination and control of multiple microspacecraft moving in formation. *Journal of the Astronautical Sciences*, 44(3):315–355, 1996.

[108] H. Wong and V. Kapila. Spacecraft formation flying near Sun-Earth L_2 Lagrange point: Trajectory generation and adaptive output feedback control. In *Proceedings of the American Control Conference*, pages 2411–2418, Portland, USA, 8-10 June 2005.

[109] F. Bauer, J. Bristow, D. Folta, K. Hartman, D. Quinn, and J.P. Howt. Satellite formation flying using an innovative autonomous control system (autocon) environment. In *AIAA Guidance, Navigation, and Control Conference*, pages 657–666, New Orleans, USA, 11-13 August 1997.

[110] E.I. Grøtli. *Modeling and Control of Formation Flying Satellites in 6 DOF*. PhD thesis, Norwegian University of Science and Technology, 2005.

[111] B.D.O Anderson, B. Fidan, Y. Changbin, and D. Van Der Walle. UAV formation control: Theory and application. In *Lecture notes in control and information sciences*, pages 15–33. Springer Berlin/Heidelberg, 2008.

[112] H.G. Tanner, A. Jadbabaie, and G.J. Pappas. Flocking in fixed and switching networks. *IEEE Transactions on Automatic Control*, 52(5):863–868, 2007.

[113] J. Wessnitzer, A. Adamatzky, and C. Melhuish. Towards self-organising structure formations: A decentralized approach. In *Book Series Lecture Notes in Computer Science*, pages 573–581. Springer Berlin/Heidelberg, 2001.

[114] E. Bahceci, O. Soysal, and E. Sahin. A review: Pattern formation and adaptation in multi-robot systems. In *Robotics Institute, Carnegie Mellon University, Tech. Rep. CMU-RI-TR-03-43*, Pittsburgh, PA, October 2003.

[115] B. Nabet, N.E. Leonard, I.D. Couzin, and S.A. Levin. Leadership in animal group motion: A bifurcation analysis. In *Proceedings of the 17th International Symposium on Mathematical Theory of Networks and Systems*, Kyoto, Japan, 24-28 July 2006.

[116] B. Varghese and G.T. McKee. Modeling and simulating a mathematical tool for multi-robot pattern transformation. In *Proceedings of International Conference on Computer Modeling and Simulation*, pages 21–27, Macau, China, 20-22 February 2009.

[117] T. Alterovitz, R. Simon and K. Goldberg. The stochastic motion roadmap: A sampling framework for planning with markov motion uncertainty. In *Motion Planning in Medicine: Optimization and Simulation Algorithms for Image-Guided Procedures*, volume 50, pages 75–89. Springer Berlin/Heidelberg, 2008.

[118] P.C. Parks. Lyapunov's stability theory: 100 years on. *IMA Journal of Mathematical Control and Information*, 9:275–303, 1992.

[119] R.E. Kalman and R.E. Bertram. Control system analysis and design via the second method of Lyapunov part I: Continuous systems. *Transactions of ASME: Journal of Basic Engineering*, 82:371–393, 1960.

[120] R.E. Kalman and R.E. Bertram. Control system analysis and design via the second method of Lyapunov part II: Discrete systems. *Transactions of ASME: Journal of Basic Engineering*, 82:394–400, 1960.

[121] F. McQuade. *Autonomous Control for On-orbit Assembly using Artificial Potential Functions*. PhD thesis, University of Glasgow, 1997.

[122] R. Thom. *Structural Stability and Morphogenesis: An Outline of a General Theory of Models*. Benjamin/Cummings Publishing, Reading, MA., 1975.

[123] Y.A. Cengel and R.H. Turner. *Fundamentals of Thermo-Fluid Sciences*. McGraw-Hill, 2001.

[124] C.M. Bender and S. A. Orszag. *Advanced Mathematical Methods for Scientists and Engineers: Asymptotic Methods and Perturbation Theory*. Springer, 1978.

[125] L. Rade and B. Westergren. *Mathematics Handbook for Science and Engineering*. Studentlitteratur, 1989.

[126] W. Bong. *Space Vehicle Dynamics and Control*. American Institute of Aeronautics and Astronautics, Reston, VA, 2nd edition, 2008.

[127] C.R. McInnes. Vortex formation in swarms of interacting particles. *Physical Review E: Statistical, Non-linear, and Soft Matter Physics*, 75(3):032904, 2007.

[128] M.H. Mabrouk and C.R. McInnes. Non-linear stability of vortex formation in swarms of interacting particles. *Phys. Rev. E*, 78(1):012903, Jul 2008.

[129] K. Sigurd and How. J. UAV trajectory design using total field collision avoidance. In *AIAA Guidance, Navigation and Control Conference*, Austin, Texas, USA, 11-14 August 2003.

[130] N. Yen, C.J. Fong, V. Chu, A. Hsiao, T. Tsai, and C.Y. Huang. FORMOSAT-3/COSMIC mission to global earth weather monitoring: Early orbit, orbit transfer and mission operation overview. In *1st FORMOSAT-3/COSMIC Data Users Workshop*, Boulder, Colorado, USA, October, 16-18 2006.

[131] N.H. Hamilton. Formation flying satellite control around the L_2 Sun-Earth libration point. Master's thesis, George Washington University, 2002.

[132] A. Sparks. Satellite formation keeping control in the presence of gravity perturbations. In *Proceedings of the American Control Conference*, Chicago, Illinois, USA, June 2000.

[133] V. Vaddi. *Modelling and control of satellite formations*. PhD thesis, Texas A and M University, 2003.

[134] H. Schaub and K.T. Alfriend. J_2 invariant relative orbits for spacecraft formations. In *Celestial Mechanics and Dynamical Astronomy*, volume 79. Springer Netherlands, 2001.

[135] C. Sabol, R. Burns, and C.A. McLaughlin. Satellite formation flying design and evolution. *Journal of Spacecraft and Rockets*, 38(2):270–278, 2001.

[136] A. Golikov. Evolution of formation flying satellite relative motion: Analysis based on the theona satellite theory. In *Proceedings of the 17th International Symposium on Space Flight Dynamics*, Moscow, Russia, 16-20 June 2003.

[137] K.T. Alfriend, H. Yan, and S.R. Vadali. Non-linear considerations in satellite formation flying. In *AIAA/AAS Astrodynamics Specialist Conference and Exhibit*, Monterey, California, 5-8 August 2002.

[138] G. Radice and D. Biamonti. Quasi-optimal spacecraft formation maneuvering via Lyapunov functions. *Journal of Aerospace Engineering, Sciences and Applications*, I(1):18–24, 2008.

[139] S. Gong, J. Li, H. Baoyin, and Y. Gao. Formation reconfiguration in restricted three body problem. In *Acta Mechanica Sinica*, volume 23. Springer Berlin/Heidelberg, 2007.

[140] M. Innocenti, F. Giulietti, and L. Pollini. Intelligent management control for unmanned aircraft navigation and formation keeping. In *RTO AVT Course on Intelligent Systems for Aeronautics*, Belgium, 13-17 May 2002.

[141] M. Sadraey and R. Colgren. UAV flight simulation: Credibility of linear decoupled vs. non-linear coupled equations of motion. In *AIAA Modelling and Simulation Technologies Conference and Exhibit*, San Francisco, California, 15-18 August 2005.

[142] A.M Hyslop and J.S. Humbert. Wide-field intergration methods for autonomous navigation of 3D environments. In *AIAA Guidance, Navigation and Control Conference and Exhibit*, Honolulu, Hawaii, 18-21 August 2008.

[143] E.J. Davidson. The robust control of a servomechanism problem for linear time-invariant multi-variable systems. *IEEE Transactions on Automatic Control*, 21(1):25–34, 1976.

[144] K. Nomura and H. Nishimura. *The Basics of Control Theory Using Matlab*. Tokyo Denki University Press, 1998.

[145] M. Bartolozzi, D.B. Leinweber, T. Surungan, A.W. Thomas, and Williams A.G. Scale-free networks in complex systems. In *SPIE International Symposium: Microelectronics, MEMS, and Nanotechnology*, Brisbane, Australia, 11-15 December 2005.